PUB-433
RECEIVED
MAY 1 1984
PUB FILE
LBL LIBRARY

μSR NEWSLETTER

Lawrence Berkeley Laboratory, University of California
Meson Science Laboratory, University of Tokyo, Japan

EDITORS:

K. M. Crowe	LBL
A. M. Portis	UC Berkeley
T. Yamazaki	U of Tokyo

CONTRIBUTING EDITORS:

J. H. Brewer	TRIUMF
F. N. Gygax	SIN
V. W. Hughes	Yale
C. Kittel	UC Berkeley
W. J. Kossler	William and Mary
P. M. Platzman	Bell Labs
A. Schenck	SIN

SECRETARY:

S. S. Rosenblum LBL

DEFINITION OF μSR

μSR stands for Muon Spin Relaxation, Rotation, Resonance, Research, or what have you. The intention of the mnemonic acronym is to draw attention to the analogy with NMR and ESR, the range of whose applications is well known. Any study of the interactions of the muon spin by virtue of the asymmetric decay is considered μSR, but this definition is not intended to exclude any peripherally related phenomena, especially if relevant to the use of the muon's magnetic moment as a delicate probe of matter.

No. 29 April 5, 1984

TABLE OF CONTENTS

Page

Muon Diffusion in the Metal Hydrides $LaNi_5H_6$ and β-PdH_x 1474
F.N. Gygax, A. Hintermann, W. Rüegg, A. Schenck, W. Studer, and A.J. van der Wal

Diffusion and Localization of Positive Muons in Niobium Single Crystals at Low Temperatures in the Presence of Impurities Measured in Zero and High Transverse Field 1491
F.N. Gygax, A. Hintermann, N. Kaplan, W. Rüegg, A. Schenck, W. Studer, and A.J. van der Wal

μ^+-Knightshift Studies and the Electronic Structure of Hydrogen in Metals 1510
F.N. Gygax, A. Hintermann, W. Rüegg, A. Schenck, W. Studer, and A. van der Wal

Quantum Diffusion of Positive Muons in Iron 1553
E. Yagi, G. Flik, K. Fürderer, N. Haas, D. Herlach, J. Major, and A. Seeger

A Comparison of Spin-Glass Dynamics Determined by the Muon-Spin Relaxation and Neutron Spin-Echo Techniques 1564
R.H. Heffner, D.E. MacLaughlin

Effects of Superconductivity on Rare-Earth Ion Dynamics in $(Ho_xLu_{1-x})Rh_4B_4$* 1582
R.H. Heffner, D.W. Cooke, R.L. Hutson, M. Leon, M.E. Schillaci, J.L. Smith, A. Yaouanc, S.A. Dodds, L.C. Gupta, and D.E. MacLaughlin

Muon Spin Relaxation in Spin Glass PdMn 1594
R.H. Heffner, M. Leon, M.E. Schillaci, S.A. Dodds, G.A. Gist, D.E. MacLaughlin, J.A. Mydosh, and G.J. Nieuwenhuys

For Reference
Not to be taken from this room

PUB-433 4-84/265 This work was supported by the U.S. Department of Energy under Contract No. DE-AC03-76SF00098
Lawrence Berkeley Laboratory is an Equal Opportunity Employer

PUB-433

MUON DIFFUSION IN THE METAL HYDRIDES $LaNi_5H_6$ AND β-PdH_x

F.N. Gygax, A. Hintermann, W. Ruegg, A. Schenck,
W. Studer and A.J. van der Wal

Institute for Medium Energy Physics, ETH-Zurich, c/o
SIN, CH-5234 Villigen, Switzerland

and

F. Stucki and L. Schlapbach

Laboratory for Solid State Physics, ETH-Zurich,
CH-8093 Zurich, Switzerland

Contribution to the International Meeting on Hydrogen in Metals, Wroclaw, Poland, September 1983

DISCLAIMER

This document was prepared as an account of work sponsored by the United States Government. While this document is believed to contain correct information, neither the United States Government nor any agency thereof, nor the Regents of the University of California, nor any of their employees, makes any warranty, express or implied, or assumes any legal responsibility for the accuracy, completeness, or usefulness of any information, apparatus, product, or process disclosed, or represents that its use would not infringe privately owned rights. Reference herein to any specific commercial product, process, or service by its trade name, trademark, manufacturer, or otherwise, does not necessarily constitute or imply its endorsement, recommendation, or favoring by the United States Government or any agency thereof, or the Regents of the University of California. The views and opinions of authors expressed herein do not necessarily state or reflect those of the United States Government or any agency thereof or the Regents of the University of California.

Abstract

Zero and transverse field μ^+SR measurements have been performed in $LaNi_5H_6$ and in PdH_x (x from 0.59 to 0.86) between 16 K and room temperature. The μ^+ depolarization is due to the spread in nuclear dipole fields originating predominantly from the protons. Motional averaging is caused by the combined motion of protons and the μ^+. The results show a surprising low correlation rate $1/\tau_c$, which points to a highly correlated μ^+-proton diffusion or to μ^+ trapping within regions of largely immobile hydrogen configurations. In $LaNi_5H_6$ muon trapping or a localized μ^+ jump mode could be considered. In that sample a linear decrease of the second moment with temperature between 20 K and 120 K is measured, in contrast to the unchanged relaxation observed by proton NMR.

1. Introduction

Spin relaxation experiments with positive muons in metal hydrides offer the possibility to compare directly the μ^+ diffusion with the proton diffusion. The proton diffusion is usually well known from other experiments.

In systems like $LaNi_5H_6$ or β-PdH_x the μ^+ depolarization is predominantly caused by the spread in nuclear dipole fields originating from the protons. The μ^+ relaxation function is as usual characterized by two parameters: (i) M_2, the second moment of the dipolar field spread, mainly determined by the structural arrangement of protons around the μ^+, (ii) τ_c, the correlation time originating from the fluctuations in the dipolar field components due to the motion of both μ^+ and proton.

Assuming an uncorrelated motion of muon and protons, the correlation rate $1/\tau_c$ can be written as

$$\frac{1}{\tau_c} = \frac{1}{\tau_\mu} + \frac{1}{\tau_p} , \qquad (1)$$

where $1/\tau_\mu$ is the μ^+ jump rate and $1/\tau_p$ the proton jump rate. Irrespective of the motional behaviour of the muon, one would then expect to find

$$\frac{1}{\tau_c} \geqslant \frac{1}{\tau_p} ,$$

i.e. that the rate $1/\tau_c$ would never be slower than the proton jump rate. For $LaNi_5H_6$ and β-PdH_x $1/\tau_p$ is known from NMR and neutron diffraction measurements [1-9].

2. $LaNi_5H_6$

The sample used for the μSR experiments was only hydrogenated two times in order to avoid Ni precipitation on the surface which could lead to an artificial increase of the μ^+ relaxation rate [10]. The resulting powdery material was sealed in a spherical quartz ampoule.

Fig. 1 shows the measured temperature dependence of the muon depolarization rate Λ ($1/\Lambda$ is the time for which the polarization decreases to 1/e). Measurements were performed in transverse field (200 G) as well as in zero field, both techniques yielding identical results. (For the zero field case, Kubo-Toyabe functions are taken to fit the data. The dipolar field spreads σ_{ZF} have to be scaled down by a factor 2/5 for direct comparison with the transverse field damping rates, according to theory.) The scaled line width of a proton NMR experiment by Halstead [1] is displayed for comparison in fig. 1. (The scale of the NMR line width has been determined from the square root of the reported second moment times 2/3 to account for the difference between the like spin

case [p-p] and the unlike spin case [μ-p].)

For T < 120 K one sees that the NMR damping is constant (which is confirmed by Barnes et al. [2]), whereas the muon depolarization rate decreases gently to a plateau value of 0.13 μs^{-1} around 150 K (dotted level in fig. 1). No diffusion occurs below 150 K, all zero field measurements are clearly best fitted by a static Kubo-Toyabe function.

Above 160 K motional averaging sets in and the data are analysed either with the usual transverse field motional narrowing function or with the dynamic Kubo-Toyabe function, using $\sigma = 0.13\ \mu s^{-1}$ (or $\sigma_{ZF} = 5/2 \times 0.13\ \mu s^{-1}$). Fig. 2 shows the results for $1/\tau_c$ plotted in logarithmic scale vs. 1/T. The straight solid line in fig. 2 represents corresponding data from a proton NMR study by Halstead et al. [3]. These data are in good agreement with other NMR and neutron diffraction experiments [1,4,5].

In the temperature region of diffusive motion, three striking differences between μ^+ and proton behaviour are apparent:

(i) The muon data differ from an Arrhenius like behaviour for T > 250 K. The observed negative curvature of the ln $1/\tau_c$ versus 1/T relation is peculiar. It cannot be explained by a classical sum of activated processes, which

would result in a positive curvature.

(ii) The activation energy for μ^+ diffusion (~ 150 meV, at least defined for the lower temperatures where an Arrhenius relation has been assumed) is smaller than for proton diffusion (~ 250 meV).

(iii) $\tau_c(\mu^+) > \tau_p$, although it seems that at the onset of diffusion the rates are of the same magnitude. In view of Eq. (1) this points to a considerably decreased mobility of the protons in the vicinity of the μ^+ and with respect to the μ^+. Such a behaviour may indicate a highly correlated motion of protons and the μ^+. It might also hint to the trapping of μ^+ in areas of largely immobile protons.

An alternative explanation could be the following: The contribution from the ^{139}La nuclei to the observed second moment cannot be ignored [2]. At low temperature we have measured the muon spin relaxation in a metallic $LaNi_5$ block. This allowed us to estimate a ^{139}La contribution of about 0.06 μs^{-1} to the σ for the immobile μ^+. Let us assume now that almost up to room temperature the μ^+ stays trapped in the lattice. This could be so if the muon either occupies one single location or has entered a rapid localized jumping mode as considered for the proton in

$LaNi_5H_6$ by different authors [11,12]. The μ^+ then is less mobile because it requires a larger local lattice expansion due to its higher zero point energy compared to the proton. The motion of the protons would reduce a fraction of the field spread at the μ^+ (averaging starting at 160 K and roughly completed at 250 K), but the fraction due to ^{139}La would remain effective (at least partially in the case of localized jumping).

3. PdH_x

Our sample was a polycristalline Pd sphere (purity 5 N, diameter 15 mm) charged in a H_2 atmosphere to the hydrogen content of x = 0.59, 0.70 and 0.75. The higher concentrations of x = 0.81 and 0.86 were reached by additional electrolytical charging; after preparation these samples were kept at liquid nitrogen temperature.

For the concentrations x = 0.70 and 0.75 stroboscopic μSR measurements [13] as well as zero field or transverse field time differential measurements were performed between 16 K and room temperature. At the three other concentrations similar measurements were effectuated for T < 77 K.

Below 50 K a static muon behaviour is indicated by the zero field measurements for all concentrations. For that temperature region fig. 3 displays the obtained static damping σ versus hydrogen concentration (the reduced value 2/5 x σ_{ZF} is shown for the zero field data). For x > 0.7 a constant value σ = 0.124 μs^{-1} is observed, compatible with the older measurements by Fiory et al. at x = 0.97 [14]. The value of σ is reduced for x = 0.70 and 0.59, but only by about 15% and 20%, respectively.

Above 50 K the relaxation data for x = 0.70 and 0.75 were analysed using motional narrowing relations. The obtained correlation rates $1/\tau_c$ are presented in the conventional Arrhenius plot of fig. 4. The results obtained from the transverse field stroboscopic data and the zero field measurements are identical. They do not point to a striking hydrogen concentration dependence .

As it can be seen (Fig. 4), the correlation rate $1/\tau_c$ is not described by a single Arrhenius law over the investigated temperature range. Above 100 K the rate follows an Arrhenius law with activation energy of ~ 53 meV and preexponential factor of about 3 x 10^7 μs^{-1} ; below 100 K the data level off.

The diffusion of protons in β-PdH has been studied by NMR [6-8] and neutron diffraction [9]; the reported activation energies E_a scatter from 100 meV to 250 meV. One solid line in Fig. 4 represents the results of Ito et al [6], with E_a = 130 meV, which were obtained from a CW-NMR study

in $PdH_{0.75}$ in the same temperature range as in our study. A second solid line shows the results of Seymour et al. [7] for x = 0.70 with E_a = 228 meV, and a third solid line links low temperature measurements by Kreitzman et al. [8] for x = 0.82. Obviously the NMR and μSR experiments yield quite different results. There is appreciable μ^+ diffusion for the low temperatures at which the protons are practically immobile. On the other side, above 180 K, the μ^+ correlation rate is significantly reduced compared to the proton NMR results. If trapping is to be made responsible for this high temperature behaviour, one has difficulties to understand the low apparent activation energy. This might again be indicative of either a slow motion inside some region in which both the μ^+ and the protons are trapped or a highly correlated μ^+-proton displacement.

The fact that σ is constant for T < 50 K and x > 0.7 suggest that the μ^+ has an identical proton environment for this concentration range.

References

[1] T.K. Halstead, J. Solid State Chem. 11 (1974) 114.

[2] R.G. Barnes, W.G. Harper, S.O. Nelson, D.K. Thome and D.R. Torgeson, J. Less-Common Met. 49 (1976) 483.

[3] T.K. Halstead, N.A. Abood and K.H.J. Buschow, Solid State Comm. 19 (1976) 425.

[4] R.C. Bowman Jr., D.M. Gruen, and M.H. Mendelsohn, Solid State Comm. 32 (1979) 501.

[5] D. Richter, R. Hempelmann and L.H. Vinhas, J. Less-Common Met. 88 (1982) 353.

[6] T. Ito and T. Kadowaki, Phys. Lett. 54A (1975) 61.

[7] E.F.W. Seymour, R.M. Cotts, and W.D. Williams, Phys. Rev. Lett. 35 (1975) 165.

[8] S.R. Kreitzman and R.L. Armstrong in Electronic Structure and Properties of Hydrogen in Metals, ed. P. Jena and C.B. Satterthwaite (Plenum, 1983).

[9] G. Nelin and K. Sköld, J. Phys. Chem. Sol. 36 (1975) 1175.

[10] F.N. Gygax, A. Hintermann, W. Ruegg, A. Schenck, W. Studer, L. Schlapbach, and F. Stucki in Recent Developments in Condensed Matter Physics, ed. F.T. DeVreese et al., Vol. 2 (Plenum, 1981).

[11] J.C. Achard, A.J. Dianoux, C. Lartigue, A. Percheron-Guegan and F. Tasset in Rare Earth in Modern Science and Technology, Vol. 3, ed. J. McCarthy and J.J. Rhyne (Plenum, 1981).

[12] D.G. Westlake in Electronic Structure and Properties of Hydrogen in Metals, ed. P. Jena and C.B. Satterthwaite (Plenum, 1983).

[13] F.N. Gygax, A. Hintermann, W. Ruegg, A. Schenck, W. Studer, A.J. van der Wal and L. Schlapbach, Hyperfine Interactions, to be published,

F.N. Gygax, A. Hintermann , W. Ruegg, A. Schenck and W. Studer, Solid State Comm. 38 (1981) 1245.

[14] A.T. Fiory, D.E. Murnick, R.P. Minnich and W.J. Kossler, Solid State Comm. 21 (1977) 747.

Figure Captions

Fig. 1: Measured muon depolarization rate Λ versus temperature in $LaNi_5H_6$. ($1/\Lambda$ is the time for which the polarization decreases to 1/e of its initial value.) The dotted level indicates the static Gaussian damping rate reached before onset of motional narrowing. The dashed curve represents the proton NMR line width [1] scaled down for comparison with μ^+ depolarization.

Fig. 2: Correlation rate $1/\tau_c$ (logarithmic scale) versus inverse temperature for μ^+ in $LaNi_5H_6$. The straight solid line represents proton NMR results [3]. A data point from proton diffusion studied by quasielastic neutron scattering [5] is also indicated.

Fig. 3: Static Gaussian damping rate σ versus hydrogen concentration x measured for μ^+SR in PdH_x below 50 K. The different measurement techniques are indicated. (The reduced value 2/5 x σ_{ZF} is represented for the zero field data.) The transverse field measurement by Fiory et al. [14] is also shown.

Fig. 4: Correlation rate $1/\tau_c$ (logarithmic scale) versus inverse temperature for μ^+ in β-PdH_x. For comparison proton NMR results by Ito et al. [6], Seymour et al. [7] and Kreitzman et al. [8] are also indicated.

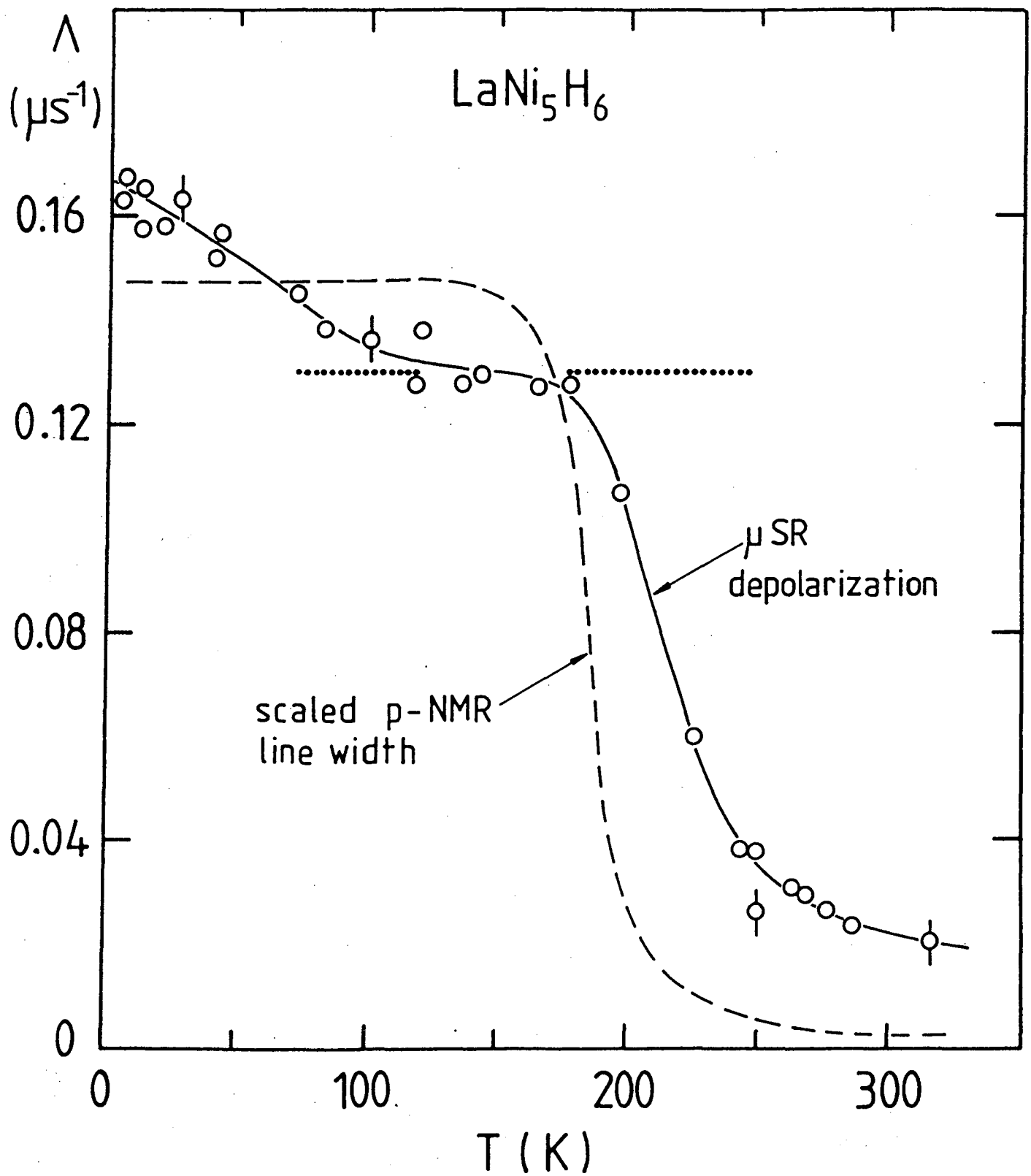
Λ
(μs⁻¹)
LaNi5H6
0.16
0.12
0.08
0.04
0
0
100
200
300
T (K)
μ SR
depolarization
scaled p-NMR
line width

Figure 1

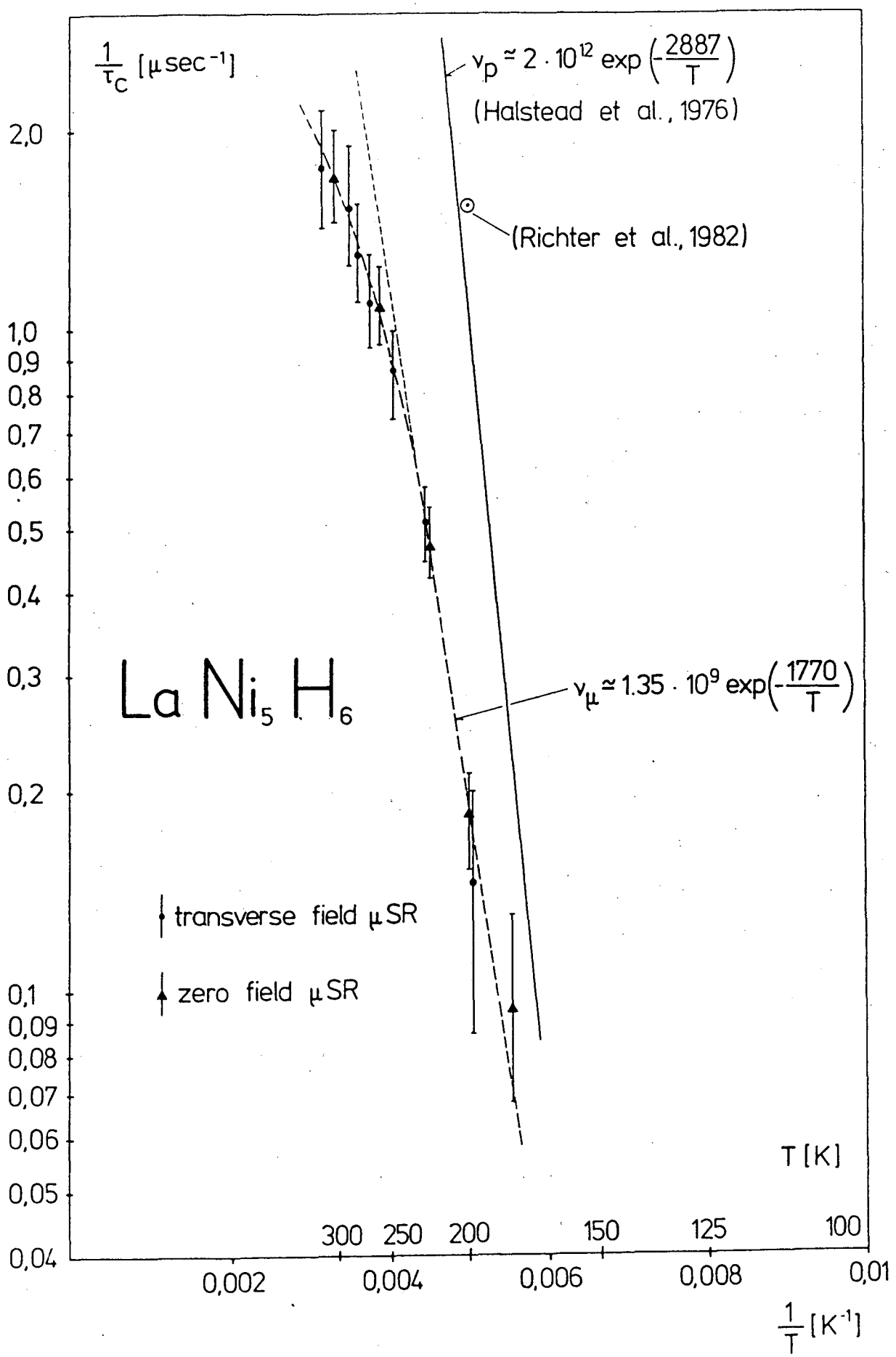
$\frac{1}{\tau_c}$ [μsec⁻¹]
$\nu_p \simeq 2 \cdot 10^{12} \exp\left(-\frac{2887}{T}\right)$
(Halstead et al., 1976)
(Richter et al., 1982)
$\nu_\mu \simeq 1.35 \cdot 10^9 \exp\left(-\frac{1770}{T}\right)$
La Ni5 H6
transverse field μSR
zero field μSR
T [K]
300 250 200 150 125 100
2,0
1,0
0,9
0,8
0,7
0,6
0,5
0,4
0,3
0,2
0,1
0,09
0,08
0,07
0,06
0,05
0,04
0,002
0,004
0,006
0,008
0,01
$\frac{1}{T}$ [K⁻¹]

Figure 2

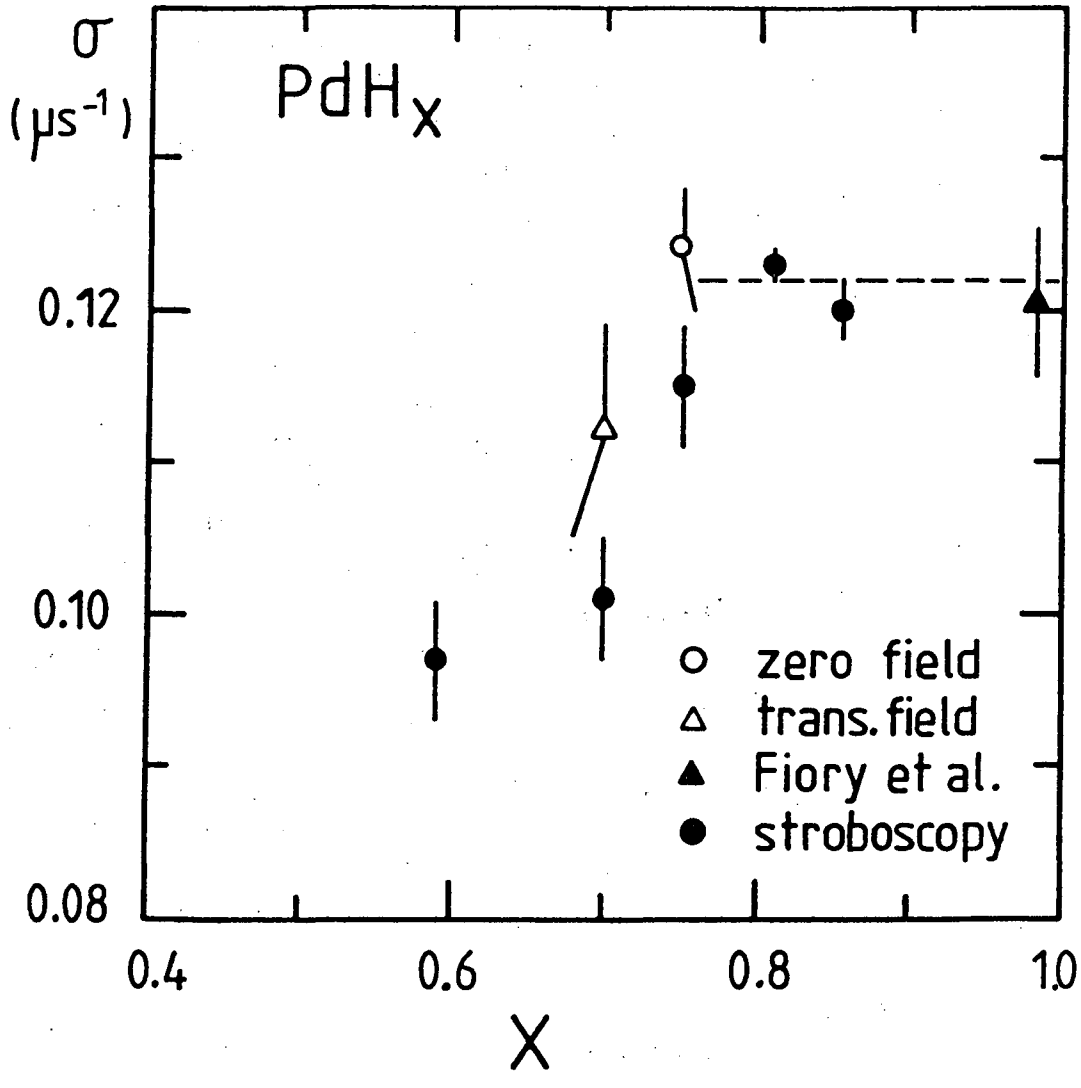
σ
(μs⁻¹)
PdHx
0.12
0.10
0.08
0.4
0.6
0.8
1.0
X
zero field
trans. field
Fiory et al.
stroboscopy

Figure 3

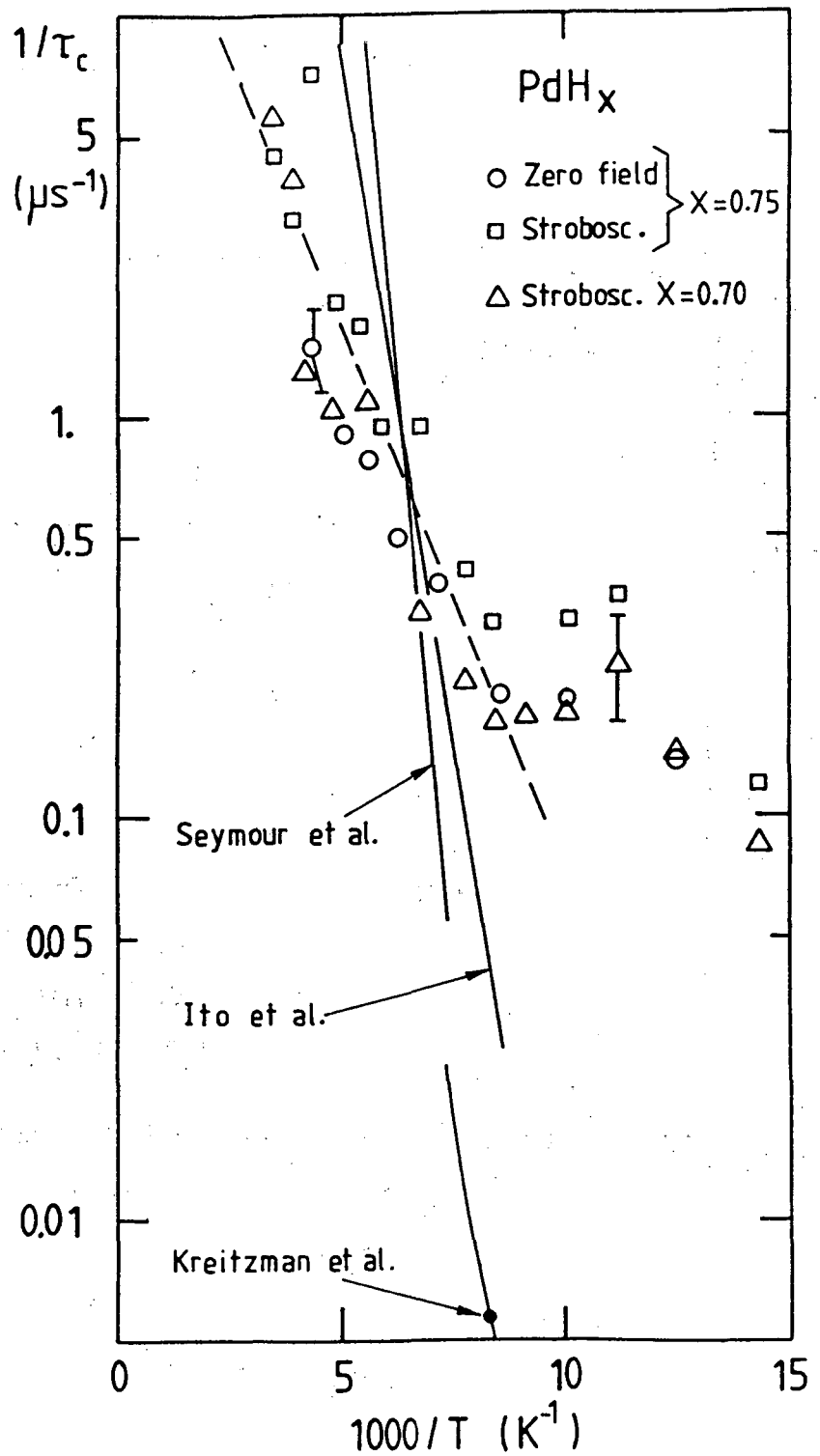
1/τc
5
(μs-1)
1.
0.5
0.1
0.05
0.01
PdHx
Zero field
Strobosc.
X=0.75
Strobosc. X=0.70
Seymour et al.
Ito et al.
Kreitzman et al.
0
5
10
15
1000/T (K-1)

Figure 4

DIFFUSION AND LOCALIZATION OF POSITIVE MUONS IN NIOBIUM SINGLE CRYSTALS AT LOW TEMPERATURES IN THE PRESENCE OF IMPURITIES MEASURED IN ZERO AND HIGH TRANSVERSE FIELD

F.N. Gygax *, A. Hintermann *, N. Kaplan **, W. Ruegg *, A. Schenck *, W. Studer * and A.J. van der Wal *

* Institute for Medium Energy Physics of ETHZ, c/o SIN, CH-5234 Villigen, Switzerland

** Racah Institute of Physics, Hebrew University of Jerusalem, Israel

Presented as "Hydrogen in Metals" Conference, Wroclaw, September 1983

(to be published in J. Less Common Met.)

ABSTRACT

We have studied the trapping and diffusion behavior of positive muons in Nb single crystals by comparing the measured depolarization rate with model calculations. Zero field μSR measurements reveal the temperature dependence of the diffusion coefficient and also clearly indicate that the different trap configurations above and below $\sim$ 22 K are correlated. The activation energy needed to escape from the low temperature traps was found to be 200 $\pm$ 20 K (17 $\pm$ 1.5 meV). Subsequently, the angular dependence of the depolarization rate has been measured at 14.0 and 36.8 K in a transverse field of 7.47 kG by rotating a Nb single crystal around its <110> axis, which was kept perpendicular to both field and μ^+ polarization. This allows one to determine the site symmetry of the trapped muon as well as the lattice distortions around it. For 36.8 K the trapping site could be identified as a tetrahedral site next to a Ta impurity, possibly also close to an interstitial (N or O) impurity. A local lattice relaxation Δ R/R of 6.7(6)% for nn and of -6(2)% for nnn has been deduced. The low temperature curve shows a much more pronounced angular dependence than the high temperature curve, indicating a completely different μ^+-environment. A satisfactory explanation for these data has not yet been found.

INTRODUCTION

In general, a close analogy exists between the diffusion behavior of light interstitials in metals, such as hydrogen, and the positive muon, the main differences stemming from the mass ratio of about ten. In contrast, the depolarization rate of positive muons implanted in relatively pure bcc Nb vs. temperature shows intriguing aspects, not observed in the temperature dependence of the relaxation of hydrogen in this metal [1,2]. Among the fascinating features that puzzle both theoreticians and experimenters is the occurrence of a distinct dip at $\sim$ 22 K. Although such a dip in the μ^+-depolarization rate is not seen in other well-studied metals like e.g. Cu [3,4], this feature is not unique. Similar structures have been observed in Bi, Ta and V.

At low temperatures the depolarization rate in Nb shows two plateau regions separated by a more or less pronounced dip at 22 K, depending on the concentration of residual impurities [1,2,5,6]. For temperatures higher then $\sim$ 50 K the depolarization rate decreases to zero, as motional narrowing sets in. In the case of ultrapure Nb, however, it was found [7,8] that the μ^+-depolarization rate is relatively low, with hardly any structure from 5-50 K. Hartmann et al. [8] also demonstrated that small amounts of impurities (10-50 ppm) such as Ta and N already suffice to create the dip, although it appears difficult to clearly separate their individual effects.

EXPERIMENT AND DISCUSSION

I. Zero-field experiments

Two different theories have been forwarded to account for the observed behavior [1,2,9]. Petzinger [10] pointed out that zero-field experiments could distinguish between diffusion towards or escape from traps and therefore might discriminate between the two proposed descriptions.

Therefore, we measured the depolarization rate in a Nb single crystal of cylindrical shape with axis along <100> in the region of the dip in zero field [11]. Fig. 1 shows the depolarization rate vs. temperature extracted from a series of zero-field measurements by fitting a Gaussian depolarization function. The same spectra have also been fitted with the dynamic Kubo-Toyabe (DKT) function [12] and the Petzinger function

$$P(t) = \frac{1}{3} + \frac{2}{3} e^{-t/\tau_c} + \frac{2}{3} \int_0^t \frac{e^{-\tau/\tau_c}}{\tau_c} \left[1 - \sigma^2 (t-\tau)^2 e^{-\frac{1}{2}\sigma^2 (t-\tau)^2} \right] d\tau$$

where τ_c^{-1} represents the rate of a muon finding a trap, and σ the static (Gaussian) relaxation rate.

If a muon escapes from a trap and moves around, it will finally depolarize completely as reflected by the DKT function. In contrast, a finite residual polarization will remain for $t \to \infty$, if the muon becomes trapped.

From our results it is apparent that the Petzinger function fits the high temperature side of the dip (22-28 K) best, whereas the DKT function proved an excellent fit for temperatures in the range 14-22 K. In Fig. 2, the resulting correlation rates τ_c^{-1} are plotted as a function of inverse temperature. The values for τ_c^{-1} entered in Fig. 2 are obtained using static depolarization rates σ of 0.515 and 0.500 MHz for the DKT and Petzinger fits, respectively. Open circles represent the Petzinger fits and closed circles the DKT fits. Also inserted are three points (closed squares) representing τ_c^{-1} as derived from data taken on the same crystal at the low-temperature side of the dip in a transverse field of 200 G. These spectra have been fitted with the Abragam formula describing the motional averaging [13].

Since τ_c^{-1} (Petzinger) is in the present dilution proportional to the concentration of available traps in the host, and τ_c^{-1} (DKT) can be identified as the escape rate from the trap, i.e. an intrinsic trap property, the coincidence of these two rates both in slope and exponential prefactor in the same Arrhenius plot is quite striking. Although the equality of the exponential prefactors is probably fortuitious, the equality of both exponents at high- and low temperature side of the dip is clear evidence for the strong correlation of the muon motion above and below 21 K. An explanation for this phenomenon could be that one observes here a bottleneck situation in which all muons that escape for T > 14 K from the low-temperature trap are quickly trapped by deeper, less abundant traps. Thus the rate

as which muons are finding the high-temperature traps is completely determined by the escape process. This in turn would imply that the two trap configurations at 14 and 35 K, respectively would be situated relatively near to each other, though not as nearest neighbors. This last conclusion follows from the observation that the muon depolarization rate displays a clear dip, i.e. is clearly influenced by motional narrowing in going from one trap to the other.

In view of these observations and preceding the conclusions of the following section, we arrive at the following picture. At temperatures below 14 K the muon diffuses through the Nb host lattice forming a small polaron and thus finds the most abundant shallow trap near a Ta impurity, of which the exact configuration has not yet been resolved. An alternative interpretation would be that the muon is already trapped in the temperature range 5-14 K. In that case the muon is assumed to be in a spatially extended state consisting of a number of equivalent sites, between which the muon quickly traps. With increasing temperature this state contracts onto a single site, as reflected by the slow increase in σ with temperature. The fact that neither Petzinger nor DKT fits provide a satisfactory fit compared to static KT fits supports this interpretation.

At a temperature of 14 K the main fraction of muons is trapped at Ta and as the temperature increases, muons start to move out of these traps, giving rise to motional narrowing and hence the occurence of the dip in the depolarization rate. At still higher temperatures ($\gtrsim$ 21 K) the muons find deeper, less

abundant traps, which are connnected with both Ta and N (or O) impurities, as will be discussed in the next section. It is known that interstitial impurities form deeper traps than substitutional [14].

Since our present samples contain 250 ppm Ta impurities and a total of about 100 ppm interstitial impurities (O,N,C), the main fraction of muons, say 80%, follows the behavior outlined above. Of course, a remaining fraction traps directly at the Ta + N and thus does not participate in the formation of the dip. Once the muons are trapped in the Ta + N trap complex, they only can escape via temperature activated hopping at $\gtrsim$ 80 K. The connection of Ta with the plateau at $\sim$14 K and N (or O) with high-temperature traps has already been discussed by other authors [8], a new element being introduced here is the hypothesis that most of the interstitials trap near a Ta impurity both below and above the dip, as supported by the observed angular dependence of σ in the following section. Of course, the preceding discussion does not exclude that some muons might move around in bandlike states, thus not contributing to σ at all.

II. High-field angular dependence at 14.0 and 36.8 K.

In order to determine the sites at which the muon is trapped at both sides of the dip, the full angular dependence of the depolarization rate was measured by rotating a large single crystal around its <110> cylinder axis in a transverse field of 7.47 kG. In a bcc lattice the muon is expected to reside either on tetrahedral sites located in the (001) planes or on octahedral sites located in the <100> direction between two Nb sites. Theoretically, the depolarization rate can be calculated on the basis of the dipole-dipole interaction between the nuclear Nb moments ($I = 9/2$) and the muons spin ($I = 1/2$). The calculation yields the Gaussian depolarization rate in the so-called Van Vleck limit, viz. for magnetic fields high enough ($\geqslant$ 2 kG) to quench the quadrupole interaction between the Nb and the electrical field gradient induced by the positive muon.

In Fig. 3 the results are presented for the low-temperature plateau at 14.0 K (open circles) and for the high-temperature plateau at 36.8 K (closed circles). Also inserted is the result of a rigid lattice calculation in pure Nb for a tetrahedral site, appropriately averaged over all possible equivalent sites. As can immediately be seen from Fig. 3, the absolute value of the experimental depolarization rate is much smaller than the calculated one for a tetrahedral site. For an octahedral site the difference would even be larger.

In order to explain the data for the high-temperature plateau, the solid curve was calculated under the assumption that the muon is trapped at a regular tetrahedral place, one of its nearest neighbors (nn) being a Ta substitutional impurity, another nn a Nb atom shifted away from the Ta, and two unrelaxed Nb nn. Only one of the next nearest neighbors (nnn) was shifted from its ideal position. After rearranging nn and nnn in this way, all nn's and nnn's are relaxed radially (as seen from the muon) to obtain a best fit to the measured data. Details on the exact positions of the nn's and nnn's can be found in Ref. 15.

The fit resulted in a relative relaxation $\Delta R/R$ of + 6.7(6)% for nn and - (6 $\pm$ 2)% for nnn, where the minus sign refers to inward displacement. The nn value is in reasonable agreement with the value of 5.4% obtained for the lattice relaxation of Nb nn adjacent to interstitital H in α-Nb [16]. The displacements of nn's and nnn's that cause the resultant relaxation around the μ^+ to be nonradial could, apart from the presence of the Ta, be caused by an O or N interstitial located at the octahedral site between the Ta nn and a Nb nnn. The site assignment for the high temperature plateau and its possible connection with an interstitial impurity does <u>not</u> comply with the interpretation of Hartmann et al., [8], although their observations do not preclude the present site assignment of a combined Ta-N trap.

The analysis of the curve at 14 K presents more problems. Clearly the muon does not reside at an undistorted octahedral or tetrahedral site, a prime difficulty being the large difference in depolarization rate between <110> of <111> on one hand and

<100> on the other. The difference of about 30% is clearly not consistent with a tetrahedral site ($\approx$ 20%) nor with structures composed of such sites, e.g. the T_2, T_4, and T_6 tunnel states, proposed for H in Nb [17,18]. These will have an increasingly less pronounced angular dependence. Alternatively, an octahedral site assignment presents difficulties in accounting for the width of the peak around H$\parallel$<100> and the flatness of the curve around H$\parallel$<111> and <110>.

Finally, one can consider the influence of the finite extension of the muon wave function in the host matrix on the second moment and thus on the μ^+-depolarization rate. This problem is treated theoretically by various authors [19,20]. From the work of Meier [21] one knows that as long as the μ^+ wavefunction is spherically symmetric, the dipolar field and, by the same arguments, the second moment due to dipole-dipole interaction are <u>not</u> changed by the finite spatial extension. Following the work of McMullen et al. and inserting the values for the width of the μ^+ wavefunction, approximated by a nonisotropic Gaussian function, as given by Sugimoto et al. for Nb, one calculates a reduction of the second moment of only a few percent compared to a pointlike muon. For the present discussion we can therefore safely ignore the finite extension of the muon wavefunction.

In conclusion, we have been able to reproduce the high-temperature angular dependence of the depolarization rate σ with a possible trap configuration for the μ^+ in the Nb host lattice. Substitutional Ta impurities, possibly in combination with interstitial impurities like O or N , play an

essential rate in explaining the observed angular dependence of σ in high magnetic field, together with an additional substantial radial outward relaxation of the neighbors nearest to the μ^+. Moreover, zero-field data show that the low- and high-temperature plateaus around the dip at $\sim$22 K are strongly correlated, thus indicating that the majority of muons escaping from low-temperature traps find after several jumps deeper, less abundant traps. This observation is an indication that only one single fraction of muons plays a dominant role in the detrapping-trapping behavior around the dip, in contrast with mechanisms as discussed in Ref. 8. Full analysis of the angular dependence at 14 K is in progress in order to resolve the trap configuration at low temperatures and further experiments have been planned to vary the concentration of interstitial impurities in the same single crystal and repeat the angular dependence measurements around the dip.

FIGURE CAPTIONS

Fig. 1: Temperature dependence of the Gaussian depolarization rate σ of positive muons implanted in a cylindrical Nb single crystal with axis along <100> in a zero field experiment. The data-points represented by closed circles were taken about one year later than those represented by open circles.

Fig. 2: Arrhenius plot of the inverse correlation time τ_c^{-1} vs. inverse temperature. The open circles correspond to Petzinger fits and the closed circles to dynamic Kubo-Toyabe fits. Also inserted are three points (open squares) representing τ_c^{-1} as derived from data taken on the same crystal at the low-temperature side of the dip in a transverse field of $\sim$200 G and fitted with the Abragam formula pertaining to motional narrowing. The solid line is a least-squares fit to $\tau_c^{-1} = A \exp(-E/k_B T)$, resulting in an 'attempt rate' $A = 28 \pm 4$ GHz and an activation energy $E/k = 200 \pm 20$ K. The τ_c's derived from Petzinger and Kubo-Toyabe fits represent of course quite different quantities. Further discussion is deferred to the text.

Fig. 3: Angular dependence of the μ^+-depolarization rate of a muon in Nb for the two plateau temperatures, 36.8 K (closed circles) and 14.0 K (open circles),

respectively, corresponding to high and low temperature trapping sites at both sides of the dip. All measurements were done in a field of 7.47 kG with the stroboscopic μSR technique. The solid line is the result of a second moment calculation allowing for nonradial relaxation around the muon of nearest neighbors and of next-nearest neighbors, due to the presence of substitutional (Ta) and interstitial (N) impurities and the μ^+ itself. For reference, the theoretical angular dependence of a tetrahedral site in a pure Nb lattice without any relaxation is also shown.

REFERENCES

[1] H.K. Birnbaum, M. Camani, A.T. Fiory, F.N. Gygax, W.J. Kossler, W. Rüegg, A. Schenck, and H. Schilling, Phys. Rev. B17 (1978) 4143.

[2] M. Borghini, T.O. Niinikoski, J.C. Soulié, O. Hartmann, E. Karlsson, L.O. Norlin, K. Pernestål, K.W. Kehr, D. Richter, and E. Walter, Phys. Rev. Lett. 40 (1978) 1723.

[3] M. Camani, F.N. Gygax, W. Rüegg, A. Schenck, and H. Schilling, Phys. Rev. Lett. 39 (1977) 836.

[4] H. Schilling, M. Camani, F.N. Gygax, W. Rüegg, and A. Schenck, Journ. Phys. F12 (1982) 875.

[5] J.A. Brown et al., Hyperfine Interactions 6 (1979) 233.

[6] R.H. Heffner, J.A. Brown, R.L. Hutson, M. Leon, D.M. Parkin, M.E. Schillaci, W.B. Gauster, O.N. Carlson, D.K. Rehbein, and A.T. Fiory, Hyperfine Interactions 6 (1979) 237.

[7] T.O. Niinikoski, O. Hartmann, E. Karlsson, L.-O. Norlin, K. Pernestål, K.W. Kehr, D. Richter, F. Walker, and K. Schulze, Hyperfine Interactions 6 (1979) 229.

[8] O. Hartmann, E. Karlsson, R.Waeppling, D. Richter, R. Hempelmann, K. Schulze, B. Patterson, E. Holzschuh, W. Kuendig, and S.F.J. Cox, Phys. Rev. B27 (1983) 1943.

[9] V.G. Grebinnik, I.I. Gurevich, V.A. Zhukov, A. Klimov, V.N. Maiorov, A.P. Manych, E.V. Mel'nikov, B.A. Nikol'skii, A.V. Pirogov, A.N. Ponomarev, V.I. Selivanov, and V.A. Suetin, JETP Lett. 25 (1977) 298.

[10] K.G. Petzinger, Phys. Lett. 75A (1980) 225 and K.G. Petzinger, Hyperfine Interactions 8 (1981) 639.

[11] A preliminary account of these zero-field measurements has been published as F.N. Gygax, A. Hintermann, N. Kaplan, W. Rüegg, A. Schenck, W. Studer, and A.J. van der Wal, SIN-Newsletter no. 14, 1982. Similar measurements are reported by C. Boekema, R.H. Heffner, R.L. Hutson, M. Leon, M.E. Schillaci, W.J Kossler, M. Numan, and S.A. Dodds, Phys. Rev. B26 (1982) 2341.

[12] R. Kubo and T. Toyabe: In Magnetic Resonance and Relaxation, ed. by R. Blinc (North Holland, Amsterdam, 1967).

[13] See e.g., A. Abragam: Principles of Nuclear Magnetism (Clarendon Press, Oxford, 1970).

[14] See e.g. Ch.A. Wert: In Hydrogen in Matals II, ed. by G. Aleveld and J. Voelkl (Springer, Berlin, 1978) and Ref. 20.

[15] F.N. Gygax, A. Hintermann, W. Rüegg, A. Schenck, W. Studer, A.J. van der Wal, and N. Kaplan, Proceedings Yamada Conference on μSR, Shimoda 1983, to be published in Hyperfine Interactions.

[16] H. Behr, H.M. Keppler, G. Steyrer, H. Metzger, and J. Peisl, J. Phys. F13 (1983) L29.

[17] W.F. Lankford, H.K. Birnbaum, A.T.Fiory, R.P. Minnich, K.G. Lynn, C.E. Stronach, L.H. Bieman, W.J. Kossler, and J. Lindemuth, Hyperfine Interactions 4 (1978) 833.

[18] H. Wipf, A. Magerl, S.M. Shapiro, S.K. Satija, and W. Thomlinson, Phys. Rev. Letters 46 (1981) 947.

[19] T. McMullen and E. Zaremba, Phys. Rev. B18 (1978) 3026.

[20] H. Sugimoto and Y. Fukai, Phys. Rev. B22 (1980) 670.

[21] P.F. Meier: In Exotic Atoms 1979, ed. by K. Crowe, J. Duclos, G. Fiorentini and G. Torelli (Plenum, N.Y.).

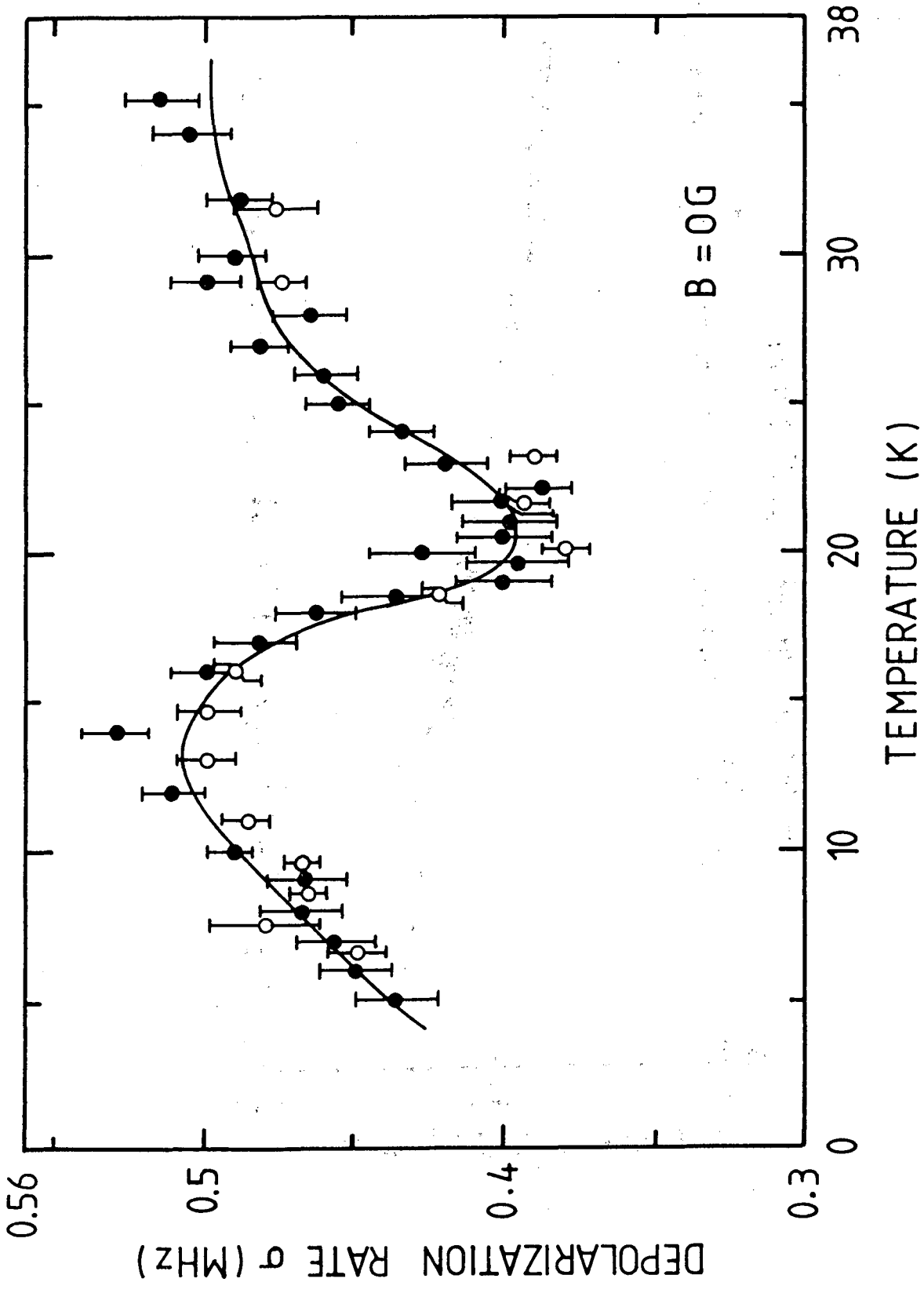
B = 0G
TEMPERATURE (K)
DEPOLARIZATION RATE σ (MHz)
0.56
0.5
0.4
0.3
0
10
20
30
38

Figure 1

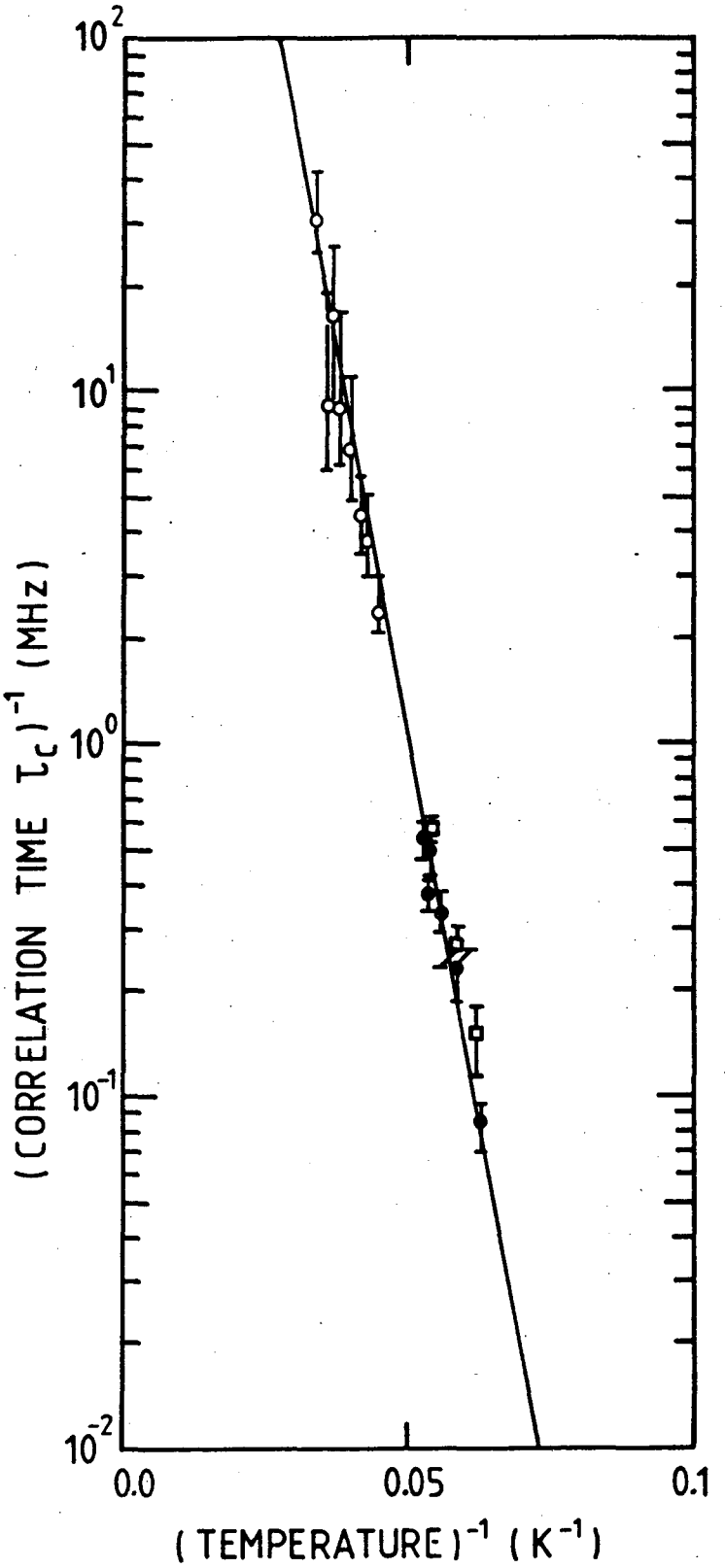
10^2
10^1
10^0
10^{-1}
10^{-2}
(CORRELATION TIME τ_c)$^{-1}$ (MHz)
0.0
0.05
0.1
(TEMPERATURE)$^{-1}$ (K^{-1})

Figure 2

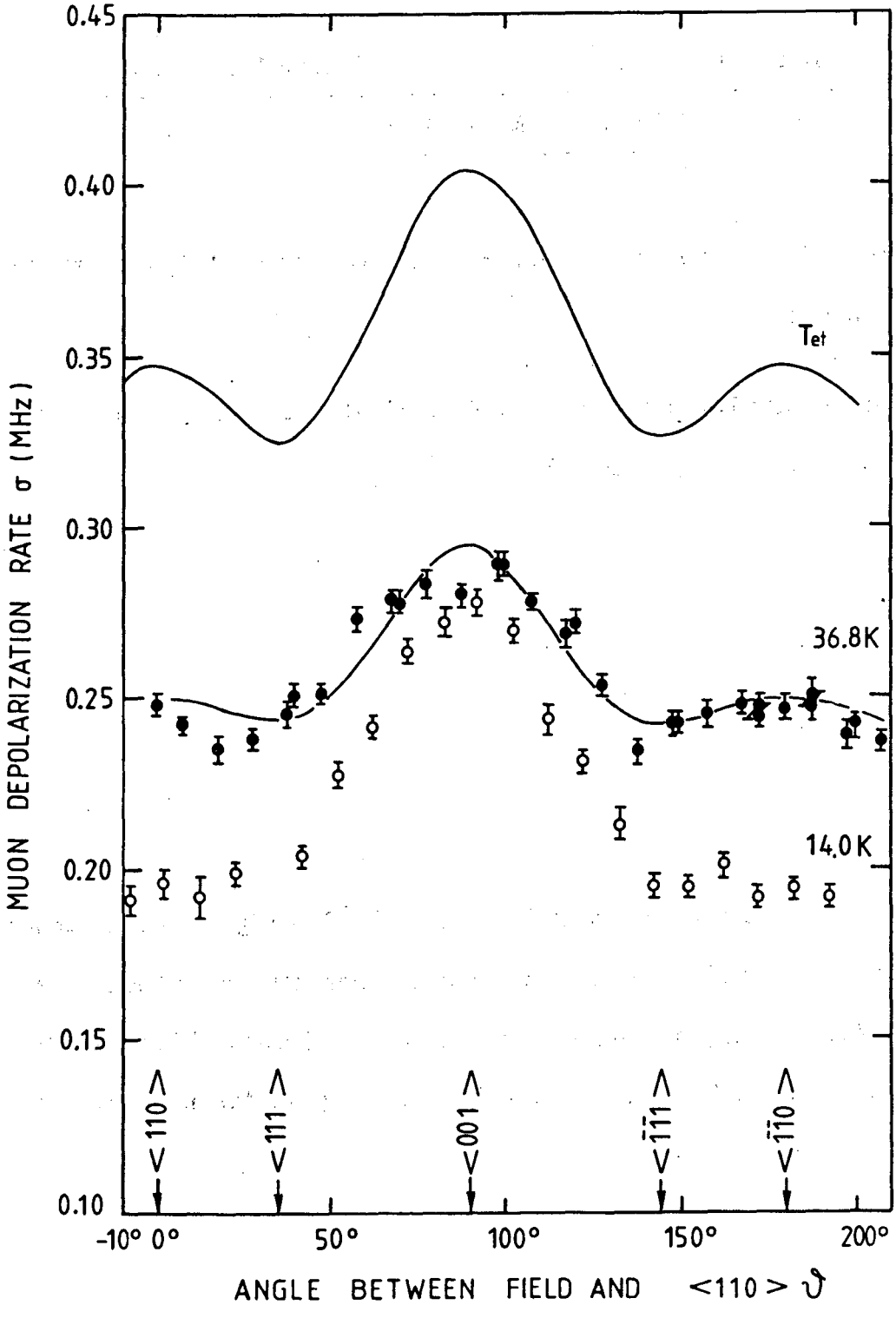
0.45
0.40
0.35
0.30
0.25
0.20
0.15
0.10
MUON DEPOLARIZATION RATE σ (MHz)
Tet
36.8K
14.0K
<110>
<111>
<001>
<$\bar{1}\bar{1}$1>
<$\bar{1}\bar{1}$0>
-10° 0°
50°
100°
150°
200°
ANGLE BETWEEN FIELD AND <110> ϑ

Figure 3

μ^+-KNIGHTSHIFT STUDIES AND THE ELECTRONIC STRUCTURE OF HYDROGEN IN METALS

F.N. Gygax, A. Hintermann, W. Rüegg, A. Schenck, W. Studer and A. van der Wal

Institute for Medium Energy Physics, ETH Zurich, c/o SIN, CH-5234 Villigen, Switzerland

Abstract

An up to data review of positive muon (μ^+) Knight shift studies in elemental non transition and transition metals and in β-palladium hydride will be presented. Implications on the local electronic structure of a hydrogenlike impurity will be pointed out.

Invited paper at International Meeting on Hydrogen in Metals (Wroclaw, September 1983)

(to be published in J. Less Common Met.)

I. Introduction

Interstitial protons or positive muons (μ^+) in a metal crystal aquire nearly the same electron distribution in their vicinity due to their identical charge state and strong Coulomb potential. Possible differences stem from their different zero point vibration amplitudes ($m_\mu \approx 1/8\ m_p$) which brings them differently close to the host lattice constituents. Aside from such effects there is basically no difference between the electronic properties of the two particles in a metal environment. Information gained on the electronic structure around a μ^+ can therefore be viewed as representative of the corresponding electronic structure around a proton. In this respect the μ^+ serves as a substitute probe in the study of the electronic structure of hydrogen in metals.

Positive muons can be implanted in any metal or metal alloy and its Knight shift can be measured by the muon spin precession (μSR) technique with high precision. In contrast the proton Knight shift can only be measured in metallic systems which absorb sufficient quantities of hydrogen to allow application of the NMR technique [1].

II. Knight shift and electronic structure

The implanted μ^+ is surrounded by electrons which form the local electronic structure and screen the positive muon charge within a radius of typically $2 \cdot a_B$ [2]. The μ^+ and the electrons interact magnetically with each other according to the Hamiltonian (in the nonrelativistic Pauli approximation)

$$\mathcal{H} = g_\mu \, \mu_\mu \, g_e \, \mu_B \, \vec{I}_\mu \cdot \sum_i \left\{ \frac{\vec{\ell}_i}{r_i^3} + \left[- \frac{\vec{S}_i}{r_i^3} + \frac{3 \, \vec{r}_i \, (\vec{S}_i \cdot \vec{r}_i)}{r_i^5} \right] + \frac{8\pi}{3} \, \delta(\vec{r}=o) \vec{S}_i \right\}$$

$$= g_\mu \, \mu_\mu \, \vec{I}_\mu \cdot \vec{H}_{eff} \qquad (1)$$

where the μ^+ is located at $\vec{r}_\mu = 0$. The index i refers to the ith electron. The first term under the sum is the orbital, the second term the dipole-dipole and the third term the Fermi contact hyperfine interaction. The sum over the first term vanishes since no net angular momentum is formed at the μ^+. However, in the presence of an external field the induced orbital motion of the electrons will lead to a diamagnetic screening field at the μ^+ (see below).

Introducing the charge density distribution

$$n(\vec{r}) = \sum_i |\psi_i(\vec{r})|^2 \qquad (2)$$

an effective magnetic field $\vec{H}_{eff}$ can be expressed in integral form as

$$\vec{H}_{eff} = g_e \mu_B \int_{V_L} n(r) \left[- \frac{\vec{S}(\vec{r})}{r^3} + \frac{3\, \vec{r}(\vec{S}(\vec{r})\cdot\vec{r})}{r^5} \right] dv$$

$$+ \frac{8\pi}{3} g_e \mu_B n(o) \vec{S} \qquad (3)$$

The integration extends in principle over the total volume of the sample, but we will assume the probe to be of spherical shape so that the demagnetization field and the Lorentz field cancel and only the integration over the Lorentz sphere remains. In the absence of magnetic ordering or an external field $\vec{H}_{eff}$ will of course be zero. In the presence of an external field B_o in, e.g. z-direction, each electronic spin will on the average acquire a small static component in z-direction which is given by

$$\langle S_z \rangle = \chi_e \cdot B_o \frac{1}{g_e \mu_B} \qquad (4)$$

where χ_e is the spin susceptibility per electron (assumed to be independent of position $\vec{r}$). As a result we find a non-vanishing H_{eff} in z-direction. The total field acting on the μ^+ is then given by

$$B_{tot}(\vec{r}_\mu = o) = B_o + H_{eff} = B_o(1+K) \tag{5}$$

where $K = H_{eff}/B_o$ is the so called Knight shift constant KS and H_{eff} the field shift. With Eq. (3) K can be written as

$$K = \frac{8\pi}{3}\, n(o)\, \chi_e + \left[\int_{V_L} n(\vec{r})\, \frac{3\cos^2\theta - 1}{r^3}\, dv\right] \chi_e$$

$$= K_{iso} + K_{ax} \tag{6}$$

where θ is the angle between the z-axis and $\vec{r}$. The second term of Eq. (6), the axial KS K_{ax}, vanishes for a charge distribution of spherical and cubic symmetry. For a charge distribution of axial symmetry K_{ax} can be written as

$$K_{ax} = \left[\int_{V_L} n(\vec{r}\,')\, \frac{3\, z'^2 - 1}{r^{13}}\, dv'\right] (3\cos^2\theta - 1)\, \chi_e \tag{7}$$

where x', y', z' refer to a new coordinate system with z' the axis of axial symmetry, usually to be identified with a certain crystal axis. θ is the angle between the z'-axis and the external field or the z-axis, respectively. A nonspherical or noncubic charge distribution, therefore, leads to an anisotropic KS. However, also the first term K_{iso}, stemming from the isotropic contact interaction may become anisotropic if the spin susceptibility is anisotropic.

In simple, nontransition metals only (s,p)-electrons at the Fermi energy will become spinpolarized in the presence of an external field (Pauli spin paramagnetism), i.e.

$$n(o) = n(o)_F = \langle|\psi(o)|^2\rangle_F$$

and principally $K_{iso} = K_s > 0$. The effect of core polarization may alter K_{iso} in both directions.

To include this effect $K_{iso} = K_s$ is often expressed in an obvious manner as

$$K_S = \frac{8\pi}{3}\,\mu_B\,\frac{n(o)^{\uparrow}-n^{\downarrow}(o)}{n_o^{\uparrow}-n_o^{\downarrow}}\,(n_o^{\uparrow}-n_o^{\downarrow})/B_o$$

$$= \frac{8\pi}{3}\,\frac{n^{\uparrow}(o)-n^{\downarrow}(o)}{n_o^{\uparrow}-n_o^{\downarrow}}\,\chi_s = \frac{8\pi}{3}\,\rho_s(o)\,\chi_s \qquad (8)$$

where $\rho_s(o)$ is the so called spin density enhancement factor and χ_s is the volume spin susceptibility of the homogeneous electron gas characterizing the conduction electrons.

In d-electron and f-electron transition metals, where the d- and f-electrons are contributing dominantly to the magnetic susceptibility, core polarization must be very important since the direct overlap of d-electron and more so of f-electron wave functions with the μ^+ is probably very small. We introduce therefore an additional term

$$K_{cp} = \frac{1}{\mu_B} B_{hf}^{\Omega a} \chi_{at}(d,f) \qquad (9)$$

where $B_{hf}^{\Omega a}$ is the induced hyperfine field at the μ^+ per unpaired d-, f-electron per atom. χ_{at} is the atomic spin susceptibility of the d-, f-electrons. In many cases $\chi(d,f)$ shows a strong temperature dependence which allows to distinguish between K_{cp} and K_s. Core polarization could in principle also contribute to the axial KS.

A last contribution to a field shift is the already mentioned diamagnetic screening analogous to the chemical shift in atoms and molecules. This negative shift constant is given by the Lamb expression

$$\sigma = - \frac{e}{3\ mc^2} \langle 0|\frac{1}{r}|0\rangle \qquad (10)$$

which yields $\sigma \approx -20$ ppm rather independent of the host metal and close to the atomic hydrogen value of - 18 ppm [3]. It involves the total charge distribution around the impurity in contrast to the contact term induced shift which depends only on the local densities at the impurity.
The total field shift (usually also called Knight shift) is then in principle composed of the following terms

$$K_\mu = K_s + K_{cp} + K_{ax} + \sigma \qquad (11)$$

III. Knight shift in nontransition metals

3.1. Systematics of isotropic Knight shift

Most of the data have already been discussed elsewhere [4, 5]. An updated compilation of all data is presented in Tab. I. New entries are the values of K_μ in Au, Zn and Cd. Revised values can be found for Be and Mg, stemming from new measurements on high purity single crystal samples. For completeness Tab. I contains also results obtained in the semi metals Sb and Bi, but these results will not be discussed here.

It was found earlier [4] that the logarithm of the induced hyperfine field per unpaired electron per atom, $B_{hf}^{\Omega a} = \mu_B K_s/\chi_{at}(s)$ *), showed a universal behavior in the cubic mono-, di- and tri-valent metals when plotted versus the molar electronic specific heat, which is proportional to the density of states at the Fermi energy (Fig. 2). It is now found that also the new values in Au and in the hcp metals Be, Zn and Cd are consistent with this universal curve. Also the revised value in Mg is now closer to this universal curve. One consequence of this universal behavior was the observation that the μ^+ KS shows a distinctive dependence on the valency of the metal and only to a lesser degree on the total conduction electron concentration in contrast to pre-

---

*) In calculating $B_{hf}^{\Omega a}$ experimental values for χ_{at} were used throughout.

Table I

Compilation of μ^+-Knight shift data in nontransition metals.

χ_s = experimental spin susceptibility (from Refs. 4, 15).

metal	r_s	$\chi_s \left\lvert \frac{emu}{cm^3} \right\rvert$	K_{iso}[ppm]	K_{ax}[ppm]	Refs.
		$\times 10^{-6}$			
Li	3.25	2.10	8.6±4.0		4, 6
Na	3.93	1.09	76.5±5.0		4, 6
K	4.86	0.90	63.2±4.5		4, 6
Rb	5.20	0.86	66.1±4.3		4, 6
Cs	5.63	0.81	31.0±4.0		4, 6
Cu	2.67	1.36	60±2.5		4, 6
Ag	3.02	0.88	94±3.5		4
Au	3.01	0.99	64±10		7
Be	1.88	~0.2	-9±1.6	-3±1.9	8, 9
Mg	2.65	~1.58	43.3±3.5	0.	new value
Ca	3.27	~1.58	21.2±6.2		4, 6
Sr	3.56	≳2.69	-18.4±6.8		4, 6
Ba	3.69	~0.99	29.6±5.0		4, 6
Zn	2.31	~0.99	60±5*	3±1.3*	8, 9, 10
Cd	2.59	~0.73	55±5*	-3.3±1.3*	8, 9, 11
Hg	2.75	~1.73	117±11**		4
Al	2.07	1.77	79.6±4.0		4
Ga	2.19	~0.7	-17±3.5		4
Pb	2.30	~2.36	105.2±3.5		4
Sb		~0.082	8700***	2200***	12, 13
Bi		~0.014	-276****	+9±6****	new value

* 20 K, ** -50° C, *** 15 K, **** 4.2 K (preliminary data), all other data are at roomtemp.

dictions by various jellium calculations on the basis of the spin density functional formalism [2].

In the meantime considerable progress has been achieved in the understanding of the gross features of the observed systematics by the work of Manninen [14]. It is essentially also a jellium calculation, but the host lattice potential is taken into account by the so-called spherical solid model, which replaces the compensating positive background charge in the conventional jellium approach.

In this model the host potential is constructed from the unscreened pseudopotentials of the host ions and subsequently a spherical average is calculated around the μ^+-site. This spherical average together with the μ^+ potential itself is then used as the relevant potential in a jellium calculation using again the selfconsistent spin density functional formalism, which includes automatically the effect of core polarization. In contrast to the conventional jellium calculations the actual lattice site of the μ^+ is now important and leads to different results. For the pseudo potentials the simple Ashcroft empty-core potentials with commonly used core radii were taken [14]. Other parameters that enter the calculations are the electron density parameter r_s and the valency Z. As an example, Fig. 2 shows a partial-wave decomposition of the electron density at the tetrahedral μ^+ site

in Cs obtained by this model. Also shown are the results of a nonpolarized jellium calculation. Clearly bound states show up showing a larger density for the spin down configuration which contribute therefore a negative hyperfine field. The continuum states, on the other side, contribute a positive hyperfine field. Compared with the jellium model the continuum states provide a considerably smaller contact density while the bound states provide a larger one, however both models yield almost the same total electron density at the μ^+-site. In the end the model is used to calculate the spin density enhancement factor $\rho_s(o)$ introduced in Eq. (8). Fig. 3 and Fig. 4 show the predictions of the spherical solid model for K_μ in mono and divalent metals. The diamagnetic contribution was calculated in the same model using a formula derived in [3]. The spin susceptibility, needed to calculate K_s, was taken to be the one of a homogeneous interacting electron gas of the appropriate density rather than the experimental value which is justified on grounds of internal consistency in using Eq. (8). It is evident from Figs. 3 and 4 that the general trend of the data with the density parameter r_s is reproduced quite well as is the grouping of the data with the valency of the host metal. However, if experimental values for the spin susceptibility were used, we would have found less agreement. This is somewhat surprising in view of the striking systematics in Fig. 1 which was obtained by using experimental values.

The situation is more clearly shown in Fig. 5 where we compare theoretical $\rho_s(o)$ from Manninen [14] with empirical ones calculated from the data as follows: $\rho_s(o) = (K_\mu - \sigma)/\frac{8\pi}{3}\chi_s$, where χ_s are experimental values [4, 15] and the diamagnetic screening constant is taken to be -20 ppm for all samples. We notice that the deviations from the predictions are most pronounced for the high density metals, although the trends are still in qualitative agreement.

Manninen [14] has also found an approximate linear relationship between log $B_{hf}^{\Omega a}$ and the atomic density of states (assuming a homogeneous electron gas picture). He dismisses this result as somewhat accidental. However in view of the empirical universal behavior in Fig. 1, which indicates that the true density of states matters indeed, we feel that it is neccessary to persue this problem further theoretically and that the present theory, although successful in reproducing the gross feature of the data, still lacks a predictive power in detail. For instance there is quite a gap between the experimental and predicted K_μ in Cu, while the experimental $B_{hf}^{\Omega a}$ is excellently accomodated by the universal curve in Fig. 1.

3.2. Axial Knight shift

Careful measurements of the angular dependence of the μ^+-KS in single crystals of the hcp metals Be, Cd and Zn [8, 9] showed the clear presence of an axial KS, while no axial KS could be observed in Mg. The axis of axial symmetry coincided generally with the crystalline c-axis. Fig. 6 shows the results obtained in Be at room temperature. In Zn an anisotropic KS could only be observed at low temperatures (< 80 K). Its size and functional dependence on angle varied between different samples and seemed to depend on the sample history, like the speed of temperature changes. At present we cannot offer any interpretation of the Zn-data. In Cd an axial KS was observable at all temperatures practically up to the melting point, however, a change of sign of K_{ax} occurred at 110 K. Fig. 7 shows the angular dependence of K_μ at 60 K and at room temperature[18]. The peculiar temperature of 110 K shows also up in the temperature dependence of the isotropic KS (see next section). If the axial KS in Cd is due to a non-spherical charge distribution around the μ^+, i.e. due to the presence of p-like states we would have observed a change of the charge distribution from oblate like (p_x, p_y components dominant) at low temperatures to prolate like (p_z component dominant) at high temperatures. On the other hand the observed anisotropy may be also due to an anisotropic χ_s as a result of an anisotropic Landé or g_e-factor of some of the

electrons contributing to the contact density. This is not an unreasonable possibility since it is known that spin-orbit coupling effects play an important role in the Cd band structure.

Since spin orbit coupling is of negligible importance in the low Z-metal Be we conclude that the observed axial μ^+ KS there presents the first evidence that also non s-like (with respect to the μ^+) electrons can be important in the local electronic structure of a hydrogenlike impurity.

3.3. Temperature dependence of K_{iso}

In nontransition metals one does not expect to find a significant temperature dependence, since the Pauli spin susceptibility is temperature independent as long as one deals with a degenerate electron system.

Indeed the μ^+ KS in Cu and Al does not display a temperature dependence within the present accuracy. In Zn one finds a slight linear increase with temperature with a slope of $(\partial K/\partial T) = 1.1 \pm 0.45$ ppm/100 K and a jump of $(12 \pm 8)\%$ when crossing the melting point [9, 10]. In contrast the μ^+ KS in Cd shows a very pronounced temperature dependence up to the melting point, but practically no change when passing into the liquid state (see Fig. 8). At 110 K we find a singularity

in the temperature dependence which has been recently identified as a band structure effect related to critical points in the vicinity of the K symmetry point of the hexagonal Brillouin zone[9,11,16].The overall temperature dependence is interpreted in analogy to the analysis of the nuclear Cd KS data [17] as a consequence of phonon-electron interactions which weaken the lattice potential and lead to an increasingly free electron character of the conduction electrons. It would be very interesting if some theorist could be motivated to calculate the concomitant change in the heat of solution for hydrogen. Remarkable is also the absence of a change of K_μ upon melting, quite in contrast to nuclear Cd Knight shift data which show a +33% jump upon melting.

3.4. μ^+ Knight shift at a structural defect in Zn

In contrast to the data obtained in polycrystalline Zn, which only showed a very weak temperature dependence, quite a different temperature dependence was found in a single crystal sample (see Fig. 9). At low and at high temperatures the data are in agreement with the polycrystalline sample results but at intermediate temperatures the KS shows a dramatic drop to large and negative values reaching its extremum at about room temperature. This behavior could not be influenced

by annealing the sample but it could be induced also in a polycrystalline sample by quenching it rapidly from a temperature close to the melting point down to 77°K [18].

The data can be understood in terms of trapping of the μ^+ at a second site involving a Knight shift of -520 ppm ± 10% which sharply contrasts with the value of 68 ± 5 ppm associated with the regular site. The escape activation energy out of this second site was determined to be 0.5 eV ± 5%, i.e. it presents a rather deep trap to the μ^+. It was also possible to obtain a rough estimate of the formation energy of this trap from the quenched polycrystalline samples: 0.5 ± 0.2 eV. The escape energy as well as the formation energy suggest that the trap site is a vacancy [11, 18]. But since it was not possible to anneal this defect by heating, such an identification seems to be ruled out. Another possibility is the formation of a multivacancy cluster or void which is thermally much more stable. Such defects will be formed from single vacancies during the temperature quench, if the quench rates are not to high. Indeed our quench rates were only of the order of 80 - 120°K/sec. Taking everything together it seems therefore quite likely that the trap site is a multivacancy cluster or small void. Manninen [14] predicts on the basis of the spherical solid model a KS of K_μ = + 280 ppm for a μ^+ at a vacancy in Zn. It was also found that the KS increases with

the vacancy or microvoid size if the μ^+ is at the center of this spherical defect [19].

The large negative KS, found experimentally, contradicts these predictions severely, indicating that the change in local electronic structure around the μ^+ by going from the interstitial site to a vacancy cluster is not really understood. Generally, information on the local electronic structure of hydrogen at a defect site appears very important, e.g. in relation to the mechanisms of hydrogen induced corrosion (weakening of metallic binding).

IV. Knight shift in transition metals

So far K_μ was determined in the group VB metals: V, Nb and Ta [4] and in the group VIII metals: Ni, Pd and Pt [20]. We will only discuss here results obtained in the latter three metals as a function of temperature. As an example Fig. 10 shows a plot of K_μ in Pt as a function of the magnetic bulk susceptibility with temperature as an implicit parameter. From such a plot one can determine the temperature independent s-electron induced KS: K_s and the d-electron

induced hyperfine field per unpaired d-electron per atom: $B^{\Omega a}_{hf,d}$ which is just the slope of the straight line in Fig. 10.

Tab. II compiles the results obtained in Ni, Pd and Pt. We notice that $B^{\Omega a}_{hf,d}$ increases by roughly a factor of 2 in going from Ni to Pd and likewise in going from Pd to Pt. For comparison Tab. II list also d-electron induced hyperfine fields at the host nuclei. Katayama et al. [21] have shown on the basis of KKR-CPA band structure calculations that the negative hyperfine field at the μ^+ in Ni originates from hydrogen-metal bonding states (involving hybridized hydrogen 1s- and Ni 3d-states), whereby the spin down state produces a larger charge density at the μ^+ than the spin up state. The observed tendency of $B^{\Omega a}_{hf,d}$ may therefore reflect an increasing spectral weight of such bonding states. Possible consequences of such a behavior for other properties of hydrogen in these metals, like local lattice relaxation, heat of solution, etc. must be investigated in the future. It may be recalled in this respect that hydrogen can be dissolved easily in Pd but not in Pt [22].

Table II

Compilation of μ^+ and nuclear Knight shfit data in Ni, Pd and Pt.

	$a(A^o)$	s-electron per atom	χ_s [emu/cm^3]	K_s^μ [ppm]	$B_{hf,d}^{\Omega_a,\mu^+}$ [kG/μ_B/at]	$B_{hf,d}^{\Omega_a,Nucl}$ [kG/μ_B/at]
Cu	3.61	1	$1.36\cdot10^{-6}$	80(3)	--	--
Ni	3.52	0.6	$0.62\cdot10^{-6}$	31(27)+	-1.224(23)+	-137
Ag	4.09	1	$0.85\cdot10^{-6}$	114(4)	--	--
Pd	3.89	0.36	$0.64\cdot10^{-6}$	62(13)	-2.39(11)	-345
Au	4.08	1	$0.99\cdot10^{-6}$	64(10)	--	--
Pt	3.92	0.2	$0.53\cdot10^{-6}$	73(15)	-5.03(43)	-1180

\+ revised value

V. Knight shift in β-PdH_x

So far all reported investigations concerned a single μ^+ (or proton) in the pure metal. This corresponds to an infinite dilute concentration of hydrogen in a metal, that is, we are within the α-phase of the metal hydrogen system. The bulk electronic structure of the host metal is only locally disturbed and effects of hydrogen-hydrogen interactions are altogether absent. The situation is quite different in the other regime of high hydrogen concentrations, i.e. in a metal hydride.

The only previous μSR KS study in a metal hydride was performed in the system $LaNi_5H_x$ [23]. Here we review some more recent investigations in β-PdH_x for concentrations of x = 0.59, 0.70, 0.75, 0.81 and 0.86. Except for x = 0.59 the KS is temperature independent [20] reflecting the fact that also the bulk magnetic susceptibility becomes practically temperature independent above x = 0.60 [24]. Fig. 11 displays the temperature ranges investigated for the various H/Pd ratios and the average KS found for each ratio. For x = 0.59 one finds a significant drop in K_μ when going from room temperature and above to 4.2 K. This is probably related to a transition from the β-phase to the mixed α+β phase just slightly below room temperature.This has to be investigated in more detail in the future, but if the change in K is really asso-

ciated with a phase transition an interesting field of further studies is opened up.

Fig. 12 displays the observed shifts corrected for a diamagnetic contribution of -20 ppm, as a function of hydrogen concentration. Indicated are also two points stemming from proton KS measurements by NMR [25]. Excellent agreement between the NMR and μSR data can be stated, indicating that isotope effects are only of minor importance. It appears that the KS in β-PdH_x rises linearly with the H-concentration. Also indicated in Fig. 12 is the temperature independent s-electron induced K_s obtained in pure Pd (see Tab. II). Since the d-band is completely filled in PdH_x for $x \gtrsim 0.6$ and falls below the Fermi energy it is tempting to trace the observed temperature independent μ^+ KS in β-PdH_x back to s-electrons too. Obviously then K_s is quite different in pure Pd and in its hydride. The Pauli spin susceptibility χ_s of the hydride is estimated to be 1.8×10^{-6} emu/cm^3 [26] which is much larger than the value estimated for pure Pd (see Tab Tab. II). Hence, one would have expected a much larger K_s in the β-hydride phase. On the other hand there is no indication that χ_s is dependent on x for $x \geqslant 0.70$ [26]. The x-dependence of K_s must therefore be of a different origin [25].

The situation becomes even more puzzling if one compares the Knight shift data with predicitions obtained from proton Korringa relaxation rate $(T_{1e} \times T)^{-1}$ measurements [27, 28, 29] by applying the Korringa relation. The predicted values are also displayed in Fig.12. There seems to be no x-dependence between x = 0.70 and 0.80, essentially in accordance with a constant χ_s. A remarkable discrepancy between the derived numbers and the measured shifts in PdH_x is apparent. These conflicting results can be reconciled if one postulates two x-dependent contributions K_1, K_2 cancelling partially in K_μ (and K_p) but adding constructively in the Korringa relaxation rate. However, no obvious interpretation of two contributions is at hand. Another possibility is to assume that an abnormally large and x-dependent diamagnetic shielding reduces the total Knight shift without affecting the Korringa relaxation rate. A required diamagnetic screening of the order of -65 ppm would point to a very peculiar electron distribution around the μ^+ or proton, which is not indicated so far by other measurements.

VI. Summary

What has been learned from the present μ^+ Knight shift studies about the local electronic structure of this hydrogenlike impurity? The conclusions may be summarized as follows:

a) hydrogen in simple, nontransition metals

A screened proton picture, underlying the spherical solid model calculations, provides an adequate model to explain the gross features of the observed KS systematics. In addition to scattering states bound states seem to be very important in producing a negative contribution to the KS which is essential in reproducing the data. The influence of the host neighbor potentials resulted in a further enhancement of the spectral density of the bound states on the expense of continuum scattering states. Implications on other properties like the heat of solution of hydrogen in these metals have still to be investigated theoretically. Lacking agreement in detail indicates that further refinements are necessary, perhaps by applying more realistic cluster or band structure calculations, including also the effect of lattice relaxation around the impurity.

The observation of anisotropies in the μ^+ KS, notably in Be, suggests that also non s-electron like states can contribute

to the local electronic structure in a non negligible way. This needs to be explored further in future experimental investigations as well as in theoretical studies. Unexplained is the drastic change of the μ^+ KS in Zn when trapped in a structural defect (probably a multivacancy cluster).

b) hydrogen in d-electron transition metals

The μ^+ KS studies in Ni, Pd and Pt show that d-electrons play an important role in the formation of the total spin density at the μ^+. This may be interpreted in various ways. The KKR-band structure calculations of Katayama et al. [21] suggest that this is the result of the formation of bonding states involving hybridized hydrogen 1s and host metal d-wave functions. This would support the covalent hydrogen model suggested for transition metal hydrides [30]. What is needed now are more calculations extended to Pd and Pt in order to understand also the observed trends in $B^{\Omega a}_{hf,d}$.

c) metal hydrides

The as yet incomplete measurements in β-PdH_x promise to elucidate various properties: (i) change of the local charge density at the μ^+ with the hydrogen concentration, (ii) possible influence of electrons from the fully occupied

d-band taking both the KS and T_{1e}-data into account, (iii) behavior of the local electronic structure at the boundary between different phases. We hope to have more on this by the time of the next conference on hydrogen in metals.

Acknowledgements

The experiments on PdH_x have been performed in collaboration with L. Schlapbach and his group. This work has been supported in part by the Schweizerisches Institut für Nuklearforschung, Villigen.

References

[1] see e.g. R.M. Cotts in Hydrogen in Metals, Vol. 1, Eds. G. Alefeld, J. Völkl (Springer Verlag, 1978).

[2] P. Jena, in Treatise on Materials Science and Technology, Vol. 21, p. 351 (Academic Press, 1981).

[3] E. Zaremba and D. Zobin, Phys. Rev. B22 (1980) 5490.

[4] A. Schenck, Helv. Phys. Acta 59 (1981) 471.

[5] A. Schenck in Electronic Structure and Properties of Hydrogen in Metals, Eds. P. Jena and C.B. Satterthwaite (Plenum Press, 1983).

[6] M. Camani et al., Phys. Rev. Lett. 42 (1979) 679.

[7] F.N. Gygax et al., Proceed. Yamada Conf. μSR (1983), Eds. T. Yamazaki, K. Nagamine (to be published in Hyperfine Interactions).

[8] W. Studer et al., loc. cit. ref. 7.

[9] W. Studer, thesis (ETH Zürich, 1983) unpublished.

[10] F.N. Gygax et al., Phys. Rev. Lett. 51 (1983) 505.

[11] W. Studer et al., loc.cit. ref. 7.

[12] O. Hartmann et al., Hyperfine Interactions 6 (1979) 47.

[13] J.H. Brewer et al., Solid State Communic. 46 (1983) 863.

[14] M. Manninen, Phys. Rev. B27 (1983) 53.

[15] G.G. Carter, L.H. Bennett, D.J. Kahan, Metallic Shifts in NMR, Part 1, Progr. Mat. Sci. Vol. 20 (Pergamon Press, 1977).

[16] W. Studer et al., to be published.

[17] R.V. Kasovski, Phys. Rev. 187 (1969) 891.

[18] F.N. Gygax et al., loc. cit. ref. 5, p. 407.

[19] R.M. Nieminen et al., loc.cit. ref. 7.

[20] F.N. Gygax et al., Proceed. Int. Conf. Hyperf. Interactions (Groningen, 1983), to be published in Hyperf. Interactions.

[21] H. Katayama et al., Solid State Communic. 29 (1979) 431.

[22] J.K. Norskov, Phys. Rev. B26 (1982) 2875.

[23] F.N. Gygax et al., in Recent Developments in Condensed Matter Physics, Vol. 2, Eds. J.T. Devreese et al., (Plenum Press, 1981).

[24] H. Frieske and E. Wicke, Ber. Bunsenges. Phys. Chem. 77 (1973) 48.

[25] P. Brill and J. Voitländer, Ber. Bunsenges. Phys. Chem. 77 (1973) 1097.

[26] H.C. Jamieson et al., J. Phys. F2 (1972) 323.

[27] G.K. Schoep et al., Physica 75 (1979) 297.

[28] D.A. Cornell et al., J. Less-Common Metals 39 (1975) 43.

[29] C.L. Wiley et al., Phys. Rev. B17 (1978) 3462.

[30] C.D. Gelatt et al., Phys. Rev. B17 (1978) 1940.

Figure captions

Figure 1

Semilogarithmic plot of the induced hyperfine field $B_{hf}^{\Omega a} = \mu_B \cdot K_s/\chi_{at}$ versus the molar electronic specific heat.

Figure 2

Partial wave decomposition of the electron density at the μ^+ at a tetrahedral site in Cs from spherical solid model calculations. The dotted dashed line is the electron density (spin up or down) from a nonpolarized jellium model [14].

Figure 3

Spherical solid model predictions for K_μ in monovalent metals versus the density parameter r_s [14].

Figure 4

Spherical solid model predictions for K_μ in divalent metals. The upper values are for μ^+ at the octahedral interstitial site, the lower ones at the tetrahedral site [14].

Figure 5

Comparison of spin density enhancement factors $\rho_s(o)$ from the spherical solid model calculation [14] and from the experimental KS values using experimental spin susceptibility data [4].

Figure 6

Angular dependence of K_μ in Be at 293 K. θ is the angle between the crystalline c-axis and the applied field [9].

Figure 7

Angular dependence of K_μ in Cd at 60 K and at 293 K. θ is the angle between the crystalline c-axis and the applied field [18].

Figure 8

Temperature dependence of K_μ in polycrystalline Cd [11].

Figure 9

Temperature dependence of the apparent K_μ in a single crystal sample of Zn [10].

Figure 10

Plot of K_μ versus magnetic susceptibility in Pt. Temperature is an implicit parameter [20].

Figure 11

Temperature range of K_μ measurements in PdH_x. K_μ is temperature independent except for x = 0.59.

Figure 12

Plot of K_s versus hydrogen concentration x in PdH_x. Indicated are also results from proton KS measurements [25] and calculated values (via the Korringa relation) from T_{1e}-relaxation data [27-29].

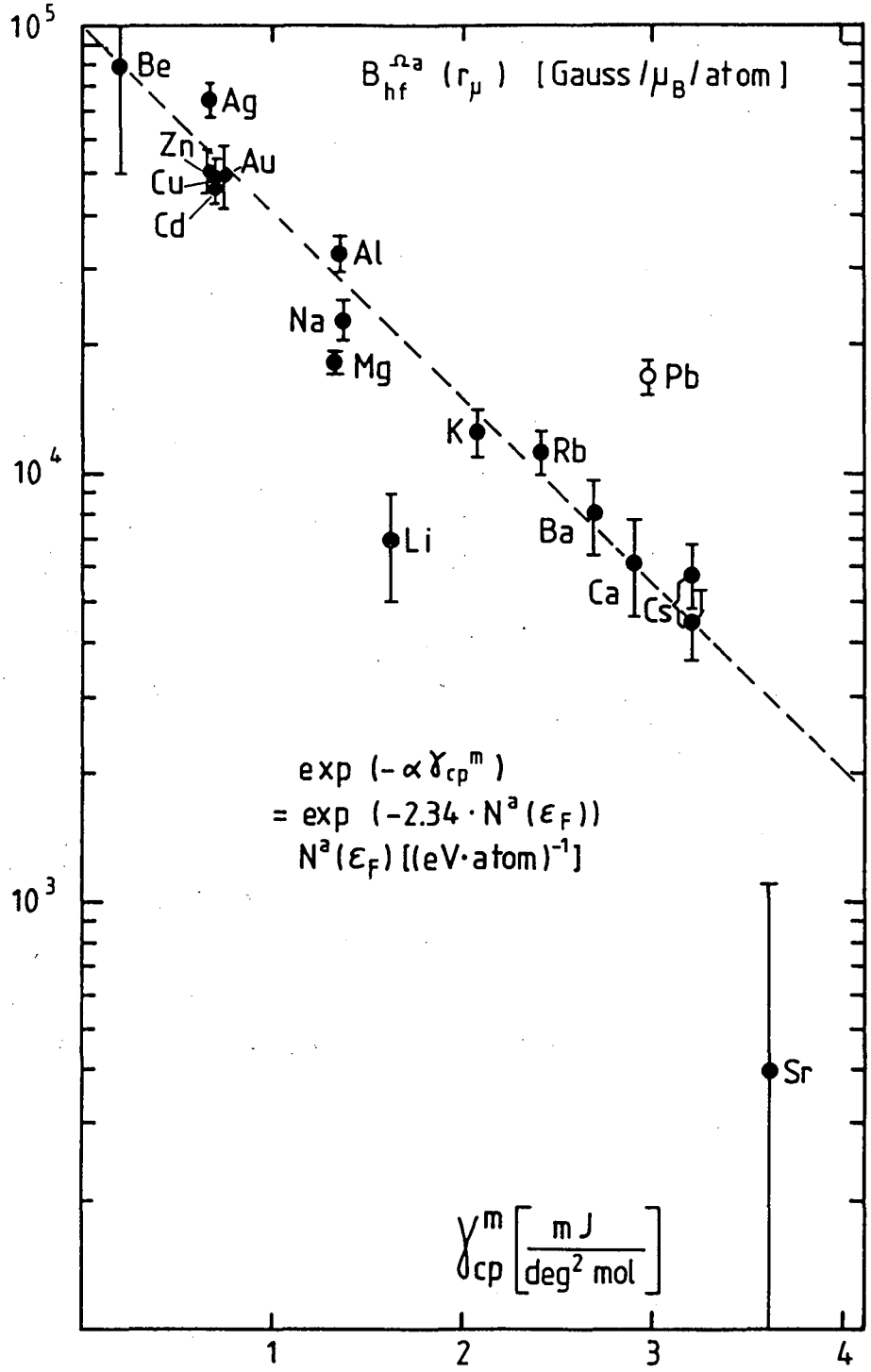
10^5
10^4
10^3
$B_{hf}^{\Omega a}(r_\mu)$ [Gauss/μ_B/atom]
Be
Ag
Zn
Au
Cu
Cd
Al
Na
Mg
Pb
K
Rb
Li
Ba
Ca
Cs
Sr
exp $(-\alpha \gamma_{cp}^m)$
= exp $(-2.34 \cdot N^a(\varepsilon_F))$
$N^a(\varepsilon_F)$ [(eV·atom)$^{-1}$]
$\gamma_{cp}^m \left[\frac{mJ}{deg^2\ mol}\right]$
1
2
3
4

Fig. 1

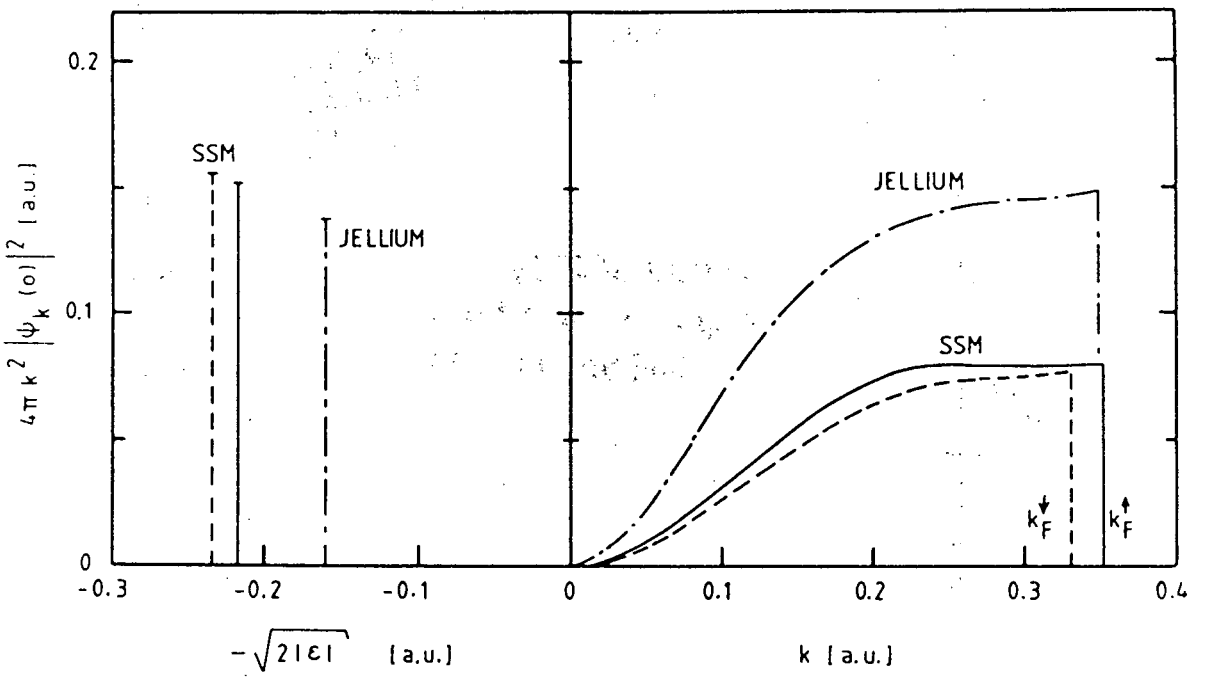
0.2
0.1
0
$4\pi k^2 |\psi_k(o)|^2$ [a.u.]
SSM
JELLIUM
JELLIUM
SSM
$k_F^{\downarrow}$
$k_F^{\uparrow}$
-0.3
-0.2
-0.1
0
0.1
0.2
0.3
0.4
$-\sqrt{2|\varepsilon|}$ [a.u.]
k [a.u.]

Fig. 2

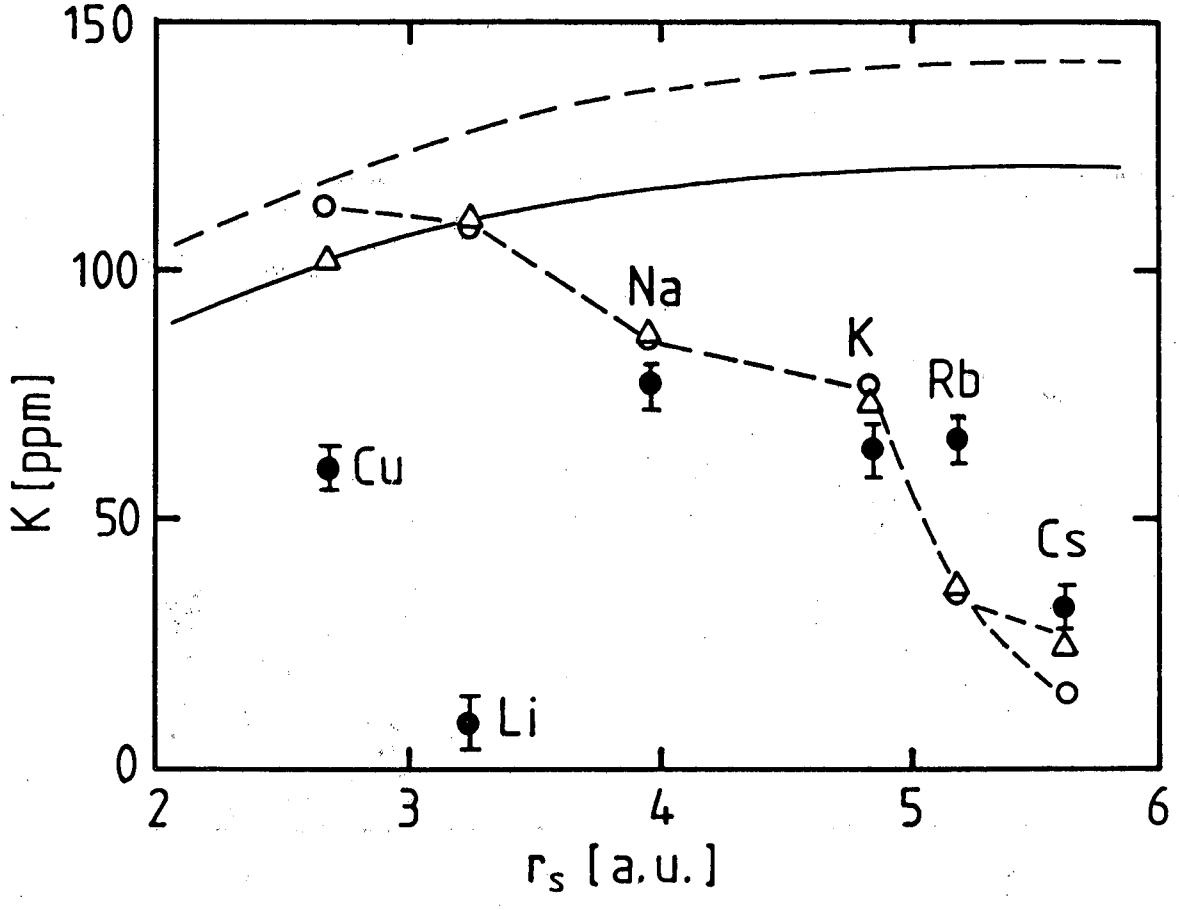

Fig. 3

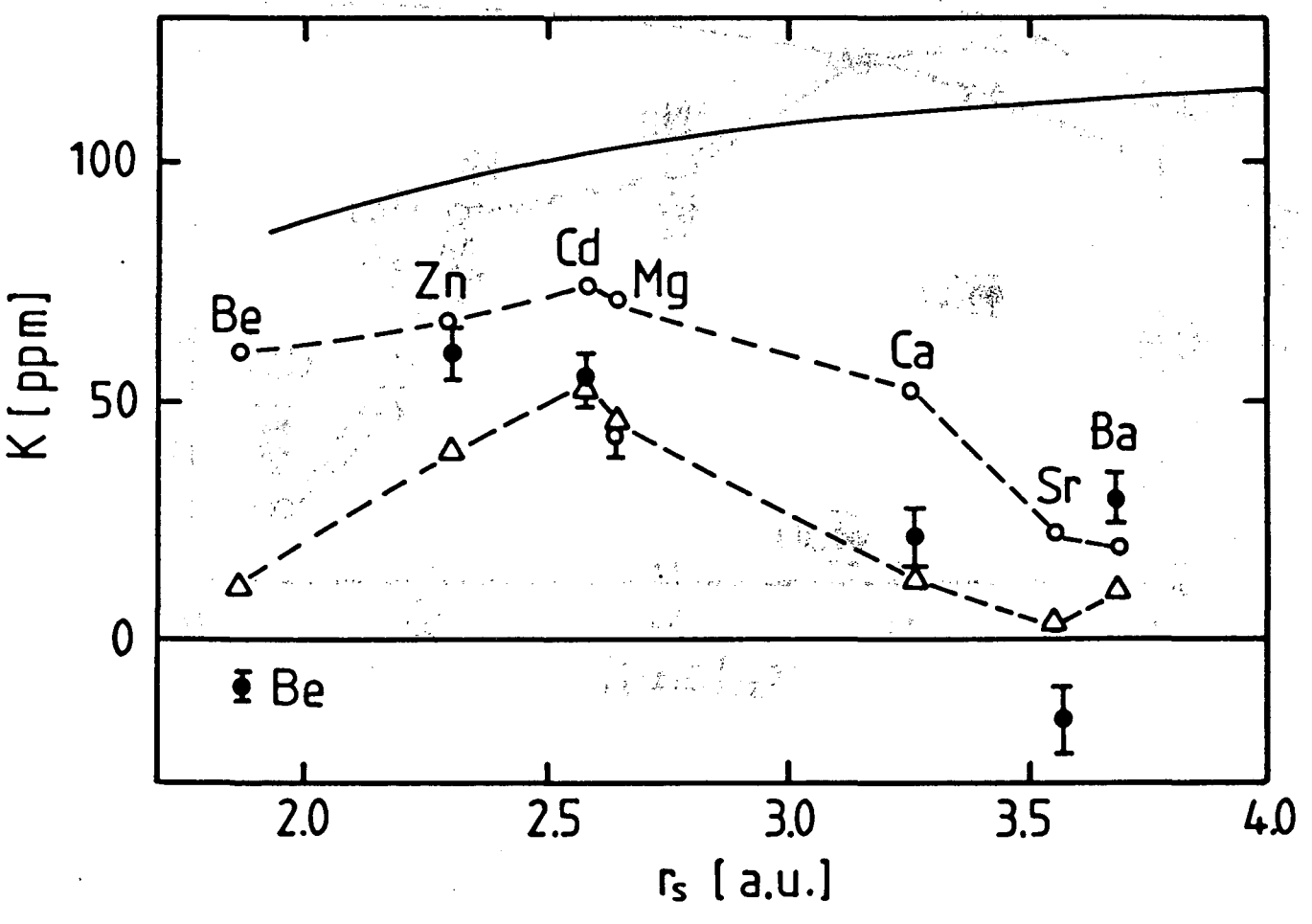

Fig. 4

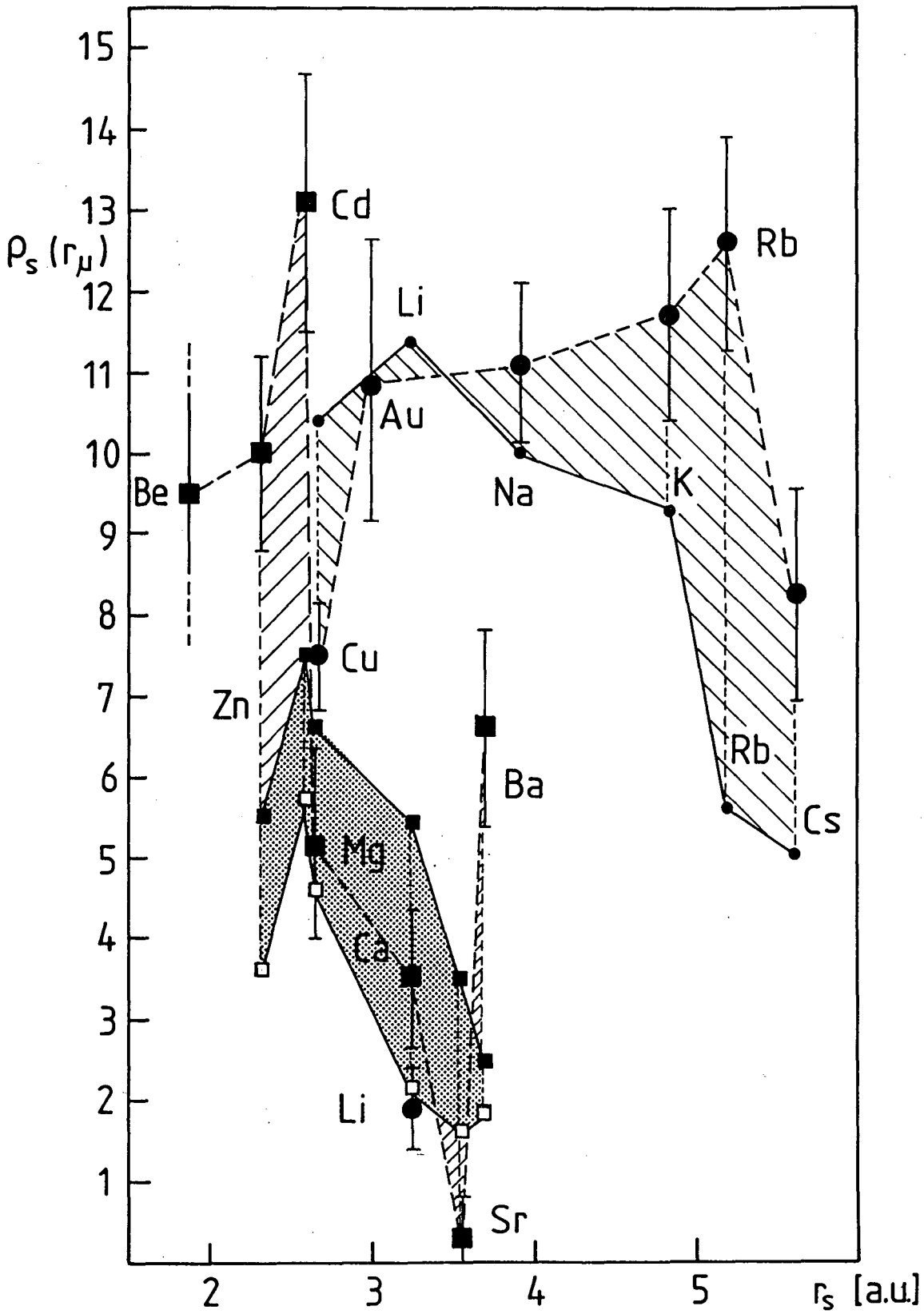
15
14
13
12
11
10
9
8
7
6
5
4
3
2
1
$\rho_s\,(r_\mu)$
Cd
Li
Au
Be
Na
K
Rb
Cu
Zn
Ba
Rb
Cs
Mg
Ca
Li
Sr
2
3
4
5
r_s [a.u.]

Fig. 5

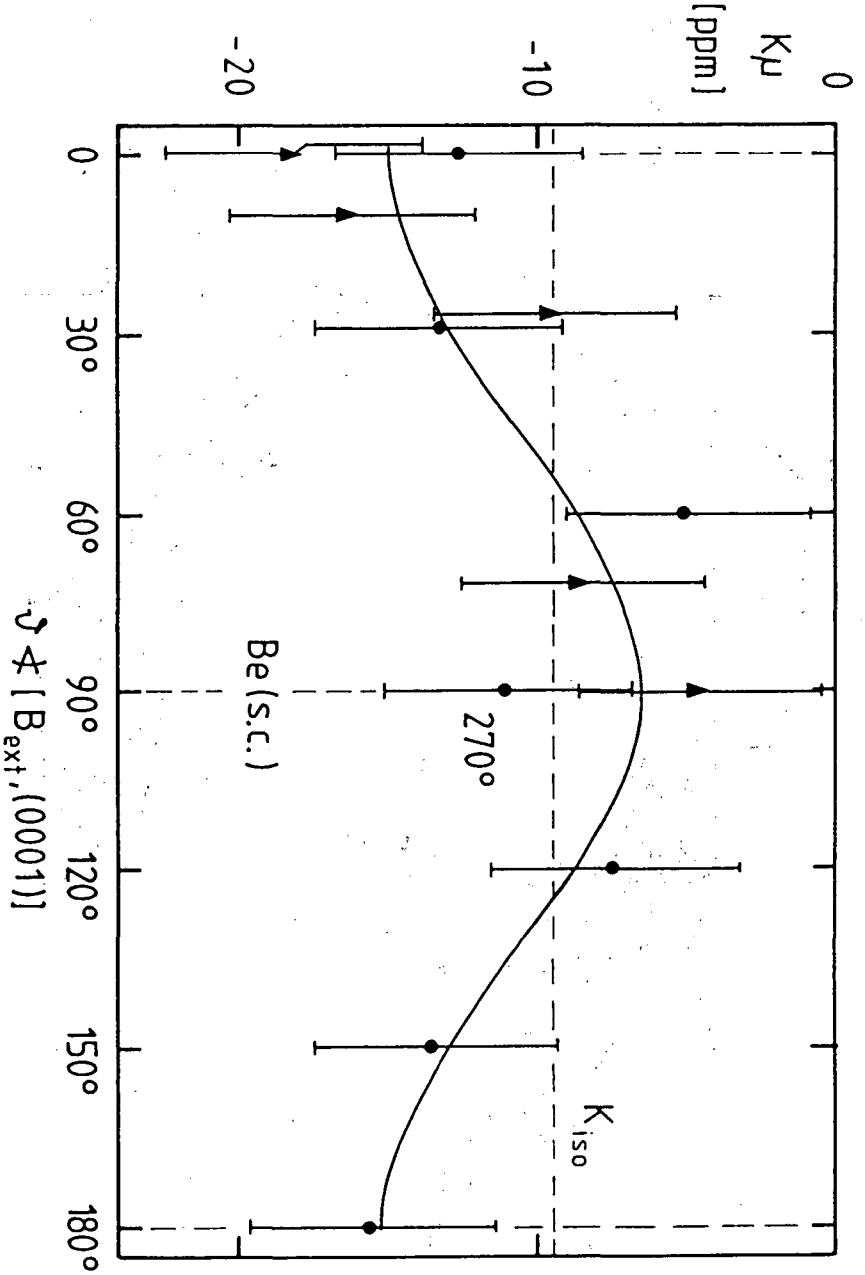

Fig. 6

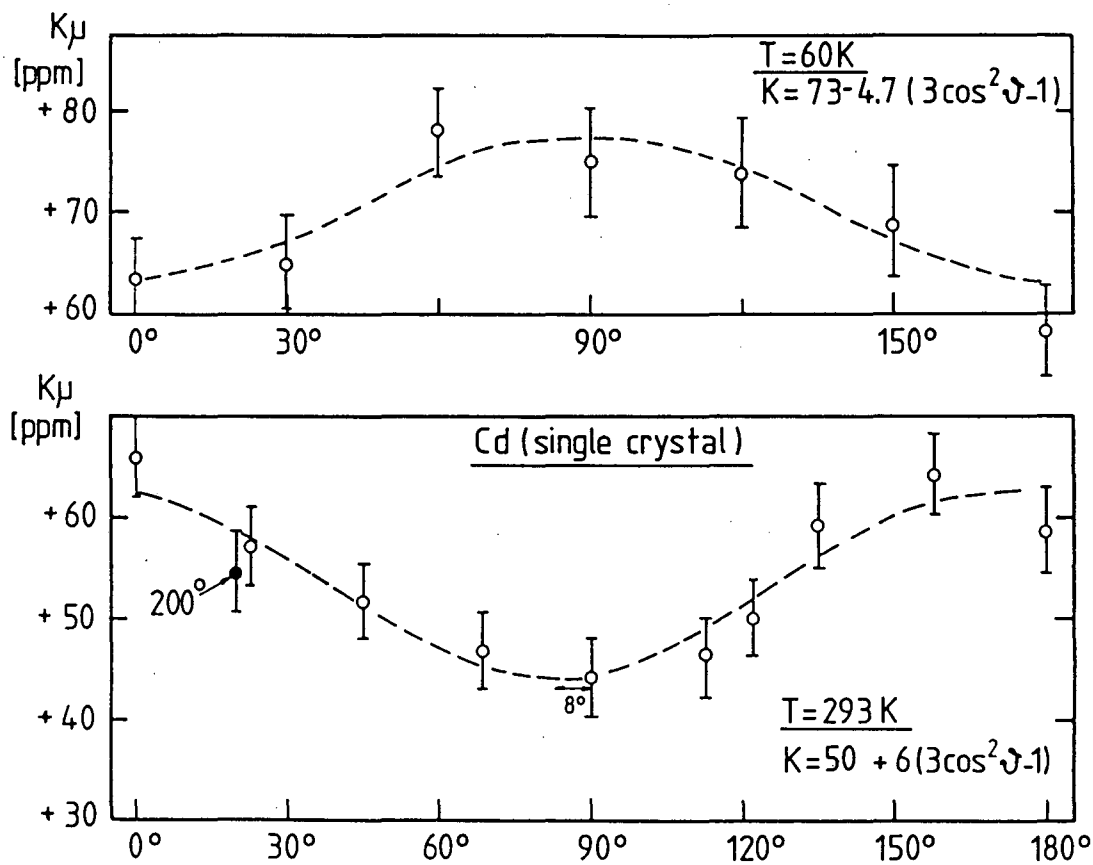
Kμ
[ppm]
+80
+70
+60
T=60K
K=73-4.7 (3cos²ϑ-1)
0°
30°
90°
150°
Kμ
[ppm]
Cd (single crystal)
+60
+50
+40
+30
200°
8°
T=293 K
K=50 +6(3cos²ϑ-1)
0°
30°
60°
90°
120°
150°
180°

Fig. 7

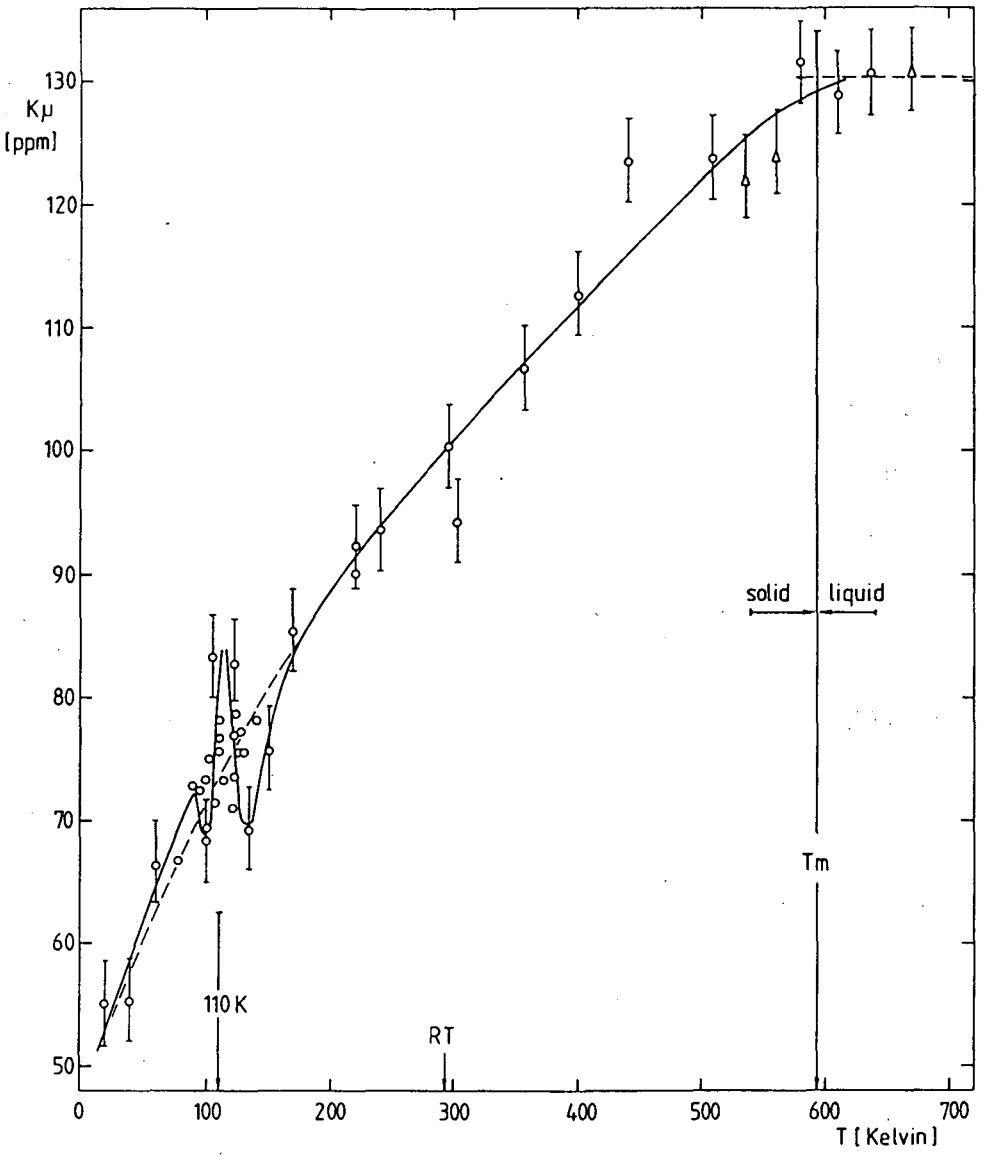
130
Kμ
[ppm]
120
110
100
90
80
70
60
50
0
100
200
300
400
500
600
700
T [Kelvin]
solid
liquid
Tm
110 K
RT

Fig. 8

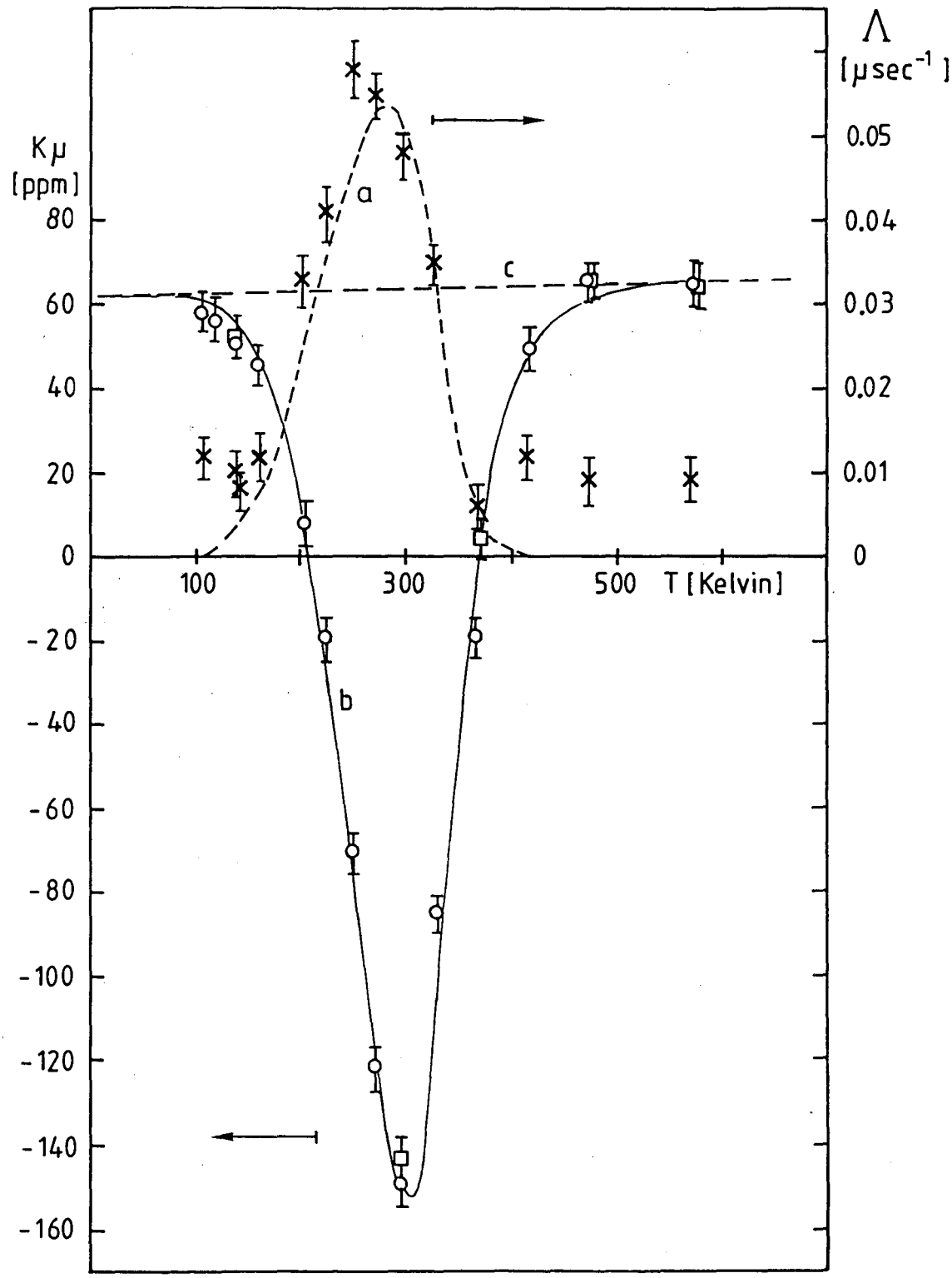
Λ
[μsec⁻¹]
Kμ
[ppm]
80
60
40
20
0
-20
-40
-60
-80
-100
-120
-140
-160
0.05
0.04
0.03
0.02
0.01
0
100
300
500
T [Kelvin]
a
b
c

Fig. 9

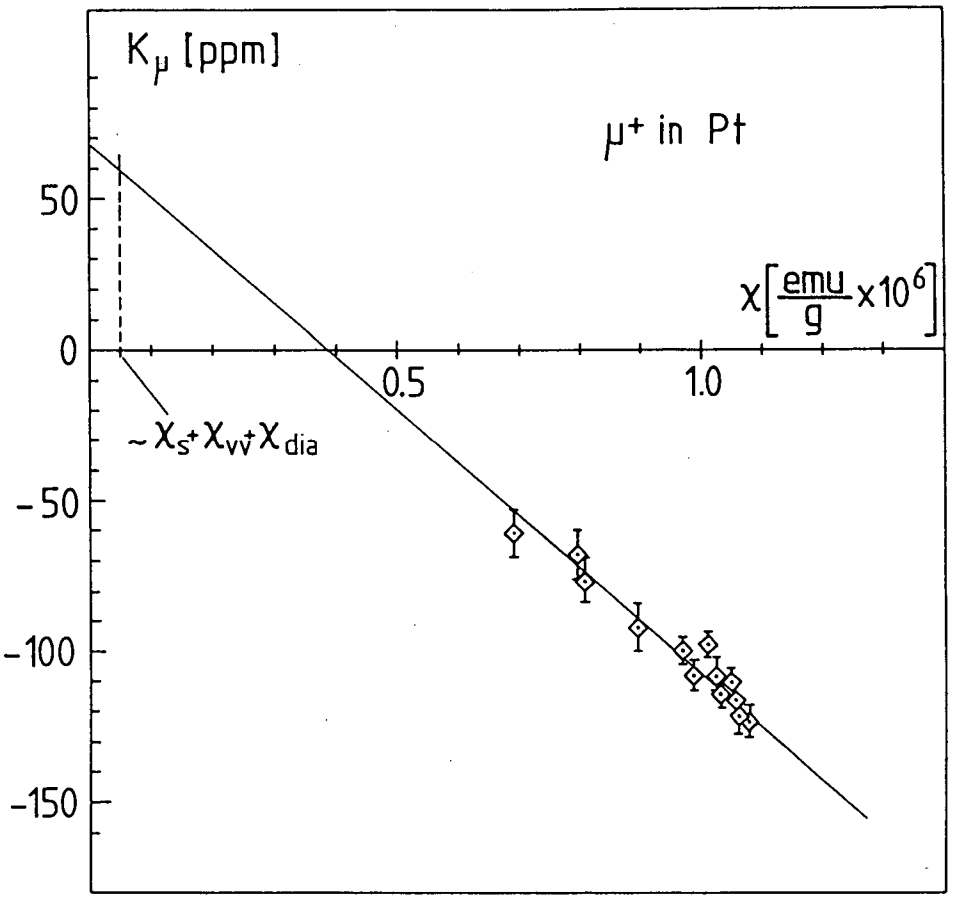
K_μ [ppm]
μ^+ in Pt
50
0
-50
-100
-150
0.5
1.0
$\chi\left[\frac{emu}{g} \times 10^6\right]$
$\sim \chi_s + \chi_{vv} + \chi_{dia}$

Fig. 10

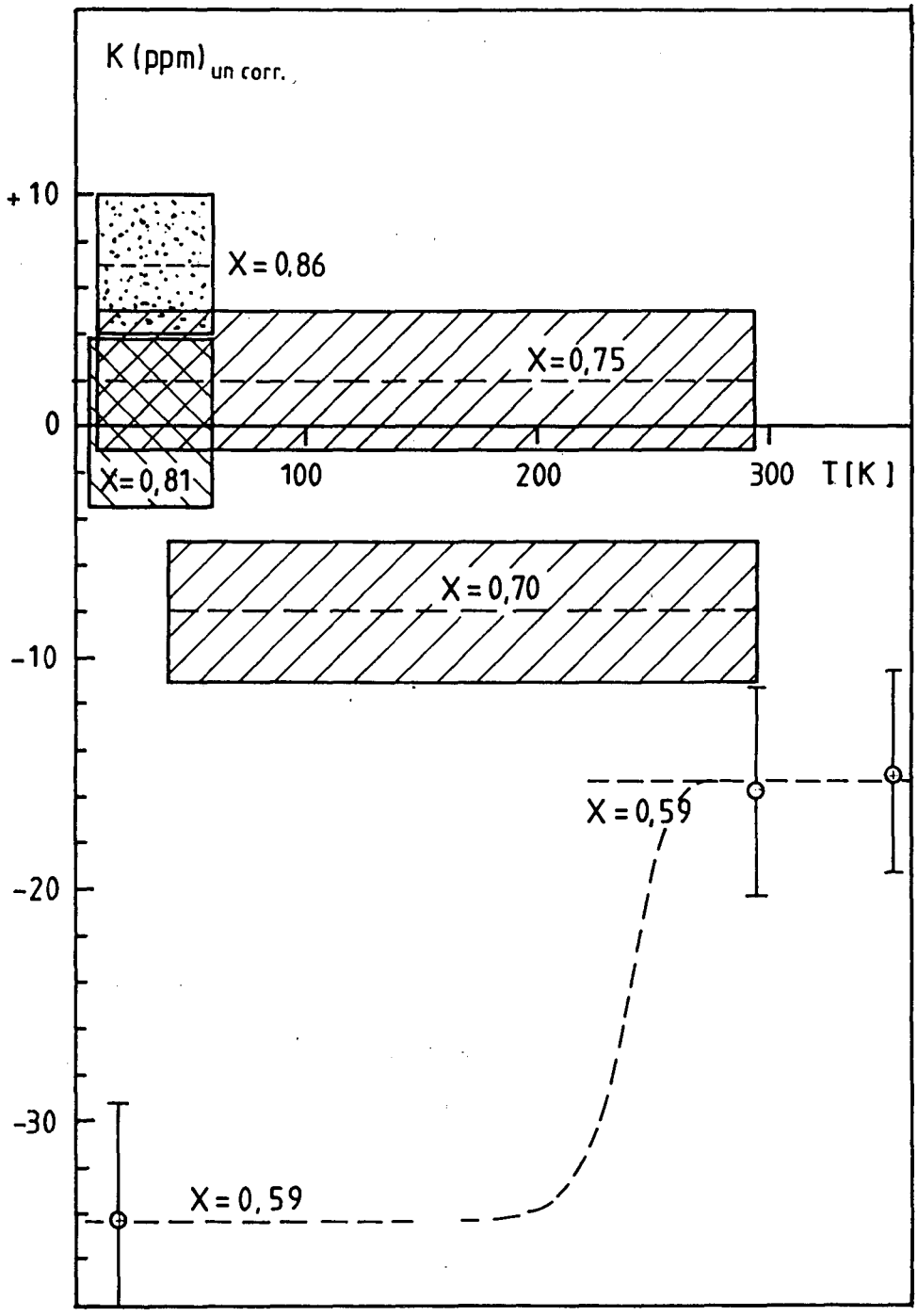
K (ppm) un corr.
+10
0
-10
-20
-30
X = 0,86
X = 0,75
X = 0,81
X = 0,70
X = 0,59
X = 0,59
100
200
300
T [K]

Fig. 11

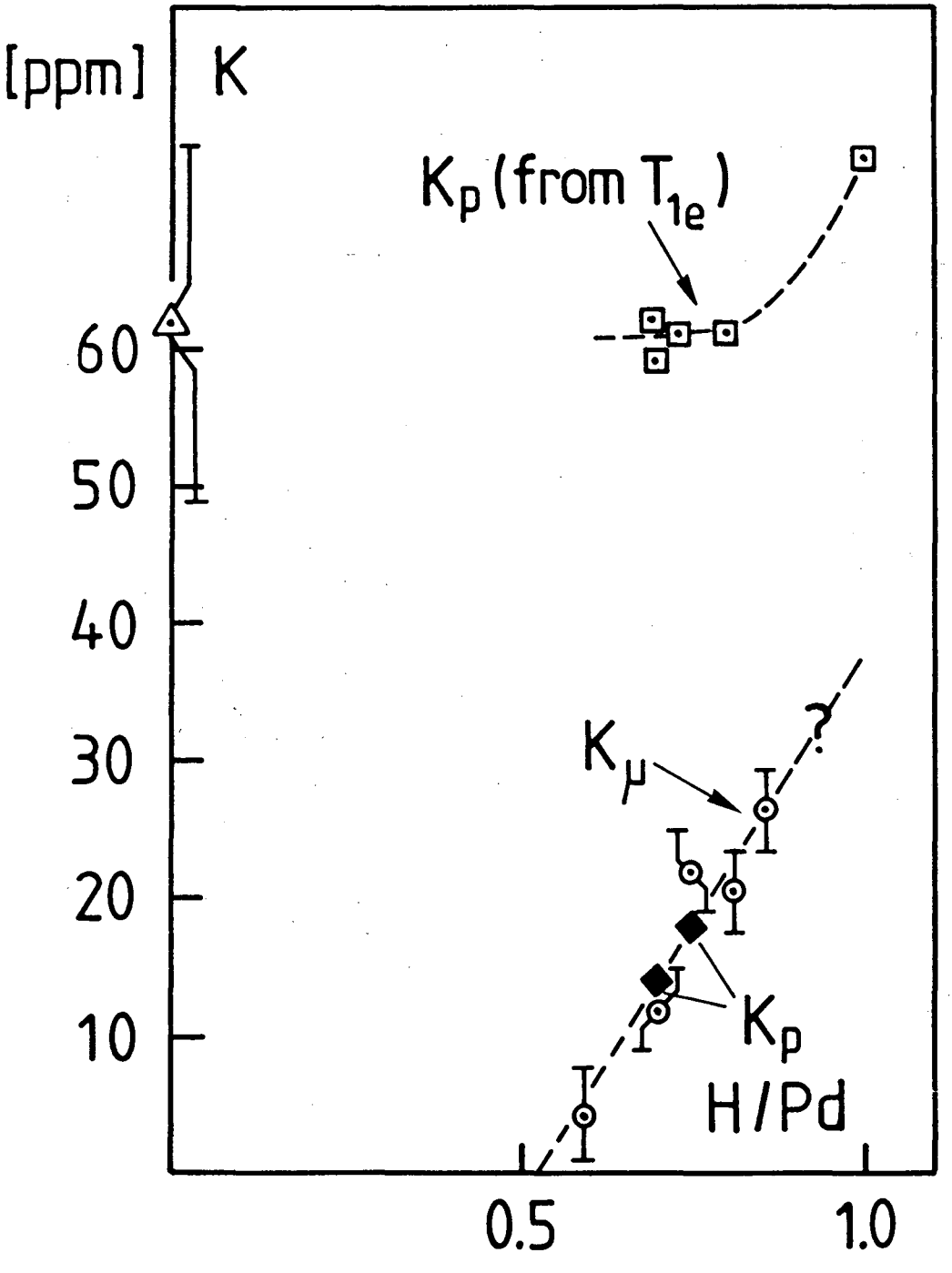

Fig. 12

Quantum Diffusion of Positive Muons in Iron

E. Yagi[(a)], G. Flik, K. Fürderer, N. Haas, D. Herlach,
J. Major[(b)], and A. Seeger

Universität Stuttgart, Institut für Theoretische und Angewandte Physik,
and Max-Planck-Institut für Metallforschung, Institut für Physik,
Postfach 800665, D-7000 Stuttgart, Germany

and

W. Jacobs, M. Krause, M. Krauth, H.-J. Mundinger, and H. Orth

Physikalisches Institut der Universität Heidelberg, D-6900 Heidelberg 1,
Germany

(Received 1983)

The longitudinal muon-spin relaxation rate Γ_1 of a spherical α-iron single crystal in an applied magnetic field of 4.5 T parallel to <111> shows a maximum at T = 3.7 K. Near the maximum $\Gamma_1(T)$ is in agreement with a muon diffusivity D^{μ^+} proportional to the temperature T and hence with one-phonon-assisted tunnelling. The results strongly support the view that the stable muon site is the tetrahedral interstice. Below about 3 K evidence for metastable occupancy of a second type of site has been found.

PACS numbers: 66.30.Jt, 76.60.Jx, 76.90.+d

The study of the diffusivity D^{μ^+} of positive muons (μ^+) in metals has been one of the main incentives for the development of the theory of quantum diffusion in crystals and, at the same time, its main testing ground.[1] The longitudinal spin relaxation of μ^+ in α-Fe is particularly well suited for quantitative studies of $D^{\mu^+}(T)$.[2-4] Measurements of the longitudinal relaxation rate Γ_1 are insensitive against trapping effects due to impurities or other imperfections[5] and hence superior to transverse relaxation

measurements. In studying α-Fe we take advantage of its ferromagnetism and the lower-than-cubic point symmetry of its interstices. This leads to strong dipolar magnetic fields $\vec{B}_{dip}$ acting on the magnetic moments of the μ^+ located on interstitial sites. When the μ^+ diffuse by jumping between neighbouring interstices, the dipolar fields felt by the μ^+ magnetic moments change. Provided the applied magnetic field $\vec{B}_{appl}$ is chosen appropriately, this affects the muon polarization so strongly that Γ_1 can be determined over a very wide temperature range.

In the body-centred cubic (bcc) structure of α-Fe the interstitial sites most likely to be occupied by μ^+, the tetrahedral (T) and octahedral (O) interstices, possess tetragonal point symmetry. In the demagnetized state the local magnetization $\vec{M}_{domain}$ is parallel to <100>. The dipolar fields at O or T sites[6] are then parallel to $\vec{M}_{domain}$, so that $\Gamma_1 \equiv 0$. Consequently, the longitudinal relaxation measurements must be carried out on single crystals with $\vec{M}_{domain}$ rotated away from <100> by a suitably oriented and sufficiently strong external field $\vec{B}_{appl}$.

A complete theory of spin relaxation due to the hopping motion of μ^+ between the above-mentioned sites in ferromagnets has been worked out by Seeger and Monachesi[7]. If a single correlation time $\tau_c = \tau_c(T)$ suffices to describe the μ^+ diffusion, Γ_1 is given by

$$\Gamma_1 = 2\hat{\Gamma}_1\tau_c/\hat{\tau}_c(1+\omega_\mu^2\tau_c^2) \quad , \qquad (1)$$

where $\hbar\omega_\mu$ denotes the Zeeman splitting of the μ^+ spin levels. Due to the compensation of the Lorentz field $B_{LORENTZ} = \mu_o M_{sp}/3$ (M_{sp} = spontaneous magnetization) and the demagnetizing field, for magnetically saturated spherical samples

$$\omega_\mu \equiv \gamma_\mu B_\mu = \gamma_\mu (B_{appl} + B_{FERMI}) \qquad (2)$$

holds ($\gamma_\mu = 8.561 \cdot 10^8$ rad $s^{-1}T^{-1}$ = gyromagnetic ratio of the muon, $\vec{B}_{FERMI}$ = contact field due to the spin polarization of the conduction electrons). According to Eq.(1), Γ_1 shows a maximum $\hat{\Gamma}_1$ at that temperature $\hat{T}$ at which

$$\omega_\mu \tau_c(\hat{T}) \equiv \omega_\mu \hat{\tau}_c = 1 \quad . \qquad (3)$$

$\hat{\Gamma}_1$ depends on the crystallographic orientation of $\vec{B}_{appl}$ and assumes its maximum value

$$\hat{\Gamma}_1^{<111>} = \frac{1}{4}(\gamma_\mu B_{dip}^{\parallel})^2 \hat{\tau}_c \qquad (4)$$

for $\vec{B}_{appl}$ along <111>. If ω_μ is known, we may use Eqs.(3) and (4) to deduce $|B_{dip}^{\parallel}|$, which is characteristic of the sites occupied by the muons.

According to Teichler, Seeger and Schmidt[8,9], in bcc metals the low-temperature muon hopping should be governed by one-phonon incoherent tunnelling processes. This mechanism yields $D^{\mu^+} \propto T$ and hence

$$\tau_c = \beta\, T^{-1} \quad , \qquad (5)$$

where β is a constant determined by the muon-phonon interaction. Insertion of Eq.(5) into Eq.(1) gives us, together with Eq.(4),

$$1/T\Gamma_1^{<111>} = A + B/T^2 \quad , \quad T/\Gamma_1^{<111>} = B + AT^2 \qquad (6a,b)$$

with $A = 2/\beta(\gamma_\mu B_{dip}^{\parallel})^2$ and $B = 2\beta(\omega_\mu/\gamma_\mu B_{dip}^{\parallel})^2$.

At SIN, Villigen, Switzerland, we have measured $\underline{\Gamma}_1$ on a spherical α-Fe crystal[10] in the ranges 300 K $\geq \underline{T} \geq$ 0.85 K and 4.9 T $\geq \underline{B}_{appl} \geq$ 1.2 T. For the lowest temperatures, the apparatus[5,11] was equipped with a large-impedance ^{3}He evaporation cryostat. Operated with ^{4}He as cryogenic fluid, the base temperature measured with a Ge resistor at $\underline{B}_{appl}$ = 0 was 0.85 K. The Ge resistor and a carbon glass sensor were calibrated between 8.3 K and 0.85 K in applied fields 2.0 T $\leq \underline{B}_{appl} \leq$ 4.5 T, using a $SrTiO_3$ capacitor for temperature control.

From measurements between 300 K and 4 K the following conclusions relevant for the present work have been drawn[5,12,13].

(i) The dependence of $\underline{\Gamma}_1$ on the crystallographic direction of $\vec{\underline{B}}_{appl}$ is in excellent agreement with exclusive occupancy of sites of tetragonal symmetry down to 6 K, the lowest temperature at which the orientation dependence of $\underline{\Gamma}_1$ was investigated.

(ii) Height and position of the maximum of $\underline{\Gamma}_1(\underline{T})$ at 32 K (Fig.1) are field-independent between 1.2 T $\leq \underline{B}_{appl} \leq$ 4.9 T; hence it cannot be the maximum associated with (3). It is attributed to a transition from exclusive occupancy of T sites below about 15 K to a thermal-equilibrium distribution of μ^+ on T and O sites at high temperatures .

(iii) Below about 20 K the dependence of $\underline{\Gamma}_1$ on $\underline{B}_{appl}$ becomes noticeable (Fig.1), indicating that we might be approaching the maximum associated with (3).

Fig.1 shows longitudinal relaxation rates $\Gamma_1^{<111>}$ recently determined between 8.3 K and 0.85 K by fitting single exponentials to the measured relaxation functions at times $\geq$ 60 ns after μ^+ implantation (full symbols) together with the earlier results[5,12]

(open symbols and crosses). The data at B_{appl} = 4.5 T satisfy (6) quite well (Fig.2), indicating that the maximum $\hat{\Gamma}_1^{<111>} = 7.5 \cdot 10^6\ s^{-1}$ at $\hat{T}$ = 3.7 K is indeed the maximum predicted by (1) at $\omega_\mu \tau_c = 1$. The dashed lines in Fig.1 represent the fit of Fig.2 for B_{appl} = 4.5 T and the corresponding curve for B_{appl} = 2.0 T as calculated from (1) and (2) with the same parameters and B_{FERMI} = -1.126 T.

The deduction of B_{FERMI} (required in order to obtain ω_μ, $\hat{\tau}_c = \omega_\mu^{-1}$ and, with Eq.(4), $(B_{dip}^{\parallel})^2$) from the spin precession frequency in zero applied field,

$$\omega_\mu^o = \gamma_\mu (B_{LORENTZ} + B_{FERMI}) \quad , \qquad (7)$$

needs some discussion. The temperature dependence of $|\omega_\mu^o|$ [14] (inset of Fig.1) shows a kink at about 6 K, for which a satisfactory interpretation has not been given. For the main conclusions of the present paper it is irrelevant whether the full-line or the dashed-line extrapolation (both linear in T) of ω_μ^o is used since the uncertainty in ω_μ is not more than ±0.2%. A convincing explanation for the kink is, nevertheless, desirable. The following proposal ties together several observations in the present experiments.

In accordance with (i) and (ii) we take the full line in the inset of Fig.1 as representing the muon spin precession frequency ω_μ^T at T sites. The extrapolation to low temperatures gives us $|\omega_\mu^T| = 3.28 \cdot 10^8$ rad s^{-1} and, together with $\mu_o M_{sp}$ = 2.222 T and the fact[15] that the direction of $\vec{B}_{LORENTZ} + \vec{B}_{FERMI}$ is opposite to $\vec{M}_{domain}$, B_{FERMI}^T = -1.126 T. The deviation of the experimental data from this extrapolation is attributed to the occupancy,

increasing with decreasing temperature, of octahedral sites in addition to tetrahedral sites. The implication that μ^+ at O sites are metastable with respect to T-site occupancy is compatible with (ii). If for an order-of-magnitude estimate we assume that at T = 0 the probability of occupation is the same for both types of site, we find $\underline{B}_{FERMI} \approx -1.175$ T.

Insertion of $\underline{B}^T_{FERMI}$ into Eq.(2) gives us, at $\underline{B}_{appl} = 4.5$ T, $\underline{\omega}_\mu = 28.7 \cdot 10^8$ rad s^{-1}, hence from Eq.(3) $\hat{\underline{\tau}}_c = \underline{\tau}_c(3.7\ K) = 3.5 \cdot 10^{-10}$s, and from Eq.(5) $\underline{\beta} = 13 \cdot 10^{-10}$s K. From Eq.(4) we find $|B^{\parallel}_{dip}| = 0.34$ T. The interpretation of the latter value as $|\underline{B}^T_{dip}|$ is consistent with our earlier conclusion[5] and with footnote[6].

Two results of our experiments have not yet been discussed:

(a) At short times the majority of the measured relaxation functions deviate strongly from a single exponential. At first sight, this effect, which is not due to experimental inadequacies, is very surprising, since under quite general assumptions[2,7] the longitudinal relaxation function of a spin-1/2 system in contact with a heat bath should be exponential. The observed deviations point strongly towards metastability effects.

(b) Below about 5 K the longitudinal relaxation rates measured at 2 T deviate strongly from $\underline{\Gamma}_1^{<111>}(\underline{T})$ as deduced above (Fig.1).

Both phenomena are accounted for by the model proposed for the interpretation of $\underline{\omega}^O_\mu(\underline{T})$. Immediately after their implantation, μ^+ occupy both T sites (stable) and O sites (metastable). The long-time longitudinal relaxation is always describable by a single exponential, i.e. by a relaxation rate constant. This constant (plotted in Fig.1) is given by $\underline{\Gamma}_1^{<111>}$ or the transition rate from octahedral to tetrahedral sites (equal to $4\underline{\nu}_{OT}$ in the notation of ref.7), depending on which one is smaller. At $\underline{B}_{appl} = 4.5$ T

(corresponding to B_μ = 3.37 T) this is $\Gamma_1^{<111>}$ over the entire temperature range investigated, whereas at B_{appl} = 2.0 T (B_μ = 0.87 T) a cross-over takes place between 2 K and 3 K. Hence below about 5 K the 2 T rates plotted in Fig.1 are only lower limits to $\Gamma_1^{<111>}$.

As a result of the present work, the following conclusions may be added to (i)-(iii) and those of[12]:

(iv) The maximum predicted by (1) at $\omega_\mu \tau_c = 1$ has been found. From its temperature and height one may conclude that under equilibrium conditions at low temperatures positive muons in α-Fe occupy tetrahedral and not octahedral interstices. The dipolar field felt by the μ^+ in tetrahedral interstices with tetragonal axis parallel to the magnetization is given by B_{dip}^T = -0.34 T.

(v) Between 0.85 K and 12 K the μ^+ jump frequency between tetrahedral interstices is proportional to the absolute temperature T; the diffusivity in this range is given by

$$D^{\mu^+}(T) = a_o^2/72\,\tau_c = 8.7\cdot 10^{-13}\,T\ m^2 s^{-1} K^{-1} \qquad (8)$$

($a_o = 2.85\cdot 10^{-10}$ m = edge length of the elementary cube). The linear temperature variation constitutes strong evidence for incoherent tunnelling by one-phonon processes.

(vi) Evidence has been found that immediately after implantation into α-Fe a certain fraction of the μ^+ occupy metastable sites.

This work was financially supported by the Bundesminister für Forschung und Technologie, Bonn. Discussions with Dr. L. Schimmele, the technical assistance of M. Krenke, and the support of SIN are gratefully acknowledged.

[a] Alexander von Humboldt scholar 1978-80; permanent address: RIKAGAGKU KENKYUSHO, The Institute of Physical and Chemical Research, HIROSAWA, WAKO-SHI, SAITAMA, JAPAN.

[b] permanent address: Hungarian Academy of Sciences, Research Institute for Technical Physics, BUDAPEST, HUNGARY.

[1] For up-to-date references see Proc. Yamada Conference on Muon Spin Rotation and Associated Problems, Shimoda, Japan, Hyperf. Int. 17/18/19 (1984)

[2] A. Seeger, in: Hydrogen in Metals I, edited by G. Alefeld and J. Völkl (Springer, Berlin-Heidelberg-New York, 1978), p.349

[3] D. Herlach, H. Metz, A. Seeger, E. Yagi, K.-P. Arnold, M. Gladisch, W. Jacobs, H. Orth, G. zu Putlitz, and J. Vetter, Research Proposal RA-78-02.1, SIN, Villigen, 1978

[4] Yu. M. Belousov, V.N. Gorelkin, A.L. Mikaélyan, V. Yu. Miloserdin, and V.P. Smilga, Sov. Phys.-Usp. 22, 679 (1979)

[5] E. Yagi, H. Bossy, K.-P. Döring, M. Gladisch, D. Herlach, H. Matsui, H. Orth, G. zu Putlitz, A. Seeger, and J. Vetter, Hyperf. Int. 8, 553 (1981)

[6] Throughout this paper, the magnitude $\underline{B}^{\parallel}_{dip}$ of these fields at the μ^+ sites with tetragonal axes parallel to $\vec{\underline{M}}_{domain}$ is used as a measure of $\underline{B}_{dip}$. For ideal α-Fe crystals (i.e., in the absence of μ^+) the $\underline{B}^{\parallel}_{dip}$ values are known[2] as $\underline{B}^{O}_{dip}$ = 1.86 T and $\underline{B}^{T}$ = -0.522 T, respectively. (As a convention[7], ± signs are used for fields parallel or antiparallel to $\vec{\underline{M}}_{domain}$.) On theoretical grounds, we expect that for occupied sites the absolute magnitudes of the dipolar fields are smaller than but not radically different from the values just quoted, so that $(\underline{B}^{O}_{dip})^2 >> (\underline{B}^{T}_{dip})^2$ should continue to hold.

[7] A. Seeger and P. Monachesi, Phil.Mag. B46, 283 (1982)

[8] H. Teichler and A. Seeger, Phys.Lett. 82A, 91 (1981)

[9] A. Seeger and C. Schmidt, to be published

[10] K. Lubitz and G. Göltz, Appl.Phys. 19, 237(1979)

[11] K. Maier and A. Seeger, in Electronic Structure and Properties of Hydrogen in Metals, edited by P. Jena and C.B. Satterthwaite (Plenum, New York, 1983), p. 601

[12] M. Krauth, Diploma thesis, Universität Heidelberg, 1983

[13] For further conclusions, see A. Seeger, Hyperf. Int. 17/18/19 (1984) 987

[14] H. Graf, G. Balzer, E. Recknagel, A. Weidinger, and R.Y. Grynszpan, Phys.Rev.Lett. 44, 1333 (1980)

[15] I.I. Gurevich, A.I. Klimov, V.N. Maĭorov, E.A. Meleshko, B.A. Nikol'skiĭ, V.I. Selivanov, and V.A. Suetin, Sov.Phys.-JETP 42, 222 (1976)

Figure captions

Fig.1 Longitudinal μ^+-spin relaxation rates in a spherical α-Fe monocrystal at various applied magnetic fields $\vec{B}_{appl}$ parallel to <111>. Open symbols and crosses: earlier measurements[5,12] Full symbols: present data. Inset: μ^+ precession frequency in demagnetized Fe[14]. The lines represent fits described in the text.

Fig.2 $(T\Gamma_1)^{-1}-T^{-2}$ and T/Γ_1-T^2 plots of the long-time ($t \geq 60$ ns) relaxation rates at $\vec{B}_{appl}$ = 4.5 T parallel to <111>.

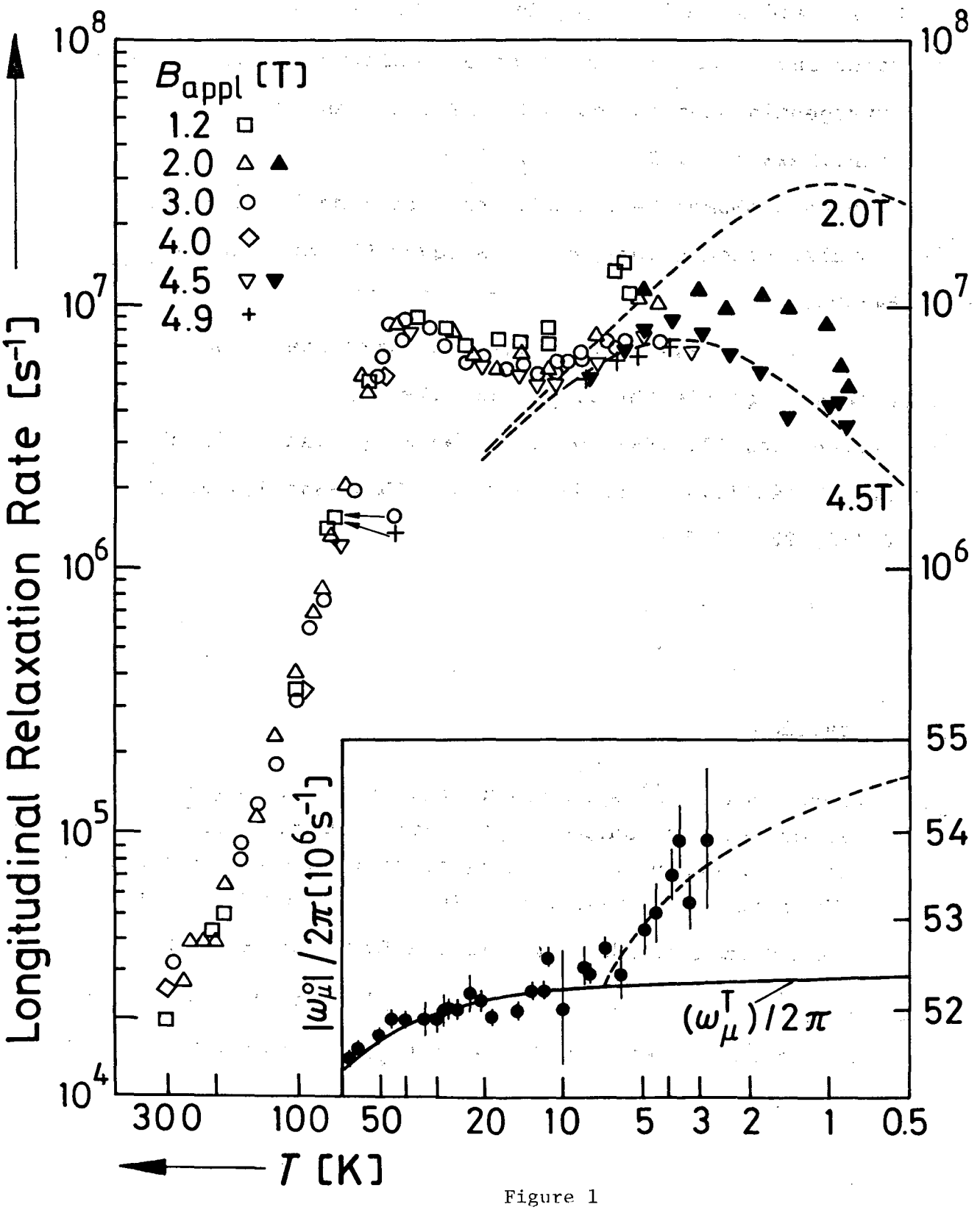
B_{appl} [T]
1.2
2.0
3.0
4.0
4.5
4.9
2.0T
4.5T
Longitudinal Relaxation Rate [s^{-1}]
10^8
10^7
10^6
10^5
10^4
$|\omega_\mu^0| / 2\pi$ [10^6s^{-1}]
55
54
53
52
$(\omega_\mu^T)/2\pi$
300
100
50
20
10
5
3
2
1
0.5
T [K]

Figure 1

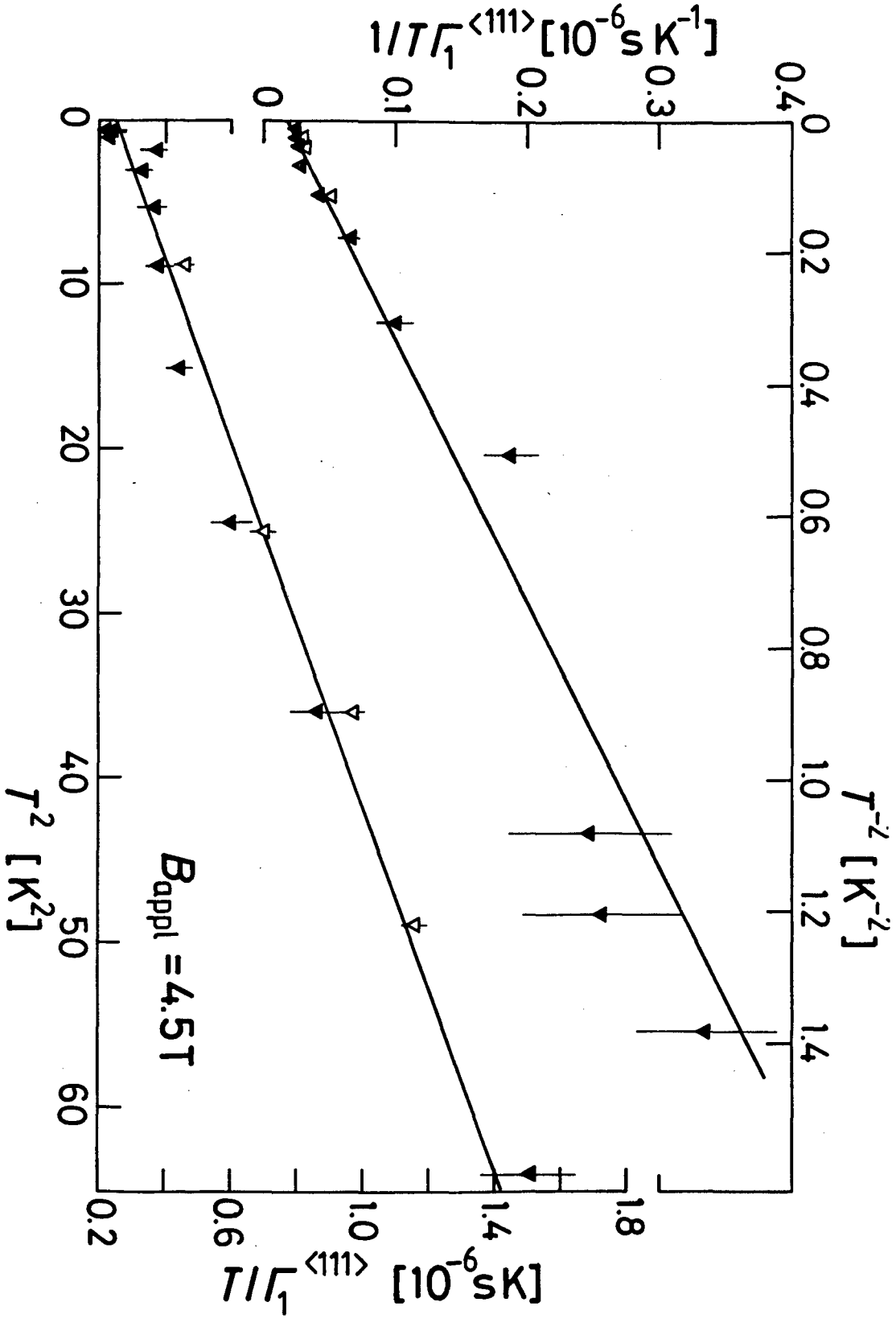
$1/T\Gamma_1^{\langle 111\rangle}$ [10^{-6}s K^{-1}]
0.4
0.3
0.2
0.1
0
T^{-2} [K^{-2}]
0
0.2
0.4
0.6
0.8
1.0
1.2
1.4
$T/\Gamma_1^{\langle 111\rangle}$ [10^{-6}sK]
0.2
0.6
1.0
1.4
1.8
T^2 [K^2]
0
10
20
30
40
50
60
B_{appl} = 4.5T

Figure 2

A COMPARISON OF SPIN-GLASS DYNAMICS DETERMINED BY THE MUON-SPIN RELAXATION AND NEUTRON SPIN-ECHO TECHNIQUES

R. H. Heffner

Los Alamos National Laboratory, Los Alamos, New Mexico 87545

D. E. MacLaughlin

Dept. of Physics, University of California, Riverside, California 92521

ABSTRACT

Impurity-spin correlation functions obtained from muon-spin relaxation and neutron spin-echo experiments are found to agree quantitatively above and below the "glass" temperature T_g. The agreement confirms the power-law decay of correlations in time near and below T_g. Features of the experimental results which depend on (quasi)static impurity-spin correlations suggest that the spatial distribution of thermally-averaged impurity-spin magnitudes is quite uniform below T_g. The stochastic behavior of dipolar fields at muon sites is essentially the same as that of the impurity spins themselves at all temperatures.

I. INTRODUCTION

The dynamic behavior of disordered spin systems possessing random exchange is a subject of considerable current interest. In simple theoretical models for crystalline (nonrandom) spin systems, such as ordered ferromagnets, it is found that the spin autocorrelation function $S_\sigma(t) = \langle\vec{\sigma}(t)\cdot\vec{\sigma}(0)\rangle$ for the stochastic time dependence $\vec{\sigma}(t)$ of the impurity spins decays exponentially in time (outside of the critical region).[1] In disordered systems, however, dynamic theories[2] and simulations[3] predict an algebraic (power-law) decay in time. It is therefore of interest to pursue experimentally the distinction between dynamics in ordered and disordered systems.

Recently two relatively new experimental techniques, neutron spin-echo (NSE) scattering and muon-spin relaxation (μSR), have been used to probe spin dynamics in metallic spin glasses. These are dilute magnetic alloys (e.g. AgMn, CuMn, AuFe), which exhibit a characteristic cusp in the ac susceptibility[4] at the glass freezing temperature T_g. The NSE technique, introduced by Mezei and Murani,[5] measures the spin correlation function $S_\sigma(\vec{q},t)$ directly, where $\vec{q}$ is the neutron momentum transfer. The μSR method[6] yields spin-lattice relaxation rates of local probes (implanted positive muons), which are sensitive to fluctuations of the (dipolar) local field $\vec{h}(t)$ at muon sites. This yields a broad average over all $\vec{q}$, as in nuclear magnetic resonance (NMR). The time dependence of the local-field correlation function $S_h(\vec{q},t)$, averaged over all $\vec{q}$, can be measured indirectly using μSR in a longitudinal applied field, and the result can then be compared to $S_\sigma(\vec{q},t)$ obtained using NSE in zero field. The two techniques are complementary in the time domain, since NSE is most sensitive to

correlation times in $S_\sigma(\vec{q},t)$ between 10^{-8} s and 10^{-12} s, whereas μSR is most sensitive to times between 10^{-4} s and 10^{-11} s.

In this paper μSR and NSE measurements of impurity-spin correlation functions in metallic spin glasses are compared. The results are also compared to dynamical theories. Preliminary results of this analysis have been previously presented.[7]

II. MUON-SPIN RELAXATION DATA

Recently the longitudinal field dependence of the muon spin-lattice relaxation rate $\lambda_\parallel$ has been reported[8] for $T < T_g$ in the spin glass $Ag_{100-x}Mn_x$, x = 1.6, 3, and 6 at.%. The technique, which is analogous to a measurement of T_1 in NMR, has been described elswhere.[9,10] The measurements were carried out in applied fields between 0.15 and 5 kOe ($g\mu_B H \ll k_B T$) and at temperatures between $0.3T_g$ and $0.92T_g$. It was found that $\lambda_\parallel = K(T)\omega_\mu^{\nu-1}$, where ω_μ is the Larmor frequency of the muon and K(T) is a temperature-dependent constant. The measured values of ν are given in Table I. Combining these results in the temperature range $0.3 < T/T_g < 0.66$ yields $\nu = 0.54 \pm 0.05$. For $T/T_g = 0.92$ one obtains $\nu = 0.24 \pm 0.02$.

For muons at rest in the sample one may argue on very general grounds[11] that $\lambda_\parallel$ is proportional to the noise power $J_h(\omega_\mu)$ in the fluctuating field at the muon Larmor frequency ω_μ, assuming that the applied field does not appreciably affect the impurity-spin dynamics. The assumption of stationary muons is known to be true at the temperatures of interest.[12] The assumption of field-independent dynamics is reasonable for small fields and temperatures well below T_g, and is borne out by NMR measurements in CuMn[13] and AgMn.[14] Near T_g a direct effect of the field on $J_h(\omega_\mu)$ cannot be ruled out, as discussed below.

III. NEUTRON SPIN-ECHO DATA

Figures 1 and 2 give NSE results[5,15] for $S_\sigma(\vec{q},t)$ in $Cu_{99}Mn_1$, $T_g = 10.1$ K (Fig. 1), and $Cu_{95}Mn_5$, $T_g = 27.5$ K (Fig. 2). The $S_\sigma(\vec{q},t)$ data were found to be essentially independent of $\vec{q}$ over the measured range ($0.045\ \text{Å}^{-1} < q < 0.36\ \text{Å}^{-1}$), and we shall write $\xi(t) \equiv S_\sigma(q,t)$ henceforth. The form of $\xi(t)$ was found to be exponential for $T \gg T_g$, but a long-time tail developed near and below T_g. The curves in Figs. 1 and 2 are model fits as discussed below.

IV. COMPARISON OF NSE AND μSR: $T < T_g$

In order to compare the NSE measurements of $\xi(t)$ to μSR spin-lattice relaxation measurements, we take a simplified form for the total spectral density

$$J_h(\omega) = A\delta(\omega) + BJ_h(\omega) \ , \tag{1}$$

of muon local-field fluctuations. Here the first term is related to the quasistatic response of the system, and the second term gives the dynamic fluctuation density. In real systems the first term may possess a nonzero (but small) width which cannot be detected using finite probe frequencies. Taking the Fourier transform of $J_h(\omega)$ yields the autocorrelation function $S_h(t)$ of the muon local field

$$S_h(t) = \int_{-\infty}^{\infty} d\omega\, J_h(\omega)\, e^{i\omega t} = A + (1 - A)F(t) \ , \tag{2}$$

where $F(0) = 1$, $F(\infty) = 0$, so that $A = S_h(\infty)$.

In a real spin glass an upper limit to the spectrum of fluctuation frequencies exists. We take this upper limit to be of the order of an exchange frequency $\omega_e \approx k_B T_g/\hbar$ ($\sim 10^{12}$ s^{-1} for $x \approx 0.01$ in CuMn and AgMn). The μSR data[8] imply a power-law form $J_h(\omega) \propto \omega^{\nu-1}$, so that

$$F(t) \approx (\omega_e t)^{-\nu} , \quad \omega_e t \gg 1 . \tag{3}$$

Using the form of the correlation function given by Eqs. (1) and (2), and the time dependence implied by the μSR results [Eq. (3)], values of $S_h(t)$ are obtained and compared with the measured $\xi(t)$ from NSE. This procedure assumes that the form of the correlation function is the same for fluctuations of the impurity spins and the muon local fields; evidence for the validity of this assumption will be given below in Sect. V. NSE measurements in CuMn will be compared to μSR measurements in AgMn and AuFe, as well as CuMn, and it must also be assumed that measured frequencies, rates, inverse times, etc., can be scaled by the respective glass temperatures of each sample.

Least-squares fits of the NSE data have been performed using Eqs. (2) and (3), with free parameters A, ω_e, and ν. In general the NSE data are not precise enough to determine all of these parameters accurately, and it must be decided instead whether a physically reasonable set of parameters are consistent with both μSR and NSE experimental results. The curves in Figs. 1 and 2 give typical fits. It can be seen that the form of Eqs. (2) and (3) represent the NSE data well, using the estimates $\omega_e = 10^{12}$ s^{-1} for $Cu_{99}Mn_1$ and 5×10^{13} s^{-1} for $Cu_{95}Mn_5$. For $T < 0.7T_g$ reasonable fits are obtained with $\nu \approx 1/2$, which is the value obtained from the μSR data,[8] although the neutron data do not determine ν well. One can see from Figs. 1 & 2

that at $T/T_g \approx 0.7$, for example, A(T) is ~0.6 for $Cu_{95}Mn_5$ and ~0.4 for $Cu_{99}Mn_1$. The NSE data therefore do not obey the expected scaling law, as noted previously.[15]

Below T_g the short-time behavior of the longitudinal muon relaxation function $G_{\parallel}(t)$ provides a direct experimental information on the distribution of static muon local fields, and is therefore related to the long-time behavior of $S_h(t)$ [i.e. the value of A in Eq. (2)]. Measurements of $G_{\parallel}(t)$ in AgMn,[10] AuFe,[16] and CuMn[17] for impurity concentrations ~1 at.% have determined the width a(T) of the Lorentzian distribution of static local fields in each of these systems. Below T_g a(T) increases with decreasing temperature from $a(T_g) \sim 0$ to the frozen-spin value a(0) for $T \ll T_g$. Figure 3 gives the dependence of $[a(T)/a(0)]^2$ on reduced temperature T/T_g for the above systems. Within about 20% uncertainty the data scale well. We note that for $T/T_g = 0.7$ the value of $[a(T)/a(0)]^2 \approx 0.4$ agrees well with the NSE value of $A(T/T_g=0.7)$ for $Cu_{99}Mn_1$ (Fig. 1), but is significantly smaller than $A(T/T_g=0.7) = 0.6$ for $Cu_{95}Mn_5$ (Fig. 2).

Walstedt and Walker[18] have shown that under some general assumptions (r^{-3} interaction, low impurity concentration) the linewidth a(T) of a probe spin (muon, nucleus) in a magnetic alloy is related to the impurity spin magnitude by

$$a(T) \propto \langle |\langle \vec{\sigma}_i \rangle_T| \rangle_i \ . \qquad (4)$$

Here $\langle\ \rangle_T$ and $\langle\ \rangle_i$ signify thermal and spatial averages, respectively. Equation (4) is valid in the rapid-fluctuation limit, i.e. for impurity-spin thermal fluctuation rates much larger than the resultant probe-spin linewidth a(T),[18] which seems to be well established for metallic spin

glasses.[10,16,17] Moreover A(T), defined in Eq. (2), is given by

$$A(T) = \langle |\langle \vec{\sigma}_i \rangle_T|^2 \rangle_i / S^2 \ . \tag{5}$$

Comparison of a(T) (μSR) and A(T) (NSE) then yields information on the <u>spatial</u> distribution of spin magnitudes $\langle \sigma_i \rangle_T$, as can be established by considering two extreme cases:[16]

I. The $\langle \vec{\sigma}_i \rangle_T$ are all the same. Then

$$\langle |\langle \vec{\sigma}_i \rangle_T|^n \rangle_i = |\langle \vec{\sigma}_i \rangle_T|^n \tag{6}$$

for any <u>n</u>, and

$$A(T) = [a(T)/a(0)]^2 \ . \tag{7}$$

As noted above, this is consistent with μSR data for x ≈ 1 at.% and the NSE results for $Cu_{99}Mn_1$ at $T/T_g = 0.7$.

B. A fraction <u>f</u> of the spins are saturated ($|\langle \vec{\sigma}_i \rangle_T| = S$), and the remaining fraction is "free" ($\langle \vec{\sigma}_i \rangle_T = 0$). Then

$$\langle |\langle \vec{\sigma}_i \rangle_T|^n \rangle_i = fS^n \tag{8}$$

for any <u>n</u>, and

$$A(T) = a(T)/a(0) = f \ . \tag{9}$$

The comparison between μSR and NSE data suggests, therefore, that the im-

purity spins are distributed in direction but not in magnitude below T_g. This in turn seems consistent with a "percolation" picture of the transition at T_g only if the "infinite cluster", the formation of which is taken to define T_g, quickly encompasses essentially all impurity spins as the temperature is lowered below T_g. NSE results at more temperatures in samples with $x \approx 0.01$ would be useful in extending this conclusion, as well as μSR data at higher concentrations.

IV. COMPARISON OF NSE AND μSR: T > Tg

The form of $\xi(t)$ as measured by NSE changes for $T > T_g$, and eventually tends toward an exponential for $T \gg T_g$. Spin probes in rapidly-fluctuating local fields are not sensitive to the functional form of $S_h(t)$,[11] but yield an effective correlation time τ defined by

$$\tau \equiv \int_0^\infty [S_h(t)/S_h(0)]\, dt \ . \tag{10}$$

Values of τ have been obtained for AgMn,[10] AuFe,[16] and CuMn[18] from zero-field μSR measurements. Figure 4 is a scaled plot of τT_g vs. T/T_g, reproduced from Ref. 10.

Mezei[15] has obtained good fits of $\xi(t)$ data obtained from NSE in $Cu_{95}Mn_5$ to the form

$$\xi(t) = \frac{1}{E_M} \int_0^{E_M} \exp[-t/(\tau_o e^{E/T})]\, dE \ , \tag{11}$$

which was motivated by considerations of distributions of barrier heights

for activated hopping. (Its validity is not necessarily a demonstration of the importance of such barriers, however.) A good fit was obtained for $E_M = 300$ K and $\tau_o = 6 \times 10^{-14}$ s. Scaled values of these parameters, together with Eqs. (10) and (11), yield the curve in Fig. 4. There is good agreement between the μSR and NSE data, with no adjustable parameters. This confirms the similarity between muon local-field and impurity-spin stochastic behavior assumed above, over a wide range of values of τ.

V. CONCLUSIONS

Muon-spin relaxation and neutron spin-echo measurements of local-field and impurity-spin correlation functions $\xi(t)$ in metallic spin glasses give consistent results for temperatures above and below T_g. The time-dependent component of $\xi(t)$ decays as $t^{-\nu}$, $\nu \simeq 1/2$, below T_g. This behavior is consistent with recent mean-field theories of spin-glass dynamics,[2] as well as with earlier Monte-Carlo simulations.[3]

For CuMn, AgMn, and AuFe spin glasses with similar values of T_g (±30%), scaled static μSR linewidths agree well below T_g. Furthermore, the relation $A(T) = [a(T)/a(0)]^2$, expected for a uniform distribution of impurity-spin moment magnitudes, is obeyed for impurity concentrations $x \simeq 1$ at.%. This agreement breaks down, however, for comparison with NSE data on $Cu_{95}Mn_5$, where, as noted by Mezei and Murani,[5,15] the larger value of A(T) implies an increase in static spectral density with increasing impurity concentration.

Near the glass temperature the relation $\xi(t) \propto t^{-\nu}$ still seems to hold, but ν deviates from 1/2 for the AgMn μSR and $Cu_{95}Mn_5$ NSE data. Curiously, the $Cu_{99}Mn_1$ NSE data still yield $\nu \simeq 1/2$ at $T/T_g \simeq 1.1$. μSR experiments are not reliable indicators of the value of ν near T_g, however, since

$J_h(\omega_\mu)$ may depend on field directly as well as via the muon Larmor frequency. Above T_g, where $\xi(t)$ tends toward an exponential form, μSR and NSE data yield consistent correlation times as seen in Fig. 4.

NSE and μSR measurements are therefore in reasonable quantitative agreement in metallic spin glasses. This implies (1) that the q independence of $S_\sigma(q,t)$, obtained from NSE measurements for a restricted range of q, apparently holds over the wider range of $\vec{q}$ values important for μSR; (2) A consistent time dependence of $S_\sigma(\vec{q},t)$ is obtained for measuring times $<10^{-9}$ s (NSE) and $>10^{-9}$ s (μSR); and (3) perhaps most importantly, more confidence in the reliability of the experimental determinations is warranted than could be given to either technique taken by itself.

Acknowledgements

We are grateful for useful discussions with D. L. Huber and R. E. Walstedt, and to M. Leon for collaboration in a preliminary version of this report. This work was performed under the auspices of the U. S. Department of Energy, and was also supported by the U. S. National Science Foundation (Grant No. DMR 81-15543).

REFERENCES

1. S.-K. Ma, Modern Theory of Critical Phenomena (Benjamin, Reading, Massachusetts, 1976).
2. H. Sompolinsky and A. Zippelius, Phys. Rev. B 25, 6860 (1982).
3. S. Kirkpatrick and D. Sherrington, Phys. Rev. B 17, 4304 (1978).
4. V. Kannella and J. A. Mydosh, Phys. Rev. B 6, 4220 (1972).
5. F. Mezei and A. P. Murani, J. Magn. Magn. Mat. 14, 211 (1979); A. P. Murani, F. Mezei, and J. L. Tholence, Physica 108B, 1283 (1981).
6. A. Schenck, in Nuclear and Particle Physics at Intermediate Energies, edited by J. B. Warren (Plenum Press, New York, 1976), p. 159.
7. R. H. Heffner, M. Leon, and D. E. MacLaughlin, in Proc. Yamada Conf. on Muon Spin Rotation and Related Problems, Shimoda, Japan, 1983 (Hyperf. Int., in press).
8. D. E. MacLaughlin, L. C. Gupta, D. W. Cooke, R. H. Heffner, M. Leon, and M. E. Schillaci, Phys. Rev. Lett. 51, 927 (1983).
9. Y. J. Uemura, K. Nishiyama, T. Yamazaki, and R. Nakai, Solid State Commun. 39, 461 (1981).
10. R. H. Heffner, M. Leon, M. E. Schillaci, D. E. MacLaughlin, and S. A. Dodds, J. Appl. Phys. 53, 2174 (1982).
11. A. Abragam, Principles of Nuclear Magnetism (Clarendon Press, Oxford, 1961).
12. R. H. Heffner, Hyperf. Int. 8, 655 (1981); M. E. Schillaci, C. Boekema, R. H. Heffner, R. L. Hutson, M. Leon, C. E. Olsen, S. A. Dodds, D. E. MacLaughlin, and P. M. Richards, in Proc. Int. Symposium on the Electronic Structure and Properties of Hydrogen in Metals, edited by P. Jena and C. B. Satterthwaite (Plenum Press, New York, 1983), p.

139.

13. H. Alloul, S. Murayama, and M. Chapellier, J. Magn. Magn. Mat. 31-34, 1353 (1983).

14. H. Alloul, in Proc. Heidelberg Conf. on Spin Glasses, edited by J. L. van Hemmen and I. Morgenstern (Lecture Notes in Physics, Springer-Verlag, Berlin, 1983), p. 18; H. Alloul, private communication.

15. F. Mezei, J. Appl. Phys. 53, 7654 (1982).

16. Y. J. Uemura and T. Yamazaki, J. Magn. Magn. Mat. 31-34, 1359 (1983).

17. Y. J. Uemura, T. Yamazaki, D. R. Harshman, M. Semba, J. H. Brewer, E. Ansaldo, and R. Keitel, in Proc. Yamada Conf. on Muon Spin Rotation and Related Problems, Shimoda, Japan, 1983 (Hyperf. Int., in press).

18. R. E. Walstedt and L. R. Walker, Phys. Rev. B 9, 4857 (1974).

19. Y. J. Uemura, T. Yamazaki, R. S. Hayano, R. Nakai, and C. Y. Huang, Phys. Rev. Lett. 45, 583 (1980).

TABLE I. Values of the power-law exponent ν of the noise spectrum below T_g in $Ag_{100-x}Mn_x$ spin glasses, $1.6 < x < 6$ at.%, obtained from μSR measurements as described in the text. Data from Ref. 8.

T/T_g	ν
0.30	0.59 ± 0.15
0.46	0.51 ± 0.07
0.66	0.55 ± 0.07
0.92	0.24 ± 0.02

FIGURE CAPTIONS

FIG. 1. Impurity-spin correlation functions $\xi(t)$ obtained from neutron spin-echo measurements (Ref. 15) for $T/T_g < 1.1$ in spin-glass $Cu_{99}Mn_1$. The curves are fits to the functional form of Eqs. (2) and (3), with parameters as indicated. The dotted lines indicate that Eq. (2) is rigorously correct for $(\omega_e t) >> 1$. The numbers in parentheses are the reduced temperatures T/Tg.

FIG. 2. Correlation functions as in Fig. 1, for $Cu_{95}Mn_5$ (Ref. 5).

FIG. 3. Dependence of the square of the reduced muon local-field distribution width $[a(T)/a(0)]^2$ on reduced temperature T/T_g in three metallic spin-glass systems.

FIG. 4. Dependence of the scaled effective correlation time τT_g on reduced temperature $T/T_g > 1$ in three metallic spin-glass systems. Data points: results of μSR measurements. Curve: fit of Eq. (11) to NSE data for $Cu_{95}Mn_5$.

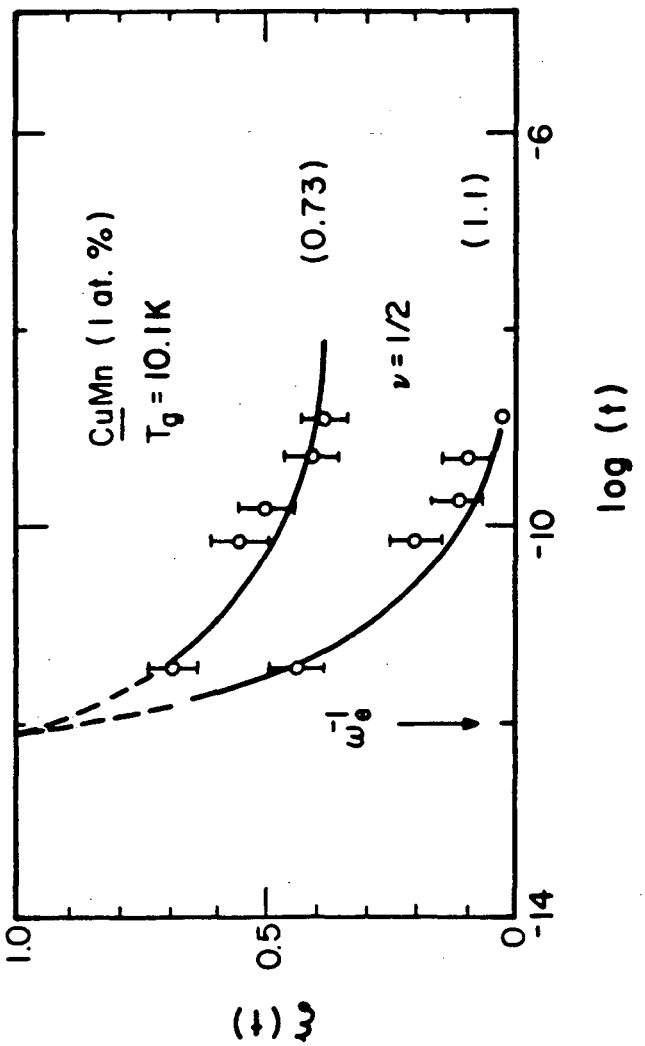

Figure 1

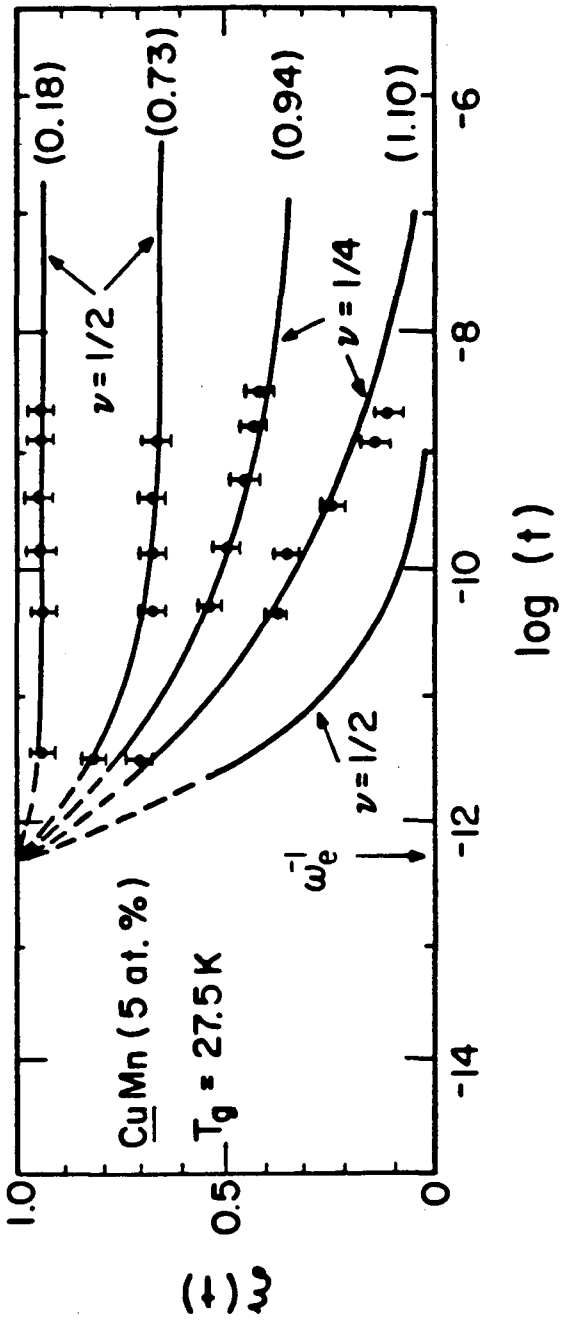
(0.18)
(0.73)
(0.94)
(1.10)
ν = 1/2
ν = 1/4
ν = 1/2
ω_e^{-1}
CuMn (5 at. %)
T_g = 27.5 K
1.0
0.5
0
-14
-12
-10
-8
-6
log (t)
ε(t)

Figure 2

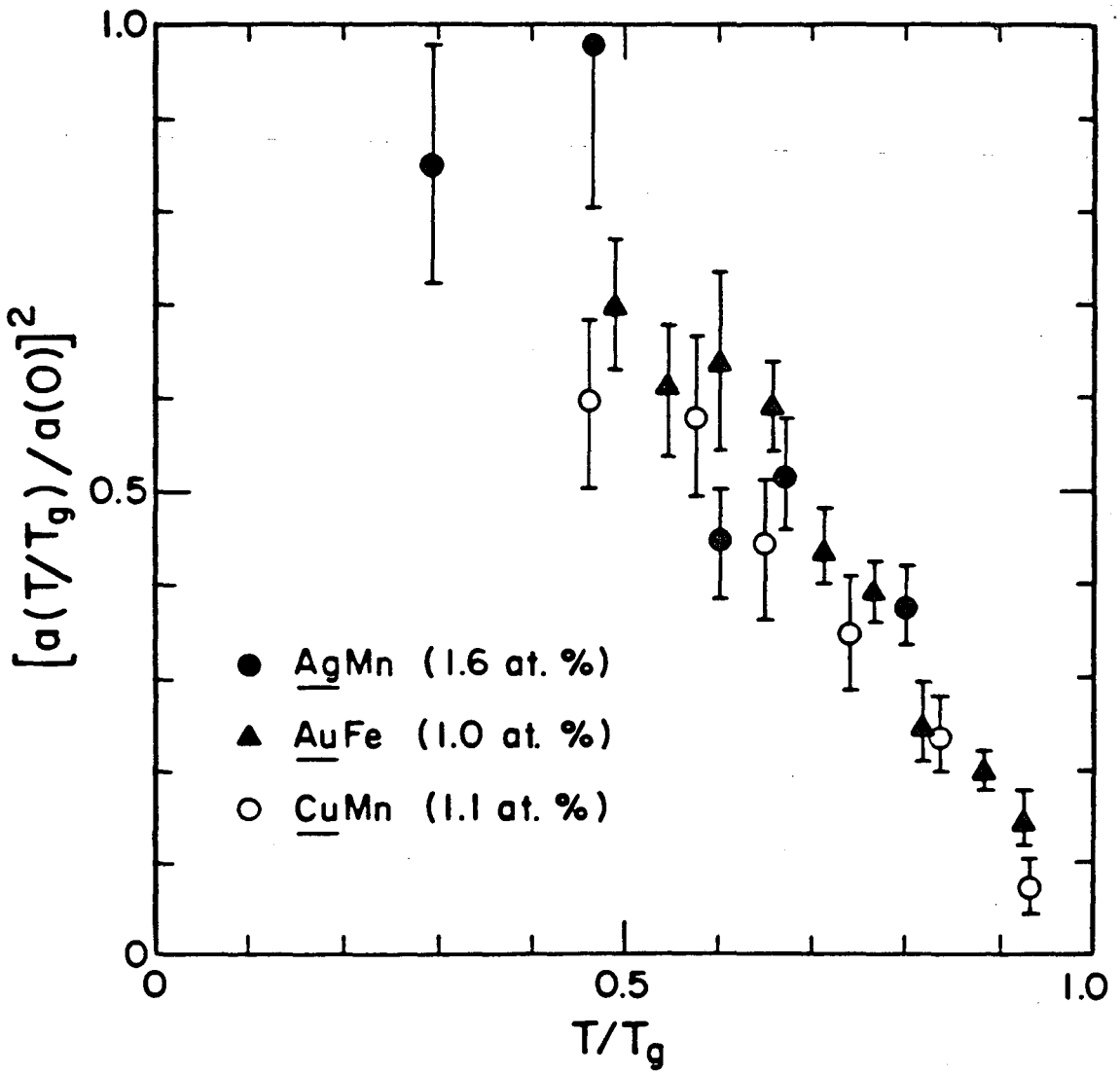

Figure 3

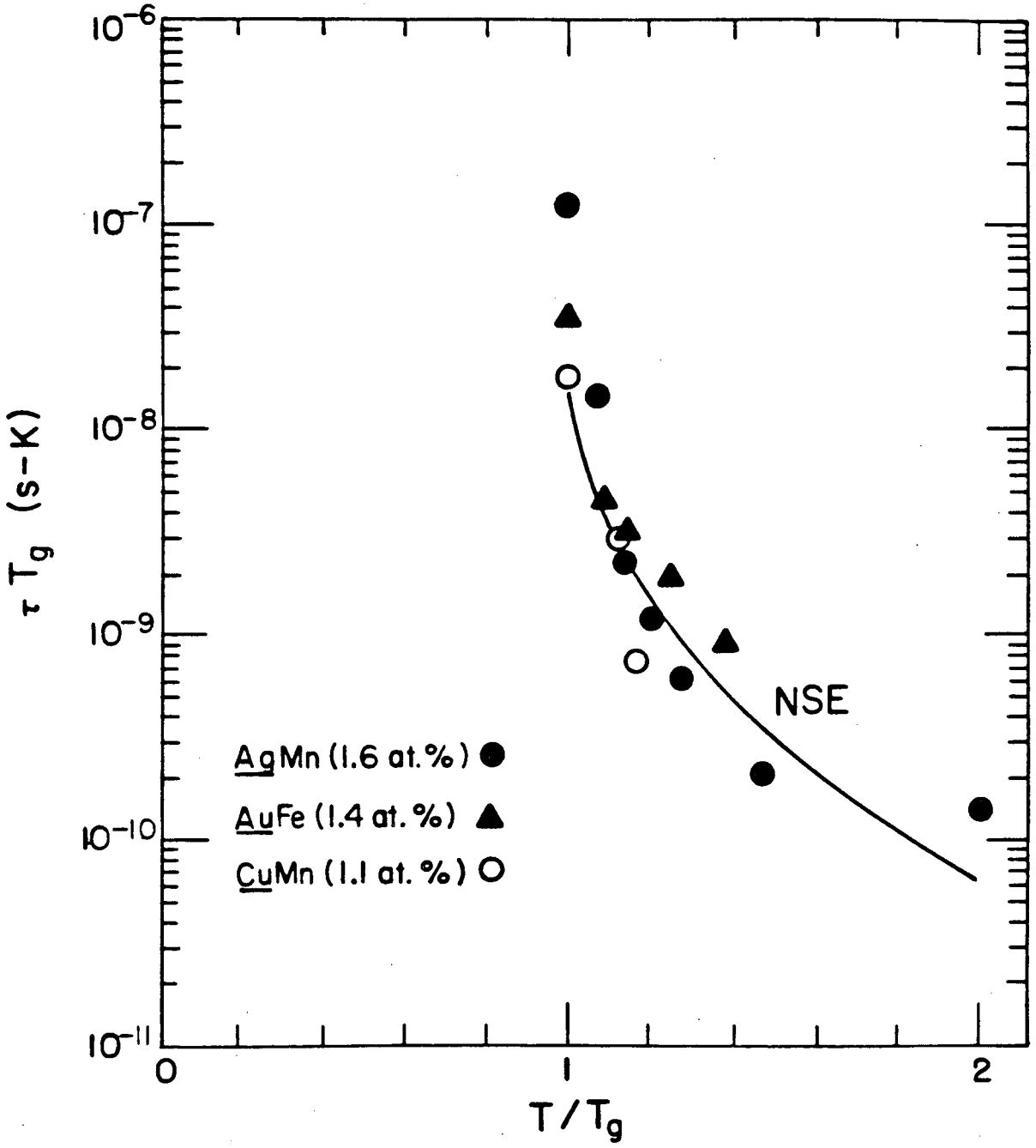
10^{-6}
10^{-7}
10^{-8}
10^{-9}
10^{-10}
10^{-11}
τT_g (s-K)
0
1
2
T/T_g
NSE
AgMn (1.6 at.%)
AuFe (1.4 at.%)
CuMn (1.1 at.%)

Figure 4

EFFECTS OF SUPERCONDUCTIVITY ON RARE-EARTH ION DYNAMICS IN $(Ho_xLu_{1-x})Rh_4B_4$*

R. H. Heffner, D. W. Cooke, R. L. Hutson, M. Leon, M. E. Schillaci,

J. L. Smith, and A. Yaouanc+

Los Alamos National Laboratory, Los Alamos, New Mexico 87545

S. A. Dodds

Rice University, Houston, Texas 77251

L. C. Gupta≠ and D. E. MacLaughlin

University of California, Riverside, California 92521

PACS numbers: 74.90.+n, 75.30.Hx, 76.90.+d

ABSTRACT

Zero-field muon spin-lattice relaxation rates have been measured in magnetically diluted $Ho_xLu_{1-x}Rh_4B_4$ ternary compounds, primarily for x = 0.02. For temperatures below ~11 K a characteristic two-component structure of the muon depolarization function is observed, which is consistent with slow (quasistatic) Ho^{3+}-moment fluctuations. We have reported similar behavior for x = 0.7, which indicates that the slow fluctuations are due to crystal-field isolation of the Ho^{3+} ground state. The observed relaxation rates in this temperature regime depend little on x, which is consistent with conduction-electron (Korringa) exchange scattering as the dominant mechanism for the fluctuations. The observed temperature dependence of muon spin-lattice relaxation in the superconducting state is not presently understood.

I. INTRODUCTION

The study of the interplay of magnetism and superconductivity, a topic of interest for some time in solid-state physics,[1] has received renewed interest following the discovery by Matthias and coworkers[2] of rare-earth (RE) ternary and pseudoternary compounds which exhibit both magnetic and superconducting phase transitions. A particular class of these compounds, the rare-earth rhodium borides ($RERh_4B_4$), has been extensively studied,[3] and the ferromagnetic, superconducting, and paramagnetic phase boundaries for these systems are by now well known.[3,4]

In previous publications[5,6] we have reported positive muon (μ^+) spin relaxation (μSR) measurements in the compounds $(Ho_xLu_{1-x})Rh_4B_4$, x = 0, 0.7, and 1.0, and in $GdRh_4B_4$. A comparison of the μSR measurements in the Ho- and Gd-based compounds has established that the Ho^{3+}-moment dynamics are strongly influenced by the crystal-field level splittings.[6] The most striking result, however, is a sharp shoulder in the temperature dependence of the μ^+ spin-lattice relaxation rate at the superconducting transition temperature T_s = 7.7 K for x = 0.7. In order to investigate further the effects of superconductivity on the Ho^{3+}-moment dynamics, we have undertaken new measurements for systems with x = 0.02 and 0.35. Here we report primarily zero-field measurements in $(Ho_{0.02}Lu_{0.98})Rh_4B_4$, which becomes superconducting at T_s = 11.3 K.

II. EXPERIMENT AND DATA ANALYSIS

The experiments were performed at the Clinton P. Anderson Meson Physics Facility (LAMPF) using the zero-field, time-differential μSR technique.[7] Sample temperatures were varied between 3 K and room temperature,

and were regulated to within 0.1 K. Sample preparation is described in Ref. 5.

Three distinct forms for the normalized muon spin relaxation function $G_z(t)$ were observed in different temperature regimes. These are plotted in Fig. 1.

A. T = 50 K

At 50 K $G_z(t)$ was found to be well described by the static zero-field relaxation function derived by Kubo and Toyabe,[8] which is appropriate for a time-independent Gaussian distribution of local magnetic fields at μ^+ sites. The measured width of the field distribution, about 4 Oe, indicates that the μ^+ spin relaxation is caused primarily by μ^+ precession about the host nuclear dipolar fields. The return of the long-time portion of $G_z(t)$ to 1/3 indicates that the local field is effectively random in direction and static in nature.[8] Furthermore, the Ho^{3+} spins must be fluctuating so rapidly at 50 K that they produce no relaxation of the μ^+ polarization.

B. 15 K < T < 50 K

As the temperature is lowered the form of $G_z(t)$ changes, until at 15 K the relaxation function can be approximated by a simple exponential $G_z(t) = \exp(-\lambda_1 t)$ (Fig. 1), where λ_1 is the μ^+ spin-lattice relaxation rate. The dominant μ^+ relaxation mechanism at 15 K is therefore fluctuations of the local field $h_L(t)$ produced by the fluctuating Ho^{3+} moments, as discussed below. In the temperature region 15 K < T < 50 K $G_z(t)$ was taken to be the product of an exponential and the Kubo-Toyabe function, because the nuclear and Ho^{3+} broadening mechanisms are independent of each other.

In principle the local-moment contribution to $G_z(t)$ in a dilute magnetic alloy at high temperatures should be approximated by the "root exponential" $G_z(t) = \exp[-(\lambda t)^{1/2}]$.[9,10] In practice the presence of the Kubo-

Toyabe function made determination of the Ho^{3+} contribution to $G_z(t)$ uncertain at high temperatures. The nuclear broadening will be quenched in a modest (~100 Oe) longitudinal field, however,[8] and future experiments in such a field will determine the form of the Ho^{3+} contribution more precisely.

C. $T < 11$ K

At $T < 11$ K the form of the relaxation function again changes, exhibiting the two-component form shown in Fig. 1 for T = 6 K. These data were fit with the function

$$G_z(t) = [1 - a] \exp(-\sigma t) + a \exp(-\lambda_2 t), \qquad (1)$$

with $\sigma \gg \lambda_2$. One finds that

i) σ is essentially independent of temperature, with an average value of $11.5 \pm 0.6\ \mu s^{-1}$, or $\sigma/\gamma_\mu \simeq 130$ Oe ($\gamma_\mu = 8.51\ Oe^{-1}\ \mu s^{-1}$ is the muon gyromagnetic ratio);

ii) a is about 0.6 at T = 11 K, and falls to 1/3 for $T < 8$ K; and

iii) λ_2 falls exponentially with decreasing temperature below T_s, with an activation energy $\Delta = 9.8 \pm 1.3$ K (Fig. 2).

From these results we conclude that the stochastic motion of the Ho^{3+} moments becomes quasistatic below ~11 K. The value of 1/3 for a at low temperatures is itself indicative of a random, quasistatic field distribution.[8] Furthermore, the temperature independence of σ is evidence that the local field $h_L(t)$ reorients completely[7-9] in a time τ_m such that $\sigma\tau_m \gg 1$, whence $\lambda_2 = 2/(3\tau_m)$. A two-component form for $G_z(t)$ can also be due to limited-amplitude fluctuations of $h_L(t)$ around a static or quasistatic average value,[10] but in such a case σ increases markedly with decreasing tem-

perature as the fluctuation amplitude decreases. This is not observed in $Ho_{0.02}Lu_{0.98}Rh_4B_4$, and we conclude that $h_L(t)$ reorients completely below 8–10 K.

We have estimated the value of σ using the formalism of Walstedt and Walker[11] for dipolar coupling between μ^+ spins and dilute impurity magnetic moments. (The μ^+ hyperfine coupling to the conduction electrons is small in metals,[12] and the dipolar coupling dominates indirect mechanisms.) This calculation requires the spatial average $\langle|\mu|\rangle$ of the Ho^{3+} moment. As discussed below, crystalline-electric-field (CEF) splitting of the Ho^{3+} $^5I_8$ multiplet produces a two-level Ising-like ground state[5,6] with a magnetic dipole moment of $\sim 10\mu_B$.[13] For randomly-oriented Ho moments this calculation yields $\sigma = 6.7\ \mu s^{-1}$, or $\sigma/\gamma_\mu \simeq 80$ Oe. This indicates that Ho^{3+} dipolar fields contribute significantly to the coupling with μ^+ spins, and is consistent with identification of the two-component structure of $G_z(t)$ with quasistatic inhomogeneous broadening.

III. DISCUSSION

Identification of the mechanisms responsible for Ho^{3+}-moment relaxation is of considerable interest. Two basic processes, Korringa scattering of conduction electrons[14] and indirect exchange (RKKY) coupling between Ho^{3+} spins,[15] should be important in dilute magnetic alloys. For the Korringa mechanism the μ^+ spin-lattice relaxation rate λ should be proportional to x^2 at high temperatures, whereas $\lambda \propto x$ for the RKKY process.[15] At 100 K our measured values of λ_1 for $x > 0.35$ are proportional to x^2, which indicates that the Korringa mechanism is dominant in this temperature regime. The Korringa mechanism has also been observed by NMR in $SmRh_4B_4$ at high temperatures.[16] For $x > 0.35$ and 11 K $< T <$ 50 K the μ^+

relaxation rate is too large to be observed,[5] so that the concentration dependence of λ_1 cannot be determined in this temperature range.

Quasistatic motion of $h_L(t)$ sets in for temperatures below ~11 K for x = 0.7, as previously reported,[5] as well as in the present case x = 0.02. This concentration dependence is additional confirmation that the dramatic reduction in Ho^{3+} fluctuation rate is due to the CEF ground-state isolation, which is a single-ion effect and should not depend greatly on concentration. We have calculated CEF energies and wave functions for RE^{3+} ions in the $RERh_4B_4$ structure by diagonalizing the hamiltonian for $\bar{4}2m$ point symmetry, using the crystal-field parameters of Dunlap and Niarchos.[17] For Ho^{3+} the ground and first excited states are each doubly degenerate, with nearly pure $|J_z=\pm 8\rangle$ and $|\pm 7\rangle$ wave functions respectively. The first excited states occur at $\delta \simeq 55$ K. Allowed transitions from $|\pm 8\rangle$ to $|\mp 8\rangle$ can therefore occur only through small admixtures of different J_z eigenfunctions in the ground and excited states, which are separated by at least 55 K. The slow Ho^{3+}-moment fluctuations at low temperatures can then be accounted for by a combination of the large ground-state isolation and the weakness of $\Delta J_z = \pm 1$ transitions within the ground-state doublet.

Below ~9 K the values of λ_2 for x = 0.02 and x = 0.7, shown in Fig. 2, are remarkably similar considering the large difference in Ho concentrations. This observation can be understood if the dominant Ho^{3+}-moment relaxation mechanism is again Korringa scattering, as at 100 K, because this mechanism would result in a concentration-independent correlation time τ_m for the μ^+ local fields. Since $\lambda_2 \sim 1/\tau_m$ for quasistatic fluctuations (Sect. II.C), λ_2 would also be independent of $\underline{x}$, as the data of Fig. 2 indicate. At least one source of difference in the temperature dependence of λ_2 between x = 0.02 and x = 0.7 is the onset of ferromagnetism below the

Curie temperature T_c = 4.1 K at the latter concentration. This is presumably responsible for the "knee" in $\lambda_2(T,x=0.7)$ near T_c.

It should be noted that most of these data are for temperatures below the superconducting transition temperature T_s. The anomalous behavior of λ_2 in the superconducting state,[5] although not well understood, can therefore be attributed to Ho^{3+}-spin relaxation by scattering of excitations in the superconducting conduction-electron system.

Kumagai and Fradin[18] have reported NMR studies of very dilute alloys of Gd and Er in YRh_4B_4, which indicate that the RKKY process dominates RE fluctuations in these alloys for $T \simeq T_s$. The low-lying CEF states of these systems are very different from those of Ho^{3+} in $(Lu,Ho)Rh_4B_4$, however.

Below T_s the temperature dependence of λ_2 for x = 0.02 indicates an activation energy $\Delta \simeq 10$ K, which is much smaller than the CEF ground-state isolation δ. Since $\Delta \simeq 1.8T_s$, interpretation of Δ as a superconducting gap parameter yields a value consideraby smaller than the BCS gap parameter $\Delta_{BCS} = 3.5T_s$. Such an interpretation is, however, speculative at this time, because it is not clear how the superconducting state could reduce the activation energy for Ho^{3+} fluctuations to a value much less than δ. Further μSR experiments in dilute $(RE)Rh_4B_4$ alloys are under way to investigate this phenomenon.

*Work supported by the U.S. Department of Energy, U.S. National Science Foundation Grants DMR-7909223 and DMR-8115543, and the U.C. Riverside Committee on Research.

+Permanent address: Laboratoire d'Interactions Hyperfines, C.E.N.G., B.P. 85X, 38041 Grenoble, France.

≠Permanent address: Tata Institute of Fundamental Research, Bombay, India.

REFERENCES

1. P. W. Anderson and H. Suhl, Phys. Rev. 116, 898 (1959); L. P. Gorkov and A. I. Rusinov, Sov. Phys.—JETP 19, 922 (1964).
2. B. T. Matthias, E. Corenzwit, J. M. Vandenberg, and E. Barz, Proc. Natl. Acad. Sci. USA 74, 1334 (1977).
3. See e.g. Proc. Int. Conf. on Ternary Superconductors, edited by G. K. Shenoy, B. D. Dunlap, and F. Y. Fradin (North Holland, New York, 1981).
4. M. B. Maple, H. C. Hamaker, D. C. Johnson, H. B. McKay, and L. D. Woolf, J. Less-Comm. Met. 62, 251 (1978).
5. C. Boekema, R. H. Heffner, R. L. Hutson, M. Leon, M. E. Schillaci, J. L. Smith, S. A. Dodds, D. E. MacLaughlin, J. Appl. Phys. 53, 2625 (1982).
6. D. E. MacLaughlin, S. A. Dodds, C. Boekema, R. H. Heffner, R. L. Hutson, M. Leon, M. E. Schillaci, and J. L. Smith, J. Magn. Magn. Mat. 31-34, 497.
7. R. S. Hayano, Y. J. Uemura, J. Imazato, N. Nishida, T. Yamazaki, and R. Kubo, Phys. Rev. B 20, 850 (1979).
8. R. Kubo and T. Toyabe, in Magnetic Resonance and Relaxation, ed. by R. Blinc (North Holland, Amsterdam, 1967) p. 810.
9. Y. J. Uemura, Hyperf. Int. 8, 739 (1980).
10. R. H. Heffner, M. Leon, M. E. Schillaci, D. E. MacLaughlin, and S. A. Dodds, J. Appl. Phys. 53, 2174 (1982).
11. R. E. Walstedt and L. R. Walker, Phys. Rev. B 9, 4857 (1974).

12. A. Schenck, Helv. Phys. Acta 54, 471 (1981).

13. H. R. Ott, L. D. Woolf, M. B. Maple, and D. C. Johnson, J. Low Temp. Phys. 39, 383 (1980).

14. H. Hasegawa, Prog. Theor. Phys. 21, 483 (1959).

15. M. R. McHenry, B. G. Silbernagel, and J. H. Wernick, Phys. Rev. B 5, 2958 (1972).

16. K. Kumagai, Y. Inoue, K. Kohori, and K. Asayama, in Ref. 3, p. 185.

17. B. D. Dunlap and D. Niarchos, Sol. St. Comm. 44, 1577 (1982). The actual parameters used vary somewhat from this reference, and were obtained from B. D. Dunlap, private communication.

18. K. Kumagai and F. Y. Fradin, Phys. Rev. B 27, 2770 (1982).

FIGURE CAPTIONS

FIG. 1. Zero-field muon spin relaxation function $G_z(t)$ at representative temperatures in $Ho_{0.02}Lu_{0.98}Rh_4B_4$. The curves are fits to the appropriate functions as discussed in the text.

FIG. 2. Temperature dependence of the zero-field μ^+ spin-lattice relaxation rate in $Ho_xLu_{1-x}Rh_4B_4$, x = 0.02 (circles and solid curves) and 0.7 (triangles and dashed curves). Open symbols: relaxation rate of the full μ^+ asymmetry (relaxation rate λ_1). Filled symbols: relaxation rate of the reduced-asymmetry component of the μ^+ polarization below ~11 K (relaxation rate λ_2). Superconducting (T_s) and ferromagnetic (T_c) transition temperatures are indicated. The curves are guides to the eye.

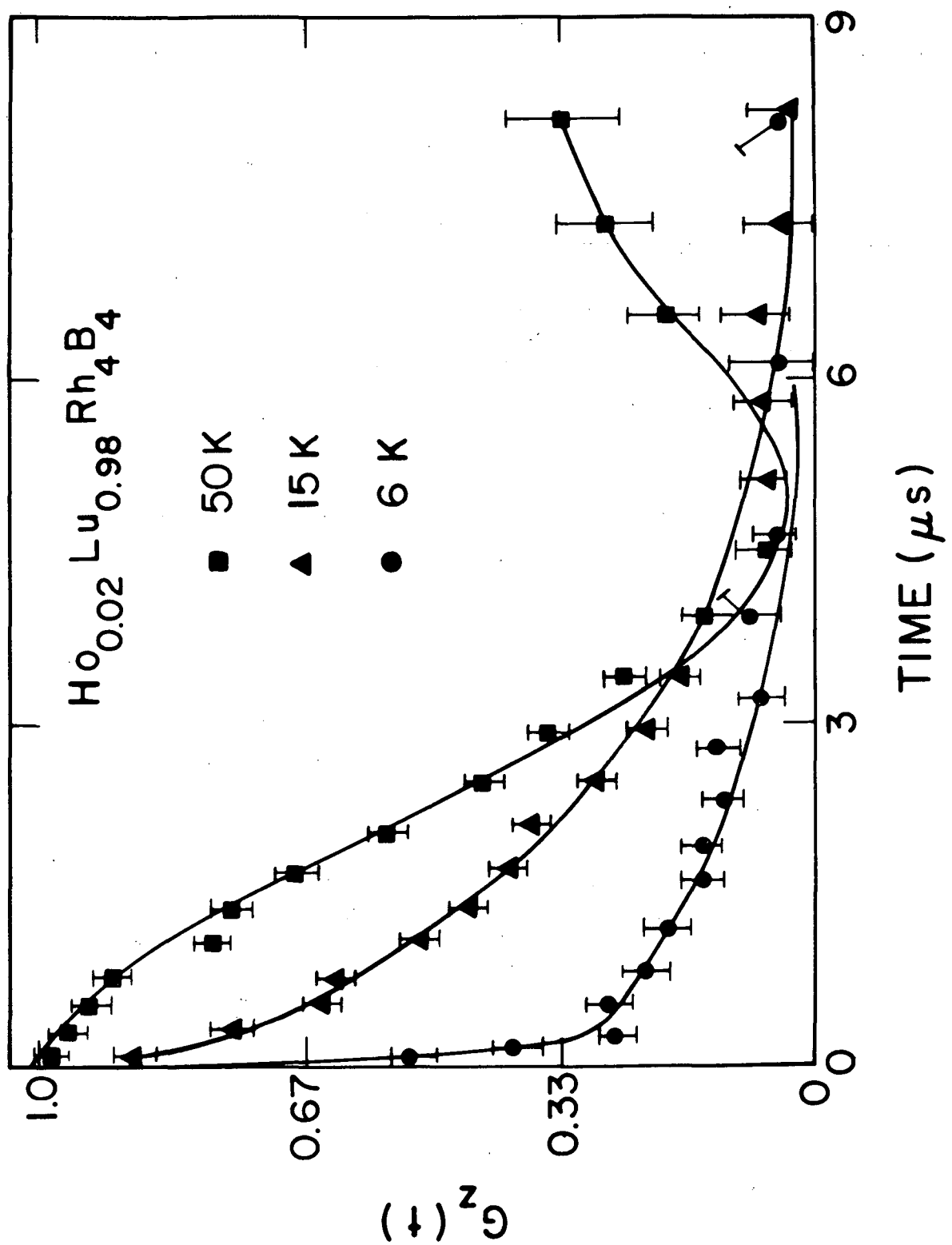
$Ho_{0.02}Lu_{0.98}Rh_4B_4$
50 K
15 K
6 K
1.0
0.67
0.33
0
$G_z(t)$
0
3
6
9
TIME (μs)

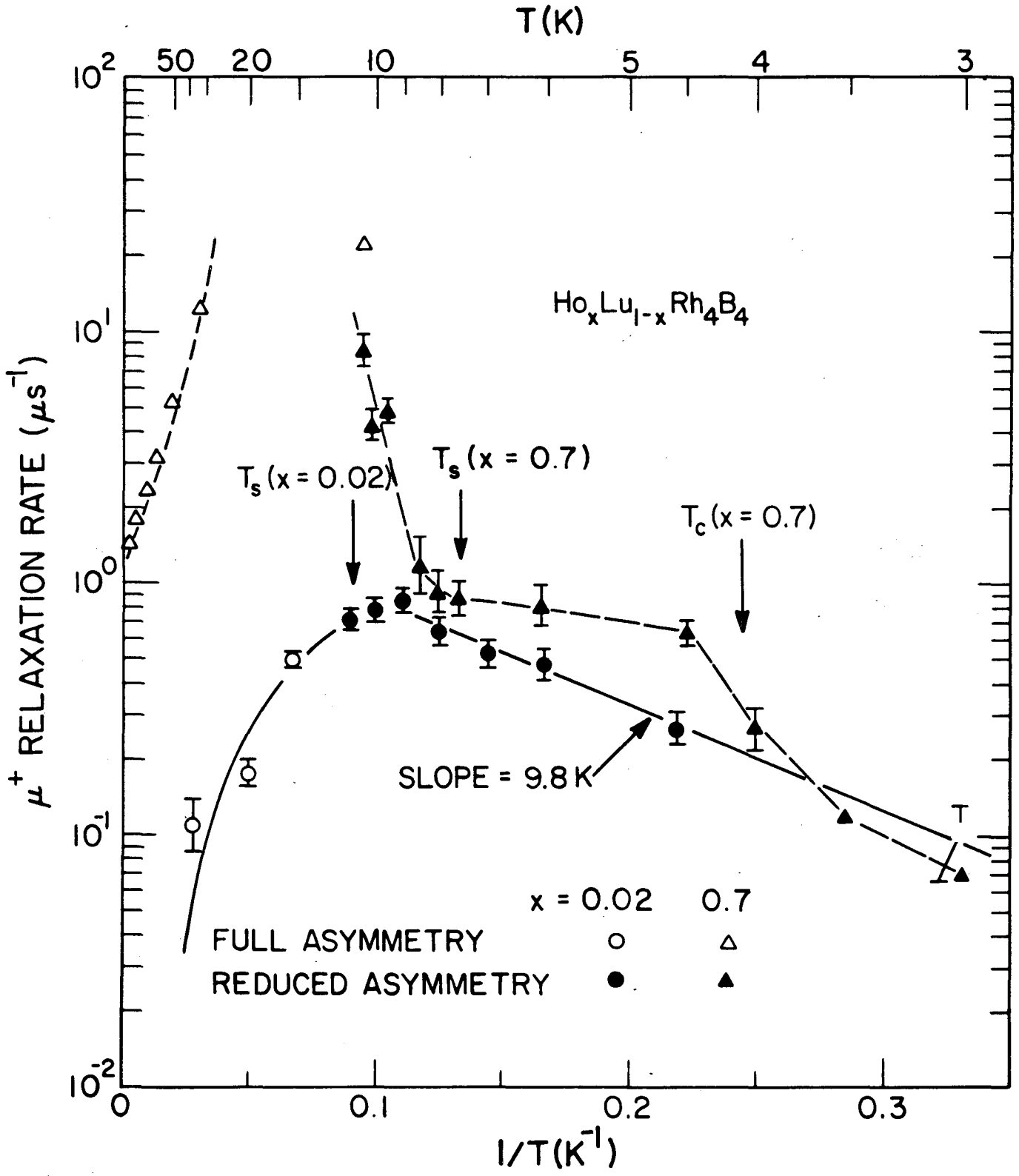
T(K)
50
20
10
5
4
3
10^2
10^1
10^0
10^{-1}
10^{-2}
μ^+ RELAXATION RATE (μs^{-1})
$Ho_xLu_{1-x}Rh_4B_4$
T_s (x = 0.02)
T_s (x = 0.7)
T_c (x = 0.7)
SLOPE = 9.8 K
T
x = 0.02
0.7
FULL ASYMMETRY
REDUCED ASYMMETRY
0
0.1
0.2
0.3
$1/T(K^{-1})$

MUON SPIN RELAXATION IN SPIN GLASS PdMn

R. H. Heffner, M. Leon, M. E. Schillaci
Los Alamos National Laboratory
Los Alamos, NM 87545

S. A. Dodds, G. A. Gist
Department of Physics, Rice University
Houston, TX 77251

D. E. MacLaughlin
Department of Physics, University of California
Riverside, CA 92521

J. A. Mydosh, G. J. Nieuwenhuys
Kamerlingh Onnes Laboratory, University of Leiden
The Netherlands

ABSTRACT

Muon spin relaxation (μSR) rates have been measured in transverse, longitudinal, and zero applied field for the spin glass PdMn (7 at. %), and are compared with a previous study of the disordered ferromagnet PdMn (2 at. %). The calculated paramagnetic state transverse field relaxation rate for non-interacting spins is much larger than the observed rate in spin glass PdMn, but is in good agreement with ferromagnetic PdMn. The zero field relaxation rate shows a sharp cusp at T_g=5K. An applied longitudinal field of 5 kG is insufficient to suppress this cusp in spin glass PdMn, but will suppress a similar cusp in ferromagnetic PdMn. Below T_g, a distribution of quasistatic local fields is observed in zero field, which has the same temperature dependence for both samples. Comparisons with model calculations are discussed.

I. Introduction

Spin glass PdMn has been widely studied as an example of a non-RKKY spin glass.[1,2] A competition between direct anti-ferromagnetic couplings and long range ferromagnetic couplings leads to a complicated phase diagram with a ferromagnetic phase for $c \lesssim 3$ at. %, and a spin glass phase for $c \gtrsim 5$ at. %.[3] In this work, muon spin relaxation (μSR) is used as a microscopic probe of the ordering in spin glass PdMn (7 at. %). The main goal of this work is to measure the temperature and field dependence of both the quasistatic local field distribution at the muon site and the muon's dynamic spin lattice relaxation. Theories of linewidths and relaxation mechanisms in dilute alloys are used to infer features of the impurity spin configuration. Comparisons with a previous study of ferromagnetic PdMn (2 at. %)[4] are used to show how the difference in magnetic ordering brought about by a change in concentration influences microscopic properties.

The experiments were carried out at the Stopped Muon Channel of the Clinton P. Anderson Meson Physics Facility (LAMPF) at the Los Alamos National Laboratory, using a standard μSR spectrometer.[5] The sample was in the form of a polycrystalline disk 3 mm thick and 30 mm in diameter; preparation techniques have been described in an earlier paper.[4] Ac susceptibility measurements showed a cusp at $T_g = 5$K, consistent with the system phase diagram.[6]

II. Quasistatic Field Distributions

Figure 1 shows measured transverse field exponential relaxation rates for applied fields of 200 G, 1 kG, and 5 kG. Measured spin lattice relaxation rates (discussed below) indicate that

the non-secular contribution to $\lambda_\perp$ is small. In addition, measurements of muon diffusion in Pd with Gd impurities indicate a negligible diffusion rate below about 100K.[7] Thus the rates shown in figure 1 represent only the quasistatic field distribution in PdMn.

Walstedt and Walker[8] (WW) have shown that if the local environment around the muon consists of non-interacting and equivalent, rapidly fluctuating spins distributed at random at concentration c, then in the dilute limit the relaxation is exponential with rate

$$\lambda_\perp = \lambda_{\perp o} \langle S_z \rangle \tag{1}$$

where $\langle S_z \rangle$ is the thermal average of the z component of the impurity spin. If the impurity spins are quasistatic (slow fluctuations) then this expression becomes

$$\lambda_\perp = \lambda_{\perp o} \langle |S_z| \rangle \quad . \tag{2}$$

For pure dipolar coupling,

$$\lambda_{\perp o} = \frac{8\pi^2}{9\sqrt{3}} N_o c \gamma_\mu g \mu_B \tag{3}$$

where N_o is the density of impurity sites, γ_μ is the muon gyromagnetic ratio, and g is the impurity spin g factor. These expressions are for the case of a large applied field, so that only components of impurity spins parallel to the applied field contribute to the z component of the local field distribution at the muon.

The observed paramagnetic susceptibility in a PdMn (5 at. %) sample is well described by a g = 2, S = 5/2 Curie law for $T \gtrsim 3T_g$

and low field,[1] so that using this Curie law for $\langle S_z \rangle$ in equation (1) gives the lines shown in Figure 1. At low temperatures, we simulate the spin glass state by assuming spins to be quasistatic and equally distributed among the 2S + 1 M_S states in calculating the order parameter $\langle |S_z| \rangle$. Equation (2) then gives the high field frozen spin linewidth

$$(\lambda_\perp)_{frozen} = 57.1\ \mu s^{-1}\ \text{(high field)}. \qquad (4)$$

A concentration of 7 at. % is not ordinarily considered to be in the dilute limit, so we have calculated a polycrystalline averaged lineshape numerically; the result differs in width from the WW result by no more than 7%.

The discrepancy in figure 1 between the $\lambda_\perp$ data and the WW prediction using a Curie law well above T_g is not understood. Similar data on the disordered ferromagnet PdMn (2 at .%)[4] show very good agreement with the WW result. We conclude that the observed discrepancy is due to the spin glass ordering, and is present for T well above T_g. Transverse field μSR results in spin glass AgMn show an increase above the WW result to at least 10 T_g.[9]

In zero applied field, the WW result is no longer valid, since all three components of the local field distribution contribute to the muon relaxation. Mikaelyan and Smilga[10] have generalized the WW expression to the case of zero field relaxation in a spin glass. The low temperature spin glass state is simulated by assuming quasistatic classical impurity spins, each of length S

and oriented along a randomly chosen local field direction. The resulting muon local field distribution is Lorentzian, with width

$$a = 0.827\ \lambda_{\perp o}\ S \tag{5}$$

which is in good agreement with the Monte Carlo simulation of Fiory.[11] For PdMn(7 at. %), equation (5) gives a zero field frozen spin linewidth

$$a_o = 78.8\ \mu s^{-1}\ \text{(zero field)}. \tag{6}$$

The zero field muon relaxation function allows a separation between a quasistatic field distribution of width a, and relaxation due to dynamic spin lattice relaxation processes. If we assume the fluctuation rate to be fast compared with a, then the long time decay will be a 'root exponential.[12] Thus for fast dynamic fluctuations, the zero field relaxation function is

$$G_z(t) = \frac{1}{3}\exp\left(-(\lambda_{\parallel} t)^{1/2}\right) + \frac{2}{3}(1 - at)\exp(-at). \tag{7}$$

The measured zero field relaxation data were fit to equation (7) for the width of the quasistatic local field distribution (a) below T_g. The temperature dependence of a is shown in figure 2, normalized to a_o. The scaled quasistatic width in ferromagnetic PdMn(2 at. %)[4] is also shown in figure 2. The similar temperature dependence in the two cases indicates that the development of a static field distribution is independent of the character of the magnetic ordering.

III. Spin Lattice Relaxation

Figure 3 presents measured muon spin lattice relaxation rates in zero and applied longitudinal field above and below T_g. Above T_g, the relaxation was fit to the 'root exponential' form appropriate for rapidly fluctuating (paramagnetic) spins in a dilute alloy,[12]

$$G_z(t) = \exp(-(\lambda_{\parallel} t)^{1/2}) \tag{8}$$

with rates plotted in figure 3. Fits of the data to a simple exponential form for $G_z(t)$ yield a similar chi-squared value, so that we have not explicity demonstrated the root exponential form. Below T_g, we expect that fluctuations will remain rapid, since this has been observed by μSR in spin glass AgMn.[13] Thus a root exponential decay of the 1/3 component (equation (7)) was used to fit the zero field data for $\lambda_{\parallel}$.

The peak in the zero field spin lattice relaxation rate at T_g is interpreted as being due to a change in the power spectrum of Mn spin fluctuations near the glass transition. Other μSR measurements in spin glass systems (AgMn, CuMn)[13,14] show a similar dramatic change in the Mn spin fluctuations around T_g. Note that a relaxation mechanism is still effective near T_g in an applied field of 5 kG, whereas in ferromagnetic PdMn (2 at. %) an applied field of 5 kG completely suppresses the fluctuation induced relaxation.[4]

At temperatures well below T_g, spin lattice relaxation is presumably due to low energy excitations of the ground state.[15]

A calculation[16] of the spectrum of excitation frequencies for spin glass PdMn(10 at. %) has shown a complicated three peak structure, with the mean spectral weight at a frequency $\sim 5\times10^{12} s^{-1}$. Since these fluctuations are much too fast to cause depolarization via the dipolar interaction in the lifetime of the muon, the observed relaxation must be due to some other, lower frequency component of the excitation spectrum. Recent analytic theories of spin wave excitations in spin glasses predict that small k magnons can propagate through the system with a dispersion relation linear in k.[17] These excitations are at frequencies lower than the localized modes, and may be responsible for the relaxation observed at low temperatures. Future zero field μSR studies in spin glasses at lower temperatures may provide useful data on relaxation for comparison with these theories.

IV. Conclusions

The transverse field relaxation rate $\lambda_\perp$ is not proportional to the observed Curie law magnetization in PdMn (7 at. %) for temperatures as high as 100K (20 T_g), where the onset of muon diffusion makes interpretation of $\lambda_\perp$ difficult. This result is especially surprising since $\lambda_\perp$ in ferromagnetic PdMn (2 at. %) is proportional to a Curie-Weiss magnetization over a wide temperature range, indicating that the observed reduction in $\lambda_\perp$ below

the Curie law prediction may be a high temperature precursor of the spin glass phase. We know of no satisfactory explanation for this effect nor for the increase in $\lambda_{\perp}$ above the measured magnetization in spin glass AgMn (1.6 at. %).

In zero field, we observe the onset of a quasistatic field distribution below T_g with a similar temperature dependence to that observed in PdMn (2 at. %). Spin lattice relaxation near T_g shows a strong cusp, indicating a change in the spectrum of Mn spin fluctuations. These fluctuations continue to induce relaxation in a large applied field, in contrast to PdMn (2 at. %).

Acknowledgements

We are grateful for helpful discussions with R. L. Hutson. This work was supported by the Department of Energy, the National Science Foundation (Grant Nos. DMR79-09223 and DMR81-15543) and the Netherlands "Stichtung voor Fundamenteel Onderzoek der Materie" (FOM).

FIGURE CAPTIONS

Figure 1. Temperature and field dependence of the transverse muon relaxation rate $\lambda_\perp$ in PdMn(7 at. %). Circles: 200 G. Triangles: 1 kG. Squares: 5 kG. The solid lines are from equation (1) using a Curie law for $\langle S_z \rangle$. $(\lambda_\perp)_f$ is the frozen spin rate (equation (4)).

Figure 2. Reduced temperature dependence of the zero field quasistatic field distribution width a(T), normalized to the theoretical zero field frozen rate a_o. Open circles: PdMn (2 at. %), $a_o = 28.\ \mu s^{-1}$, $T_c = 5.8$ K. Filled circles: PdMn (7 at. %), $a_o = 78.8\ \mu s^{-1}$, $T_g = 5.$K.

Figure 3. Temperature and field dependence of the muon spin lattice relaxation rate. Circles: zero field. Triangles: 200 G. Squares: 5 kG. Fitting functions used are described in the text.

REFERENCES

1. B. R. Coles, H. Jamieson, R. H. Taylor, A. Tari, J. Phys. F 5, 565 (1975).
2. S. C. Ho, I. Maartense, G. Williams, J. Phys. F 11, 1107 (1981).
3. H. A. Zweers, G. J. van den Berg, J. Phys. F 5, 555 (1975).
4. S. A. Dodds, G. A. Gist, D. E. MacLaughlin, R. H. Heffner, M. Leon, M. E. Schillaci, G. J. Nieuwenhuys, J. A. Mydosh, Phys. Rev. B, in press.
5. E. Karlsson, Phys. Reports 82, 271 (1982).
6. J. A. Mydosh, G. J. Nieuwenhuys, B. H. Verbeek, Phys. Rev. B 20, 1280 (1979).
7. S. A. Dodds, R. T. Stein, R. H. Heffner, R. L. Hutson, M. Leon, M. E. Schillaci, D. E. MacLaughlin, J. A. Mydosh, G. J. Nieuwenhuys, P. M. Richards, Bull. Am. Phys. Soc. 27, 162 (1982).
8. R. E. Walstedt, L. R. Walker, Phys. Rev. B 9, 4857 (1974).
9. J. A. Brown, R. H. Heffner, T. A. Kitchens, M. Leon, C. E. Olsen, M. E. Schillaci, S. A. Dodds, D. E. MacLaughlin, J. Appl. Phys. 52, 1766 (1981); R. H. Heffner, M. Leon, M. E. Schillaci, D. E. MacLaughlin, S. A. Dodds, J. Appl. Phys. 53, 2174 (1982).

10. A. L. Mikaelyan, V. P. Smilga, Sov. Phys. JETP 53, 1216 (1981).

11. A. T. Fiory, Hyp. Int. 8, 777 (1981).

12. M. R. McHenry, B. G. Silbernagel, J. H. Wernick, Phys. Rev. B 5, 2958 (1972).

13. R. H. Heffner, M. Leon, M. E. Schillaci, D. E. MacLaughlin, S. A. Dodds, J. Appl. Phys. 53, 2174 (1982).

14. Y. J. Uemura, T. Yamazaki, R. S. Hayano, R. Nakai, C. Y. Huang, Phys. Rev. Lett. 45, 583 (1980).

15. D. Beeman, P. Pincus, Phys. Rev. 166, 359 (1968); A. H. Mitchell, J. Chem. Phys. 27, 17 (1957).

16. W. Y. Ching, D. L. Huber, B. H. Verbeek, J. Appl. Phys. 50, 1715 (1979).

17. B. I. Halperin, W. M. Saslow, Phys. Rev. B 16, 2154 (1977); W. M. Saslow, Phys. Rev. B 22, 1174 (1980); K. H. Fischer, Z. Phys. B 39, 37 (1980); S. E. Barnes, J. Phys. F 11, L249 (1981).

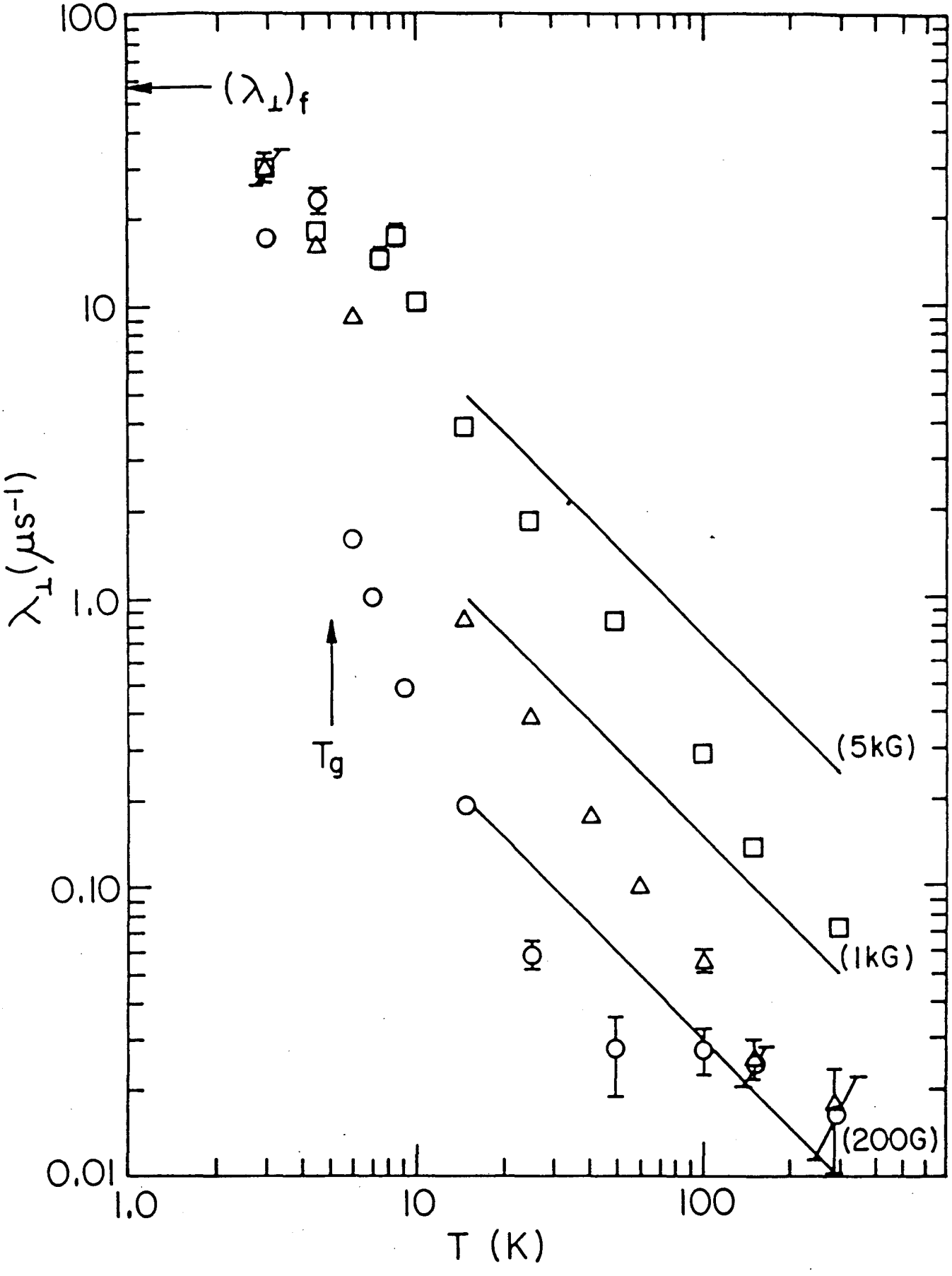
100
10
1.0
0.10
0.01
$(\lambda_\perp)_f$
$\lambda_\perp (\mu s^{-1})$
T_g
(5kG)
(1kG)
(200G)
1.0
10
100
T (K)

Figure 1

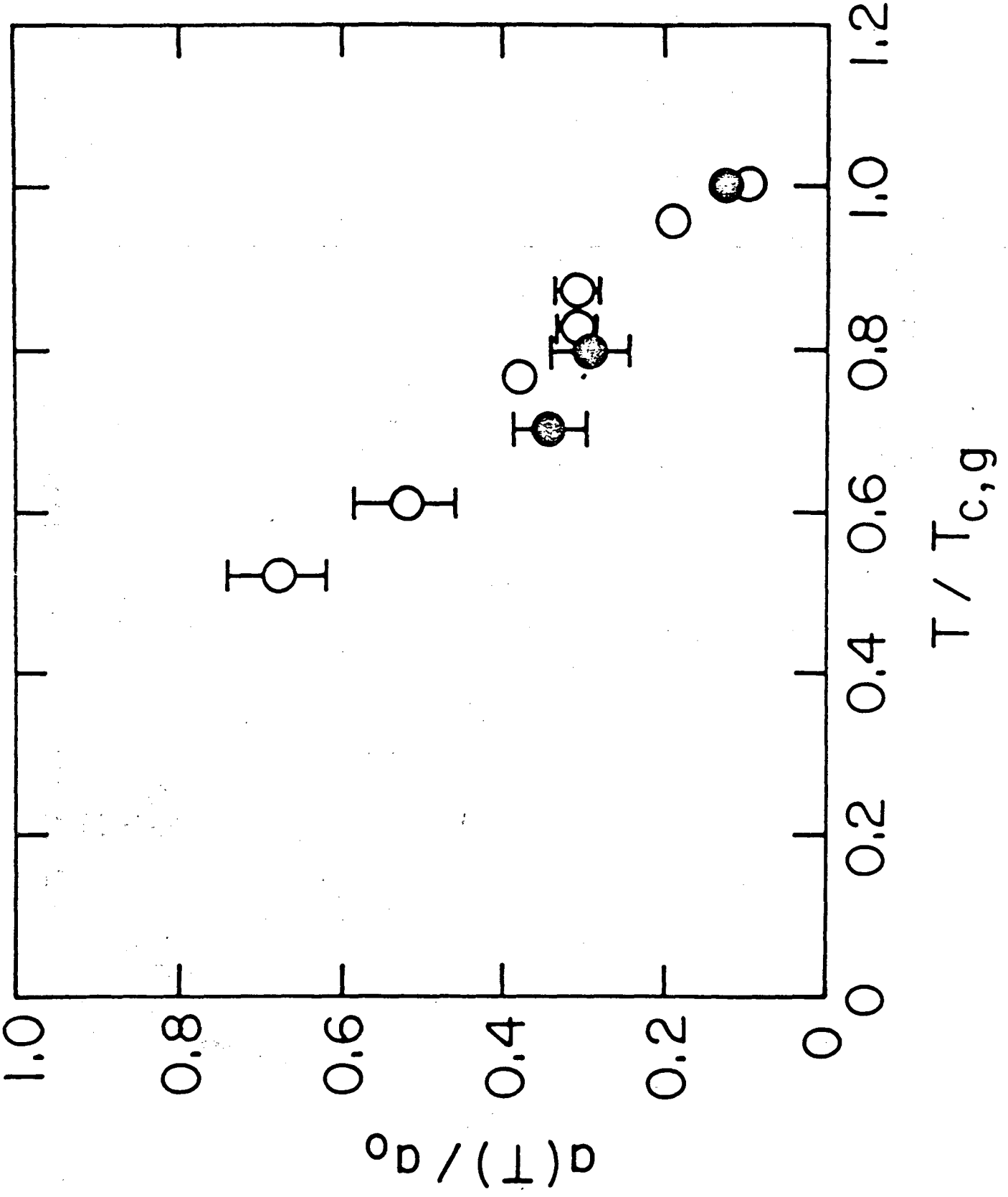

Figure 2

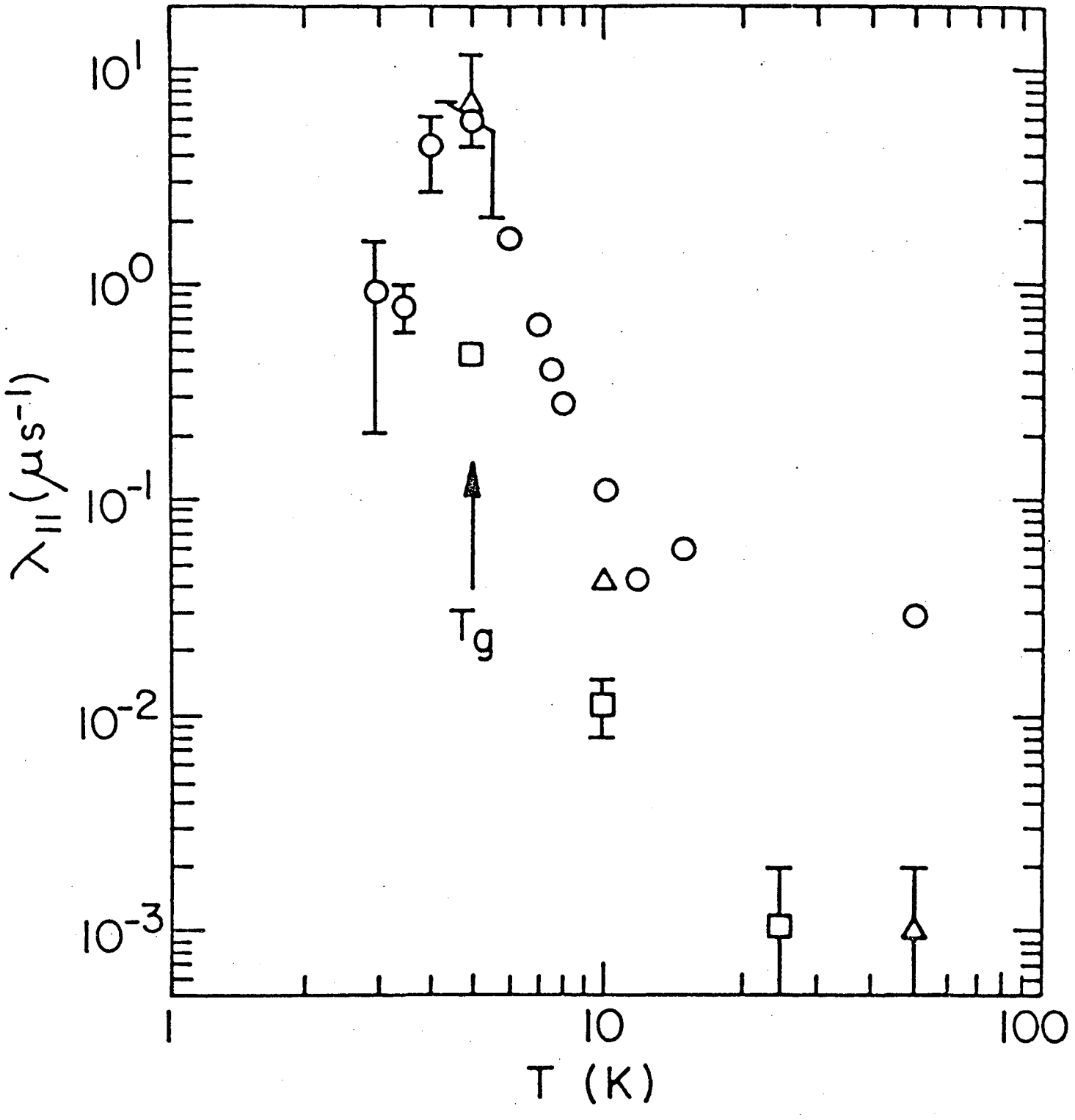

Figure 3